THE JOURNAL
OF
CHEMICAL PHYSICS

VOLUME 17, NUMBER 4 APRIL, 1949

The Mercury Photosensitized Polymerization of Cyclopropane*

H. E. GUNNING** AND E. W. R. STEACIE

(Received May 19, 1948)

An investigation has been made of the polymerization of cyclopropane with mercury ($^3P_1$) atoms in a static system over the pressure range from 1–400 mm at 30°C. The only important product of the reaction is a liquid polymer with the formula $(C_3H_6)_n$, where n is probably about 6. Small amounts of other products, of low molecular weight, are present at initial pressures below 10 mm. Data are presented which show that propylene is formed only at low initial pressures, suggesting its origin from the collision of trimethylene biradicals with the wall.

The over-all rate of consumption of cyclopropane becomes independent of initial pressures above 40 mm. The quantum yield of cyclopropane disappearance in the complete quenching region is 0.136.

A mechanism is proposed for the polymerization involving the initial formation of an energy-rich trimethylene biradical by the reaction

$$C+Hg(^3P_1)\rightarrow R_1{}^*+Hg(^1S_0). \quad (1)$$

The activated radical can then either reform cyclopropane upon collision or form a higher biradical:

$$R_1{}^*+C\rightarrow 2C, \quad (2)$$

$$R_1{}^*+C\rightarrow R_2{}^*, \text{ etc.}, \quad (3)$$

where C=cyclopropane, $R_1=\cdot(CH_2)_3\cdot$, and $R_2=\cdot(CH_2)_6\cdot$. Chain termination will occur when the polymer biradical can no longer furnish sufficient energy to break the C–C bond in cyclopropane. The radical will then stabilize itself by a proton shift. On the basis of the above mechanism, combined with the analytical data, reaction (2) must be at least 43 times faster than reaction (3).

Evidence is also presented for the fact that cyclopropane does not react with the H atoms formed by the collision of $Hg(^3P_1)$ atoms with hydrogen.

INTRODUCTION

THE polymerization of cyclopropane, sensitized by $Hg(^3P_1)$ atoms was first observed by Harris, Ashdown, and Armstrong[1] during the course of an investigation of the Raman spectrum of cyclopropane. These authors found that the rate of pressure decrease was independent of the initial pressure of the cyclopropane over the range from 0.5 to 4 atmospheres. Furthermore, they found that "the product was a viscous colorless oil having a boiling point of nearly 300°C at 760 mm, and showing continuous absorption in the ultraviolet below 2500A." They concluded that the polymer must have the formula $(CH_2)_n$.

The present investigation was undertaken in order to elucidate the mechanism of the polymerization, and to gather further information on the properties of the trimethylene biradical.

EXPERIMENTAL

Two separate series of static runs were made at 30°C. Descriptions of the apparatus used in each series follow:

Static Runs, "*K*" Series

In this series of runs a cylindrical, fused quartz cell was employed which was 10 cm in length with windows 5 cm in diameter. The cell was immersed in a metal thermostat provided with a fused quartz window. The distilled water in the bath, which was changed before each run, was maintained at 30.00±0.01°C, by means of a thermionic relay circuit, similar to the device described by Serfass.[2] The cell had a volume of 250 cc, while the volume of the entire cell system was 1052 cc. Pressure changes in the system were followed by means of a

* Joint contribution from the Department of Chemistry, University of Rochester, Rochester, New York, and the Division of Chemistry, National Research Laboratories, Ottawa, Canada. The portion of this work which was done at the University of Rochester was supported by Contract N6onr-241, Task I, with the Office of Naval Research, United States Navy.

** Department of Chemistry, Illinois Institute of Technology, Chicago, Illinois.

[1] L. Harris, A. A. Ashdown, and R. T. Armstrong, J. Am. Chem. Soc. **58**, 682 (1936).

[2] E. J. Serfass, Ind. Eng. Chem. Anal. Ed. **13**, 262 (1941).

TABLE I. Volume of system = 1050 cc.

Run no.	P_0 (mm)	$(-\Delta P/\Delta t)$ $\times 10^2$ mm/min.	$[d(CH_4)/dt]$ $\times 10^6$ moles/min.	$[d(H_2)/dt]$ $\times 10^6$ moles/min.
132K	1.79	0.69	0.032	0.013
133K	4.20	1.12	0.035	0.018
131K	7.14	1.31	0.019	0.017
130K	10.8_5	1.52	0.019	0.018
129K	19.9_5	1.91	0.014	0.020
124K	33.0_1	2.31	0.008	0.019
125K	39.8_9	2.33	0.009	0.019
126K	49.8_5	2.44	0.005	0.022
127K	57.7_3	2.46	0.009	0.022
128K	72.4_4	2.44	0.006	0.019

multirange McLeod gauge. A description of the mercury resonance lamp used and other experimental details will be found in an earlier publication.[3]

The mass spectrometric analyses on the products of the "K" runs which were condensible in liquid air were obtained through arrangement with the National Bureau of Standards. The sampling technique employed, as well as the method used in the analyses for hydrogen and methane, have been previously described.[4]

Static Runs, "P" Series

In this series of runs the cylindrical, fused quartz cell was 8 cm in length with windows 5 cm in diameter. The volume of the cell was 165 cc. Pressure measurements were made with a Pearson differential manometer, similar to the instrument described by LeRoy.[5] The manometer was carefully calibrated throughout its entire length by filling with mercury and weighing successive portions, using a one-meter cathetometer to measure the displacements in the meniscus of the mercury. The manometer was separately thermostatted to 0.1°C, to avoid changes in pressure due to fluctuations in room temperature. With this manometer it was found possible to measure changes in pressure to 0.01 mm of mercury up to absolute pressures of 500 mm.

The cell was immersed in a metal water bath at 30.00±0.01°C, exactly as in the "K" runs. The cell and the manometer made up about 80 percent of the volume of the system. The remainder of the cell system was constructed from heavy-walled capillary tubing to minimize temperature effects. The total volume of the system was dependent upon the setting of the manometer. However, all pressure rates reported in this paper have been corrected to a volume of 280 cc.

In the "P" series of runs, cyclopropane and propylene were determined by selective catalytic hydrogenation over nickel catalysts, after the method of Corner and Pease.[6] Attempts were also made to detect propylene using a Perkin-Elmer infra-red spectrometer.

The source used in this series was a Hanovia SC-2537 mercury resonance lamp, wound in the form of a five-coil helix, the coils being about 5 cm in diameter. The lamp was operated from a "neon sign" type transformer, delivering an initial voltage of 3000 volts at 30 milliamperes from the secondary.

The cyclopropane used throughout the entire investigation was the U.S.P. grade supplied by the Ohio Chemical and Manufacturing Company, Cleveland, Ohio. The gas was further purified by several trap-to-trap distillations. The middle fractions from these distillations were stored in two-liter bulbs provided with all-mercury valves of the design suggested by Warrick and Fugassi.[7] Mass spectrometric analyses of duplicate samples of the cyclopropane showed it to be 99.8 percent cyclopropane and 0.2 percent propane.

Before making a run the cell was allowed to stand for two hours in a hot chromic acid solution. It was then thoroughly rinsed with distilled water, and "flamed out" at a bright red heat in a current

TABLE II.

Run no.	P_0 (mm)	$-d/dt$ (cyclopropane)	d/dt (ethane)	d/dt (propylene)	d/dt (propane)	d/dt (methyl cyclopentane)	d/dt (methyl hexenes)	d/dt (dimethyl hexanes)
		The rates are in moles per minute $\times 10^6$.						
133K	4.20	0.85	0.006	0.10	0.03	0.007	0.02	0.007
131K	7.14	0.87	0.006	0.02	0.04	0.004	0.04	0.006
130K	10.8_5	0.88		0.01	0.04			
129K	19.9_5	1.06			0.02			
124K	33.0_1	1.34						
125K	39.8_9	1.33						
126K	49.8_5	1.37						
128K	72.4_4	1.38						

[3] H. E. Gunning and E. W. R. Steacie, J. Chem. Phys. **12**, 484 (1944).
[4] H. E. Gunning and E. W. R. Steacie, J. Chem. Phys. **14**, 544 (1946).
[5] D. J. LeRoy, Ind. Eng. Chem. Anal. Ed. **17**, 652 (1945).
[6] E. S. Corner and R. N. Pease, Ind. Eng. Chem. Anal. Ed. **17**, 564 (1945).
[7] E. Warrick and P. Fugassi, Ind. Eng. Chem. Anal. Ed. **15**, 13 (1943).

of air, to remove any polymer remaining on the cell from previous runs. One cc of distilled mercury was then added to the cell, after which the cell was attached to the system and evacuated to a "sticking" vacuum, as measured on the McLeod gauge. The desired amount of cyclopropane was then frozen in the cell system by placing liquid nitrogen around a small bulb in the system. After another evacuation to remove any non-condensible gas from the cyclopropane, the cyclopropane was allowed to vaporize and remain for 12 hours in the system before making a run, in order that the mercury might attain its vapor pressure at 30°C.

RESULTS

Results with "*K*" Series

Cyclopropane showed a similar behavior to propylene,[8] isobutene,[7] 1-butene,[9] 2-butene,[9] and isoprene[8] in that the pressure decreases linearly with time even in the initial stages of the reaction. Droplets of a clear, colorless polymer could be seen forming on the window throughout the course of a run. A study of Table I will show that the rate of pressure decrease becomes independent of the initial pressure above about 30 mm pressure. This is in agreement with the results of Harris, Ashdown, and Armstrong.[1] Also from Table I it is apparent that the rates of formation of both methane and hydrogen become independent of pressure in the complete quenching region. The increase in the rate of methane formation at low pressures would suggest wall reactions between methyl radicals and H atoms. Of course, both methane and hydrogen are very minor products in the reaction.

In Table II the results of the mass spectrometric analyses of the "*K*" runs are tabulated.

The polymer is apparently the only important product above an initial pressure of 20 mm. This polymer must therefore have the formula $(CH_2)_n$. Its vapor pressure is 10^{-4} mm at 30°C. It is interesting to note that propylene becomes a significant product at low pressures, which would suggest that the propylene might be formed in collisions of trimethylene biradicals with the wall.

Results with "*P*" Series

With the Pearson differential manometer, it was found possible to measure accurate pressure rates up to much higher initial pressures than with the McLeod gauge. Table III shows a typical run, using the manometer. It will be observed that there is a slight pressure rise at the beginning of the run. After about five minutes the pressure begins to decrease linearly with time. However, at the end of the run, the pressure falls rapidly as soon as the lamp is turned off. The linear portion of the pressure-time curve extrapolates back to 0.18 mm at zero time, while the drop in pressure after turning off the lamp = 0.21 mm. The same effect is observed with isobutene.[10] This displacement of the pressure-time curve disappears below initial pressures of 20 mm and becomes independent of initial pressure at 0.2 mm in the complete quenching region. It could conceivably be due either to desorption of gas molecules from the wall, or to the heat of reaction or to a combination of both. More data will shortly be published on this effect.[10]

TABLE III. Run no. 163*P*, $P_0 = 39.5$ mm.

Time (min.)		$-\Delta P$ (mm)
0		0.00
1		−0.01
2		0.06
3		0.14
4		0.21
5		0.28
10		0.76
15		1.25
20		1.70
25		2.18
30		2.65
35		3.11
40		3.57
45		4.03
50		4.50
55		4.96
60		5.43
.		.
.	Lamp off	.
.		.
60.3		5.54
63		5.54

The rate data are summarized in Table IV. The cyclopropane consumed was calculated from the pressure changes, corrections being applied for the non-condensible gas formed during the run. This method of calculation is valid, since the mass spectrometric analyses of the "*K*" runs (Table II) show that polymer is the only significant product of the reaction at initial pressures greater than 10 mm. The rate of consumption of cyclopropane is remarkably constant in the complete quenching

TABLE IV. Volume of system = 280 cc.

Run no.	P_0 (mm)	$-\Delta P/\Delta t$ mm/min. $\times 10^2$	d/dt (CH_4+H_2) moles/min. $\times 10^6$	$-d/dt$ (cyclo C_3H_6) moles/min. $\times 10^6$	φ cyclo C_3H_6
158*P*	17.2	7.8	0.070	1.08	0.10
157*P*	27.0	8.4	0.049	1.19	0.11
163*P*	39.5	8.7	0.038	1.25	0.12
155*P*	50.3	9.9	0.029	1.44	0.136
162*P*	156.8	9.9	0.027	1.44	0.136
156*P*	219.0	9.8	0.025	1.43	0.135
159*P*	415.2	9.9	0.027	1.44	0.136

[8] H. E. Gunning and E. W. R. Steacie, J. Chem. Phys. **14**, 57 (1946).

[9] H. E. Gunning and E. W. R. Steacie, J. Chem. Phys. **14**, 581 (1946).

[10] G. A. Allen and H. E. Gunning, J. Chem. Phys. **16**, 1146 (1948).

region, suggesting that the rate of reaction is determined entirely by the initial quenching process.

In view of the fact that propylene would seem to be a likely product of the reaction, attempts were made to detect propylene in the products by infra-red absorption and by catalytic hydrogenation.[6]

In the infra-red method of analysis, a Perkin-Elmer spectrometer was used in conjunction with a 15-cm absorption cell. Preliminary tracings showed that propylene absorbed quite strongly at 10.85 mμ, while the cyclopropane absorption at

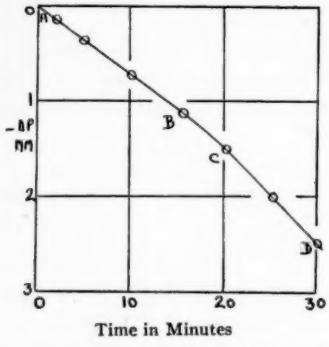

FIG. 1. Pressure *vs.* time for a mixture of 50-mm cyclopropane and 3-mm propylene.

this wave-length was very weak. In order to obtain quantitative data, a series of calibration tracings were made over a range of pressures for both cyclopropane and propylene. Five one-hour runs were then made over the pressure range from 50 to 400 mm. The products of each run were frozen into the infra-red absorption cell and tracings made with the gas. The results, corrected for cyclopropane absorption, showed no propylene to be present. It was estimated that a minimum of 500 cc-mm of propylene could be detected by this method, or about one percent by volume.

Attempts were also made to detect propylene in the products by catalytic hydrogenation over a kieselguhr-supported nickel catalyst, which had been poisoned by mercury.[6] These results were also negative. The sensitivity of this method is about the same as the infra-red technique used.

The Effect of Added Propylene

In Fig. 1 the pressure-time curve is shown for a run on a mixture of 50 mm of cyclopropane and 3 mm of propylene. The portion *AB* of the curve has a slope of 0.068 mm/min., while the *CD* portion has a slope of 0.099 mm/min. It is apparent that propylene has a strong inhibiting effect on the rate and that it is rapidly consumed, since the *CD* portion of the curve corresponds to the uninhibited rate. In Table V and Fig. 2 the initial slopes of five runs are shown at various concentrations of added propylene. Maximum inhibition appears to occur at about two percent by volume of added propylene. These results seem to offer a fairly tangible proof that propylene is not a significant product in the cyclopropane polymerization, except perhaps at low pressures, as indicated in Table II. The fact that the rate of pressure decrease becomes independent of propylene concentration in mixtures richer than two percent by volume in propylene, as seen in Fig. 2 ,would suggest that at these concentrations propylene is doing the major portion of the quenching. It follows that the quenching cross section of propylene for $Hg(^3P_1)$ atoms must be at least 50 times greater than cyclopropane. Now these values have never been determined directly. However, Steacie and LeRoy[11] found that the quenching cross section of propylene for $Cd(^3P_1)$ atoms was some forty times greater than cyclopropane, and it is probable that approximately the same ratio of cross sections would be obtained for these substances with respect to $Hg(^3P_1)$ atoms.

Hydrogenation of Cyclopropane***

Several runs were made with mixtures containing 90 percent by volume of hydrogen and 10 percent by volume of cyclopropane. The total pressure in these runs was 450 mm. Under these conditions practically all the quenching would be done by hydrogen. After a five-hour irradiation, the pressure fell by only 0.30 mm as measured on the differential manometer. The condensible gas at the end of the run was shown to be pure cyclopropane by the fact that it did not hydrogenate over the mercury-poisoned nickel catalyst, and was completely hydrogenated over the unpoisoned nickel catalyst.[6] Therefore, it is apparent that cyclopropane does not react appreciably with the H atoms generated in mercury photosensitization.

The Quantum Yield of the Reaction

In the "*K*" series of runs the light intensity was determined by filling the cell with ethylene at an initial pressure of 13 mm, and determining the initial rate of formation of hydrogen, by oxidation over copper oxide at 250°C. The average of eight runs gave $d(H_2)/dt = 2.5 \pm 0.2 \times 10^{-6}$ mole/minute. While LeRoy and Steacie[12] have reported that the quantum yield for the ethylene reaction at 13

[11] E. W. R. Steacie and D. J. LeRoy, J. Chem. Phys. 11, 164 (1943).

*** Professor H. S. Taylor has informed us that Dr. R. E. Powell, in some preliminary work at Princeton University, found that the mercury photosensitized hydrogenation of cyclopropane was slower than that of propylene by a factor of at least 100 to 150. We would like to acknowledge our indebtedness to Professor Taylor and Dr. Powell for their kindness in making this unpublished information available to us.

[12] D. J. LeRoy and E. W. R. Steacie, J. Chem. Phys. 9, 829 (1941).

TABLE V. Effect of added propylene. Pressure of cyclopropane = 50 mm.

Run no.	Percent by vol. added C_3H_6	Initial rate mm/min.
155*P*	0	0.099
164*P*	0.2	0.094
165*P*	0.5	0.088
166*P*	1.75	0.068
160*P*	3.5	0.067
161*P*	5.8	0.067

mm is 0.37, recent work at the University of Rochester[13] suggests that the quantum yield of hydrogen formation under these conditions is 0.25, and on this basis $I_{ab}=1.0\times10^{-5}$ Einstein per minute in the "*K*" series of runs. Combining this information with the data in Table II, we obtain 0.14 as the quantum yield of cyclopropane disappearance in the complete quenching region.

On the "*P*" series of runs, the light intensity was determined by using uranyl oxalate solutions,[14] which gave $I_{ab}=1.06\times10^{-5}$ Einstein per minute. The over-all quantum yield is recorded in the last column of Table IV as 0.136, in excellent agreement with the "*K*" runs, considering that two different sources were used.

DISCUSSION

Before attempting to devise a mechanism for the polymerization of cyclopropane, sensitized by $Hg(^3P_1)$ atoms, it might be wise to summarize the essential features of the reaction. These are:

(a) The pressure decreases linearly with time, even in the initial stages of the reaction.

(b) The rate of pressure decrease and the rate of cyclopropane consumption become independent of the initial pressure, in the complete quenching region, i.e., above approximately 40 mm.

(c) A colorless liquid polymer, which has the formula $(CH_2)_n$, appears to be the only significant product of the reaction in the complete quenching region.

(d) There are a large number of low molecular weight products at initial pressures below 10 mm. Propylene seems to become a significant product in this low pressure region.

(e) Small amounts of added propylene have a marked inhibiting effect upon the rate of pressure decrease, suggesting that propylene is not a product of the reaction in the complete quenching region.

(f) Runs with 9:1 mixtures of hydrogen to cyclopropane showed that cyclopropane does not react appreciably with the H atoms formed by the quenching of $Hg(^3P_1)$ atoms with hydrogen molecules.

(g) The quantum yield of cyclopropane disappearance is 0.136 in the complete quenching region.

The reaction of cyclopropane with $Hg(^3P_1)$ atoms is in remarkable contrast with its thermal behavior, since, as Corner and Pease[15] and others have shown, propylene is the main product of the thermal reaction.

In our discussion of the mechanism we will use the following abbreviations: C = cyclopropane, $R_1=\cdot CH_2-CH_2-CH_2\cdot$, $R_2=\cdot CH_2-CH_2-CH_2-CH_2-CH_2-CH_2\cdot$, etc.

Now since cyclopropane does not react with H atoms and, furthermore, since the polymer is the only significant product in the complete quenching region, we postulate that the initial quenching act must involve a C–C bond split with the formation of an activated trimethylene biradical.

$$C+Hg(^3P_1)\rightarrow R_1{}^*+Hg(^1S_0). \quad (1)$$

The C–C bond strength in cyclopropane is not known accurately. However, recent work of R. A. Ogg[15] would suggest that the C–C bond strength may be as low as 50 kcal. and, consequently, there may be as much as 62 kcal. per mole of excess energy in the trimethylene biradicals formed in quenching $Hg(^3P_1)$ atoms. These activated radicals could therefore bring about further decomposition of cyclopropane by the reaction

$$R_1{}^*+C\rightarrow R_2{}^*. \quad (2)$$

The low quantum yield of the reaction could then be explained by assuming that cyclopropane can also reform by

$$R_1{}^*+C\rightarrow 2C. \quad (3)$$

Reaction (2) should be exothermic since the net effect is the rupture of the C–C bond is cyclopropane and the formation of the C–C bond in the hexamethylene biradical. The C–C bond strength in the linear biradical would probably be about 90 kcal. per mole, with the result that reaction

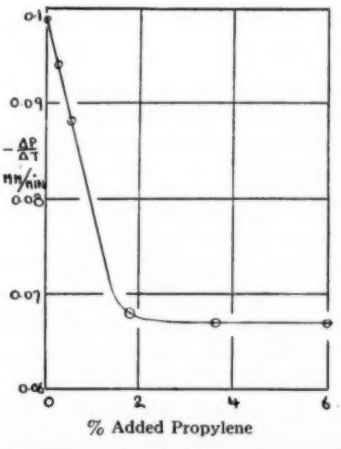

FIG. 2. The effects of added propylene on the rates.

[13] G. A. Allen and H. E. Gunning, J. Chem. Phys. **16**, 634 (1948).

[14] G. S. Forbes and L. J. Heidt, J. Am. Chem. Soc. **56**, 2363 (1934).

[15] E. S. Corner and R. N. Pease, J. Am. Chem. Soc. **67**, 2067 (1945).

[16] R. A. Ogg, private communication.

(2) could be exothermic to as much as 40 kcal., if we adopt the conclusions of Ogg as to the strength of the C−C bond in cyclopropane. Of course, the number of vibrational degrees of freedom over which this excess energy can disseminate itself has also increased during this reaction. Nevertheless, it seems plausible to assume that the energy necessary to propagate the polymer chain can be adequately supplied by a mechanism of the type suggested above.

The polymer which was obtained in this investigation can therefore be explained by the sequence

$$R_2^* + C \rightarrow R_3^* \qquad (4)$$

$$\vdots$$

$$R^*_{(n-1)} + C \rightarrow M_n, \qquad (5)$$

where M_n represents the polymer molecule. Chain termination will occur when the number of vibrational degrees of freedom has increased to such an extent that the energy available upon collision is no longer sufficient to break the C−C bond in cyclopropane. When the polymer radical has reached this degree of complexity, it could stabilize itself by a proton shift with the formation of an alkene. It is also possible that cyclization might occur during the shifting of the proton.

The presence of propylene at low pressure points strongly to its formation from a collision of a trimethylene biradical with the wall. The work of Bawn and Hunter[17] on the reaction of trimethylene bromide with sodium vapor tends to substantiate our results. They found that the isomerization of the trimethylene biradical to propylene seemed to occur mainly at the wall, while the formation of cyclopropane from the biradical occurred in the gas phase.

If we assume that the low quantum yield arises from reaction (3), it would seem plausible to assume that the reaction

$$R_2 + C \rightarrow M_2 + C \qquad (6)$$

might occur also, since Bawn and Milsted[18] found that 1,6-dibromohexane reacted with sodium vapor with the formation chiefly of cyclohexane, with some hexene. However, this reaction is precluded in our case since C_6 compounds are present only at very low pressures, suggesting that they are formed either by the recombination of monoradicals or the isomerization of biradicals at the walls.

The sequence of $n+1$ steps summarized in reactions (1) to (5) are consistent with our findings in the complete quenching region. Thus, on the assumption of steady-state concentrations for the radicals, we obtain the relation:

$$-dC/dt = n \cdot I_{ab} \cdot k_2/(k_2+k_3) = d(M_n)/dt$$

where $-dC/dt$ = rate of disappearance of cyclopropane, I_{ab} = rate of absorption of resonance radiation, $d(M_n)/dt$ = rate of formation of polymer, and n = number of units of C_3H_6 in the polymer. From Table IV, $\varphi_C = [-dC/dt] \cdot / I_{ab} = 0.136$ in the complete quenching region, and, therefore,

$$k_3/k_2 = (7.3)(n) - 1.$$

The rate of disappearance of cyclopropane on the basis of this mechanism will be independent of pressure in the complete quenching region, if the polymer chain length, n, is also independent of pressure.

Harris, Ashdown, and Armstrong[1] reported that the polymer had a boiling point of 300°C, and this is consistent with our observation that the polymer has a vapor pressure of 10^{-4} mm at 30°C. These data could be roughly identified with an octadecene, i.e., $C_{18}H_{36}$, and this would correspond to chain termination by a proton shift at $n=6$. At any rate it seems plausible from the foregoing remarks that $n=6$ would be a minimum value, and we can therefore conclude that k_3/k_2 has a minimum value of 43. In other words, the cyclopropane-reforming step (3) must be at least 43 times faster than the radical-forming step (2).

The small amounts of hydrogen, methane, ethane, and propane formed at low pressures, as shown in Tables I and II, could be adequately accounted for if we assume that the reaction

$$\text{cyclo } C_3H_6 + Hg(^3P_1) \rightarrow C_3H_5 + H + Hg(^1S_0) \qquad (7)$$

occurs to a slight extent. It is relevant to note that similar products are found in the mercury-photosensitized reactions of propylene,[19] and these products will ultimately arise in propylene from the interaction of allyl radical with H atoms, followed by hydrogenation and atomic cracking reactions.

It is, of course, possible to construct an activated molecule mechanism which could be made to fit our experimental findings. This is especially true in view of the fact that we have no direct evidence for the existence of the trimethylene biradical. The sequence

$$C + Hg(^3P_1) \rightarrow C^* + Hg(^1S_0), \qquad (8)$$

$$C^* + C \rightarrow 2C, \qquad (9)$$

$$C^* + C \rightarrow R_2, \text{ etc.} \qquad (10)$$

would yield rate expressions similar to those obtained from the mechanism postulated above, pro-

[17] C. E. H. Bawn and R. F. Hunter, Trans. Faraday Soc. **34**, 608 (1938).

[18] C. E. H. Bawn and J. Milsted, Trans. Faraday Soc. **35**, 889 (1939).

[19] H. E. Gunning and E. W. R. Steacie, J. Chem. Phys., in press.

vided that the activated cyclopropane molecule had a very long life. It is pertinent to note here that Phibbs, Darwent, and Steacie[20] found it necessary to postulate an activated molecule followed by ring opening in the mercury photosensitized decomposition of ethylene oxide, which is structurally somewhat similar to cyclopropane. In the present state of our knowledge, no definite choice can be made between the two mechanisms.

CONCLUSIONS

The reaction of cyclopropane with $Hg(^3P_1)$ atoms is in remarkable contrast to its thermal behavior, where isomerization to propylene seems to be the principal reaction occurring during the decomposition.[15] Furthermore, the cyclopropane reaction is unique among all the mercury photosensitized reactions of the hydrocarbons which have been investigated to date.[21] While it is not possible at the present time to decide whether the collision of an $Hg(^3P_1)$ atom with a cyclopropane molecule results in the formation of activated molecule or a trimethylene biradical, it seems fairly certain that the polymer chain is propagated by the successive formation of higher and higher biradicals.

Further work is now under way on the cyclopropane reaction in the laboratories of one of us (H.E.G.), together with investigations of the mercury photosensitized decompositions of the higher cyclic paraffins and olefins.

ACKNOWLEDGMENT

It is a great pleasure for the authors to acknowledge their indebtedness to Dr. Fred L. Mohler of the Mass Spectrometry Section of the National Bureau of Standards for performing the mass spectrometric analyses reported in this paper.

Our thanks are also due Mr. Yves Lupien for assistance in some of the measurements and Mr. Burton Dearing for his assistance in the infra-red measurements.

[20] M. K. Phibbs, B. de B. Darwent, and E. W. R. Steacie, J. Chem. Phys. **16**, 39 (1948).

[21] For discussions of the mercury photosensitized reactions of the hydrocarbons, see: E. W. R. Steacie, *Atomic and Free Radical Reactions* (Reinhold Publishing Corporation, New York, 1946); Keith J. Laidler, J. Chem. Phys. **15**, 712 (1947); E. W. R. Steacie, Research, in press.

THE JOURNAL OF CHEMICAL PHYSICS VOLUME 17, NUMBER 4 APRIL, 1949

The General Solution of the Secular Equation of Second Degree, with Application to the Class A_1 Vibrations of the Symmetrical Triatomic Molecule

P. TORKINGTON
39a Palliser Road, London, W., England
(Received July 8, 1948)

Various solutions of the secular equation of second degree, giving the force constants, normal coordinates, and potential energy distributions in terms of the fundamental vibration frequencies and molecular constants, have been found and their significance discussed. General formulas are obtained for certain critical solutions and illustrative numerical results given for a series of eight symmetrical triatomic molecules, with curves covering all possible solutions in three typical cases. The solution in which the ratios of the contributions to the potential energy from the two square terms in the valence-force potential energy expression are mutually reciprocal in the two normal modes is shown to be universally applicable; that in which the normal coordinate for the vibration of higher frequency is identical with the corresponding valence-force symmetry coordinate is also quite satisfactory. Both always give real results. Alternative solutions are suggested for use when the difference in frequency of the two modes is small.

I. THE SECULAR EQUATION

IF the motion of a displaced system specified by two coordinates Δ_1 and Δ_2 is simple harmonic, the potential energy, V, contains only quadratic terms and has the following general form

$$2V=d_{11}\Delta_1^2+d_{22}\Delta_2^2+(d_{12}+d_{21})\Delta_1\Delta_2, \qquad (1)$$

where the d_{ij}'s are the force constants, $(d_{12}=d_{21})$. It is assumed in this paper that Δ_1 and Δ_2 are valence-type coordinates of the required symmetry class. It is usually convenient to express them in terms of further coordinates z_1 to z_N, as follows

$$\Delta_i=\sum_{k=1}^{N} a_{ik}z_k, \qquad (2)$$

where the coefficients a_{ik} are determined by the geometry of the system. The secular equation giving the normal vibration frequencies of the system described by the force field (1) can then be written[1]

$$\begin{vmatrix} A_{11}d_{11}+A_{12}d_{12}-\lambda & A_{21}d_{11}+A_{22}d_{12} \\ A_{11}d_{21}+A_{12}d_{22} & A_{21}d_{21}+A_{22}d_{22}-\lambda \end{vmatrix}=0, \qquad (3)$$

[1] E. Bright Wilson, Jr., J. Chem. Phys. **7**, 1047 (1939).

where

$$A_{ij}=A_{ji}=\sum_{k=1}^{N} a_{ik}a_{jk}(M/m_k), \tag{4}$$

and

$$\lambda=4\pi^2\nu^2c^2M, \tag{5}$$

ν being the vibration frequency in cm^{-1}, c the velocity of light in cm sec.$^{-1}$, and M some mass, usually related to one of the m_k's, (which are the masses conjugate to the coordinates z_k), introduced in order that the A_{ij} shall be pure numbers.

An unambiguous solution for the force constants d_{ij} in terms of the vibration frequencies is not possible unless some arbitrary assumption is made as to the nature of the force field, equivalent to postulating a relationship between two of the constants. A possible exception to the above situation occurs when isotopic molecules are available for study; but, with the exception of the hydrogen-deuterium pair, the isotopic shifts are too small to be of much value. We shall examine the range of values allowed to each constant in the general problem and investigate the corresponding variation in the geometrical form and energy properties of the normal vibrations.

II. THE SOLUTION FOR THE CONSTANTS

By elimination of d_{22} from Eq. (3) we obtain the following second-degree equation in d_{11} and d_{12}

$$A_{11}d_{11}^2+2A_{12}d_{11}d_{12}+A_{22}d_{12}^2 -(\lambda_1+\lambda_2)d_{11}+(A_{22}/D)\lambda_1\lambda_2=0, \tag{6}$$

where $D=(A_{11}A_{22}-A_{12}^2)$, and λ_1 and λ_2 are the two solutions of (3) corresponding to ν_1 and ν_2. It can be shown that $(D/A_{11}^2)>0$, and that consequently Eq. (6) is that of an ellipse.[2] The center is found at $d_{11}=(A_{22}/2D)(\lambda_1+\lambda_2)$, $d_{12}=-(A_{12}/2D)(\lambda_1+\lambda_2)$, the major axis is inclined to the d_{11} axis at an angle $\theta=(1/2)$ arc $\tan[2A_{12}/(A_{11}-A_{22})]$, and the semi-axes a and b are given by the following expressions

$$\left.\begin{aligned} a^2&=(A_{22}/4D)[A_{11}\cos^2\theta+2A_{12}\sin\theta\cos\theta \\ &\qquad +A_{22}\sin^2\theta]^{-1}(\lambda_1-\lambda_2)^2 \\ b^2&=(A_{22}/4D)[A_{11}\sin^2\theta-2A_{12}\sin\theta\cos\theta \\ &\qquad +A_{22}\cos^2\theta]^{-1}(\lambda_1-\lambda_2)^2 \end{aligned}\right\}, \tag{7}$$

TABLE I. General solution of the secular equation of second degree.

	d_{12}	d_{11}	d_{22}	i	ρ_i	$V_{11}(\nu_i)$	$V_{22}(\nu_i)$	$V_{12}(\nu_i)$
Mean d_{12} (IV)	$-A_{12}''$	$A_{22}''\pm a_1D'$	$A_{11}''\mp(D'/a_1)$	1	$(a_2P_1)^{-1}$	$(B_1+A\mu_1)/4$	$(B_2+A\mu_1)/4$	$-(A\epsilon_1)/2$
				2	a_2P_2	$(B_2+A\mu_2)/4$	$(B_1+A\mu_2)/4$	$-(A\epsilon_2)/2$
Mean d_{11} (V)	$-A_{12}''\pm D'$	A_{22}''	$A_{11}''\mp 2a'D'$	1	$a'Q_1$	$(C_1\epsilon_1)/4$	$(C_2+C_1\mu_1)/4$	$-(C+C_1\mu_1)/2$
				2	$(a'Q_2)^{-1}$	$(C_2\epsilon_2)/4$	$(C_1+C_2\mu_2)/4$	$-(C+C_2\mu_2)/2$
Mean d_{22} (VI)		$A_{22}''\mp 2a_2D'$	A_{11}''	1	$(a_2Q_1)^{-1}$	$(C_2+C_1\mu_1)/4$	$(C_1\epsilon_1)/4$	$-(C+C_1\mu_1)/2$
				2	a_2Q_2	$(C_1+C_2\mu_2)/4$	$(C_2\epsilon_2)/4$	$-(C+C_2\mu_2)/2$
Min. (III) & Max. d_{12}	$-(A_{12}''\pm A'D')$	$A_{22}''\pm a_1D''$	$A_{11}''\pm(D''/a_1)$	1	$\mp(1/a_1)$	$(1+K_1\mu_1)/4$		$(1-K_1\mu_1)/2$
				2	$\pm a_1$	$(1+K_2\mu_2)/4$		$(1-K_2\mu_2)/2$
Min. d_{22} (VII)	$-A_{12}'\lambda_2$	$\lambda_1'+A\lambda_2'$	$A_{11}'\lambda_2$	1	$(1/a_2)$	$1+A\mu_1$	$A\mu_1$	$-2A\mu_1$
				2	∞	0	1	0
Min. d_{11}		$A_{22}'\lambda_2$	$\lambda_1''+A\lambda_2''$	1	a'	$A\mu_1$	$1+A\mu_1$	$-2A\mu_1$
				2	0	1	0	0
Max. d_{11} (VIII)	$-A_{12}'\lambda_1$	$A_{22}'\lambda_1$	$\lambda_2''+A\lambda_1''$	1	∞	1	0	0
				2	$(1/a')$	$A\mu_2$	$1+A\mu_2$	$-2A\mu_2$
Max. d_{22}		$\lambda_2'+A\lambda_1'$	$A_{11}'\lambda_1$	1	0	0	1	0
				2	a_2	$1+A\mu_2$	$A\mu_2$	$-2A\mu_2$
$V_{12}=0$ (I)	0	$L_1'\pm E'$	$L_1''\mp E''$	1	*	$(1\pm E)/2$	$(1\mp E)/2$	0
				2	*	$(1\mp E)/2$	$(1\pm E)/2$	
$V_{11}(\nu_1)=V_{22}(\nu_2)$ (II)	$-2A_{12}'L_3$	$F'(F\pm L_2)$	$F''(F\mp L)_2$	1	*	$F(F\pm 1)/2$	$F(F\mp 1)/2$	$-4A(L_3/L_1)$
				2	*	$F(F\mp 1)/2$	$F(F\pm 1)/2$	

See reference *, Section IV.

[2] G. Glockler and Yo-Yun Tung, J. Chem. Phys. **13**, 388 (1945).

both of which are always real and positive. The constant d_{12} varies over the range $(1/2D)[-A_{12}(\lambda_1+\lambda_2) \pm (A_{11}A_{22})^{\frac{1}{2}}(\lambda_1-\lambda_2)]$ and d_{11} over the range $(A_{22}/2D)[(\lambda_1+\lambda_2)\pm(\lambda_1-\lambda_2)]$.

Similarly, by elimination of d_{11} from Eq. (3), we obtain the second degree equation in d_{22} and d_{12}, corresponding to Eq. (6)

$$A_{22}d_{22}^2+2A_{12}d_{22}d_{12}+A_{11}d_{12}^2 - (\lambda_1+\lambda_2)d_{22}+(A_{11}/D)\lambda_1\lambda_2=0. \quad (8)$$

This is also the equation of an ellipse, whose center is at $d_{22}=(A_{11}/2D)(\lambda_1+\lambda_2)$, $d_{12}=-(A_{12}/2D)(\lambda_1+\lambda_2)$, whose major axis is inclined to the d_{22} axis at an angle $\theta'=[(\pi/2)-\theta]$ and whose semi-axes are related to a and b in Eq. (7) by $a'=(A_{11}/A_{22})^{\frac{1}{4}}a$, $b'=(A_{11}/A_{22})^{\frac{1}{4}}b$. d_{12} varies as before, and d_{22} over the range $(A_{11}/2D)[(\lambda_1+\lambda_2)\pm(\lambda_1-\lambda_2)]$.

The following relations holding at certain singular solutions are of interest:

$$\text{At } (\partial d_{11}/\partial d_{12})=0, \quad A_{21}d_{11}+A_{22}d_{12}=0. \quad (9)$$

$$\text{At } (\partial d_{22}/\partial d_{12})=0, \quad A_{11}d_{21}+A_{12}d_{22}=0. \quad (10)$$

$$\text{At } (\partial d_{12}/\partial d_{11})=(\partial d_{12}/\partial d_{22})=0, \quad (11)$$
$$A_{11}d_{11}+A_{12}d_{12}=A_{21}d_{21}+A_{22}d_{22}=\tfrac{1}{2}(\lambda_1+\lambda_2).$$

Eqs. (9) and (10) lead to the factorization of Eq. (3) into two linear equations, and Eq. (11) requires the two diagonal terms to be equal, and the subsidiary elements to be equal but opposite in sign. It is found that real solutions of d_{11} and d_{22}, with $d_{12}=0$, are only possible if the following condition is satisfied,

$$(A_{11}A_{22}/A_{12}^2)[(\lambda_1-\lambda_2)/(\lambda_1+\lambda_2)]^2 \geqslant 1. \quad (12)$$

It may be noted that in the case $\lambda_1=\lambda_2$, (degeneracy), Eqs. (6) and (8) each represent two imaginary straight lines, and the only real solution for the constants is $d_{12}=-(A_{12}/D)\lambda$, $d_{11}=(A_{22}/D)\lambda$, and $d_{22}=(A_{11}/D)\lambda$. Conditions (9), (10), and (11) then all hold simultaneously, and all possible linear combinations of Δ_1 and Δ_2 are allowed as normal coordinates.

III. THE NORMAL COORDINATES

It is found that the displacements $z_n(\nu_{1,2})$ associated with the normal modes $\nu_{1,2}$ are related to the (unnormalized) normal coordinates $\eta_{1,2}$ as follows,

$$\left.\begin{aligned} z_n(\nu_{1,2}) &= (M/m_n)[(a_{1n}A_{21}-a_{2n}A_{11})d_{21} \\ &\quad +(a_{1n}A_{22}-a_{2n}A_{12})d_{22}-a_{1n}\lambda_{1,2}]\eta_{1,2}, \\ &= (M/m_n)[(a_{1n}A_{21}-a_{2n}A_{11})d_{11} \\ &\quad +(a_{1n}A_{22}-a_{2n}A_{12})d_{12}+a_{2n}\lambda_{1,2}]\eta_{1,2}, \end{aligned}\right\} \quad (13)$$

where the force constants d_{ij} are any set satisfying the original Eq. (3). In terms of the coordinates Δ_1 and Δ_2, the geometrical form of the normal vibrations is described by the following relations

$$\left.\begin{aligned} &(\Delta_1/\Delta_2)(\nu_{1,2}) \\ &\quad =[(A_{11}\lambda_{1,2}-Dd_{22})/(A_{12}\lambda_{1,2}+Dd_{12})] \\ &\quad =[(A_{12}\lambda_{1,2}+Dd_{12})/(A_{22}\lambda_{1,2}-Dd_{11})] \end{aligned}\right\}. \quad (14)$$

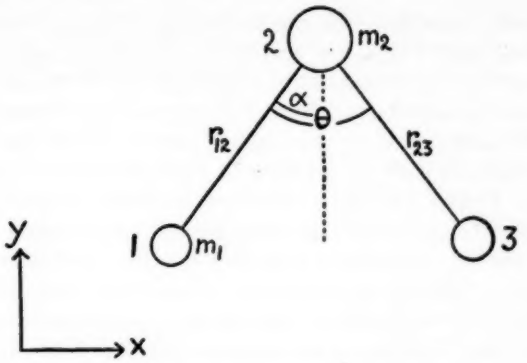

FIG. 1. Coordinates for the symmetrical triatomic molecule.

It is convenient to define two parameters

$$\rho_1=(\Delta_1/\Delta_2)(\nu_1), \quad \rho_2=(\Delta_2/\Delta_1)(\nu_2). \quad (15)$$

The normal coordinates define the directions and relative magnitudes of the atomic displacement vectors in the two modes; the alternative, energy description[3] requires a knowledge of the relative contributions to the potential energy from each of the three terms in Eq. (1), in each mode. If we write $V_{11}=\frac{1}{2}(d_{11}\Delta_1^2/V)$, $V_{22}=\frac{1}{2}(d_{22}\Delta_2^2/V)$ and $V_{12}=(d_{12}\Delta_1\Delta_2/V)$, so that $V_{11}+V_{22}+V_{12}=1$, then it can be shown that

$$\left.\begin{aligned} V_{11}(\nu_{1,2}) &= \pm(d_{11}/\lambda_{1,2}) \\ &\quad \times[(A_{11}\lambda_{1,2}-Dd_{22})/(\lambda_1-\lambda_2)] \\ V_{22}(\nu_{1,2}) &= \pm(d_{22}/\lambda_{1,2})[(A_{12}\lambda_{1,2}+Dd_{12})^2/ \\ &\quad \{(\lambda_1-\lambda_2)(A_{11}\lambda_{1,2}-Dd_{22})\}] \\ V_{12}(\nu_{1,2}) &= \pm(2d_{12}/\lambda_{1,2}) \\ &\quad \times[(A_{12}\lambda_{1,2}+Dd_{12})/(\lambda_1-\lambda_2)] \end{aligned}\right\}, \quad (16)$$

where the positive sign refers to ν_1 and the negative to ν_2.

The plot of (Δ_1/Δ_2) against d_{12} for all possible solutions, for both ν_1 and ν_2, is symmetrical about $d_{12}=-(A_{12}/2D)(\lambda_1+\lambda_2)$. At $d_{12}=-(A_{12}/D)\lambda_{1,2}$ the curve has roots at 0 and at $\pm\infty$ (asymptotic), and $[\partial(\Delta_1/\Delta_2)/\partial d_{12}]$ is infinite at the four points corresponding to maximum and minimum values of d_{12}; i.e., the curve is in two continuous halves. (See Fig. 4.) If ν_i^+ is the normal mode determined by the greater of the two roots for d_{11} corresponding to a given value of d_{12}, and ν_i^- that determined by the smaller, then if $\nu_1>\nu_2$ those portions of the curve representing ν_1^+ lie at the two extremities of one half, the central region corresponding to ν_1^-; reflection of the segments for ν_1^+ and ν_1^- at the plane of symmetry through $d_{12}=-(A_{12}/2D)(\lambda_1+\lambda_2)$ gives the segments for ν_2^- and ν_2^+, the curves intersecting at the above value of d_{12}. $[\partial(\Delta_1/\Delta_2)/\partial d_{12}]$ changes sign in passing from $\nu_{1,2}^+$ to $\nu_{1,2}^-$.

If the energy fractions V_{ij} are plotted against d_{12}, for all possible solutions, it is found that the contributions from the two square terms form one

[3] See for example O. Burkard, Proc. Ind. Acad. **8**, 365 (1938); J. Wagner, Zeits. f. physik. Chemie **B45**, 69 (1939).

closed curve for each normal mode, $V_{11}(\nu_{1,2}{}^{+})$ coinciding with $V_{22}(\nu_{1,2}{}^{-})$, and $V_{22}(\nu_{1,2}{}^{+})$ with $V_{11}(\nu_{1,2}{}^{-})$. (See Fig. 6.) $(\partial V_{ii}/\partial d_{12})$ is infinite at the two extreme values of d_{12}, where $V_{11}(\nu_i{}^{\pm})=V_{22}(\nu_i{}^{\pm})$; at the minimum of d_{12}, $V_{ii}(\nu_1)\gtrless V_{ii}(\nu_2)$, according as $d_{12}(\text{min.})\gtrless 0$; if $d_{12}(\text{min.})=0$, then $V_{ii}(\nu_1)=V_{ii}(\nu_2)=\frac{1}{2}$. V and $(\partial V/\partial d_{12})$ become zero for $V_{ii}(\nu_j{}^{+})$ at $d_{12}=-(A_{12}/D)\lambda_j$. The curves for $V_{12}(\nu_i{}^{\pm})$ are both parabolas, with axes parallel to the V axis, vertices at $d_{12}=-(A_{12}/2D)\lambda_i$, $V_{12}=(-1)^i(A_{12}{}^2/2D)\times[\lambda_i/(\lambda_1-\lambda_2)]$, $(i=1$, minimum; $i=2$, maximum), and latus rectum $(-1)^{i+1}(\lambda_i/2D)(\lambda_1-\lambda_2)$. Both curves, produced if necessary, pass through the origin, and $V_{12}(\nu_i)=0$ at $d_{12}=-(A_{12}/D)\lambda_i$. The points of intersection of the various curves are of interest; at $d_{12}=0$ and $-(2A_{12}/D)[\lambda_1\lambda_2/(\lambda_1+\lambda_2)]$, $V_{11}(\nu_1{}^{\pm})=V_{22}(\nu_2{}^{\pm})$, $V_{11}(\nu_2{}^{\pm})=V_{22}(\nu_1{}^{\pm})$, and $V_{12}(\nu_1{}^{\pm})=V_{12}(\nu_2{}^{\pm})$, while at $d_{12}=[-(2A_{12}/D)\lambda_1\lambda_2\pm(\lambda_1\lambda_2/D)^{\frac{1}{2}}(\lambda_1-\lambda_2)]/(\lambda_1+\lambda_2)$, (corresponding to $d_{11}=(2A_{22}/D)[\lambda_1\lambda_2/(\lambda_1+\lambda_2)]$, $d_{22}=(2A_{11}/D)\times[\lambda_1\lambda_2/(\lambda_1+\lambda_2)]$), $V_{ii}(\nu_1)=V_{ii}(\nu_2)$. The exact nature of these intersections depends on the sign of $d_{12}(\text{min.})$; at the upper value of d_{12} in the expression above, $V_{11}(\nu_1{}^{+})=V_{11}(\nu_2{}^{+})$, and, at the lower value, $V_{11}(\nu_1{}^{+})=V_{11}(\nu_2{}^{+})$, if $d_{12}(\text{min.})<0$, and $V_{22}(\nu_1{}^{+})=V_{22}(\nu_2{}^{+})$ if $d_{12}(\text{min.})>0$. Finally, $V_{ij}(\nu_i)=V_{jj}(\nu_i)=0$ at $d_{12}=-(A_{12}/D)\lambda_i$.

It follows from the above discussion that the two alternative sets of constants allowed at each possible value of d_{12} correspond to alternative assignments of the fundamental vibration frequencies to the two normal modes; at the extreme values of d_{12} the two solutions coincide. General solutions for singular and related points are given in Table I. The Roman numerals in the first column refer to solutions discussed in the text; where alternatives exist, the numeral refers to $\nu_{1,2}{}^{+}$. The additional symbols used in Table I are defined as follows:

$$\lambda_1'=\lambda_1/A_{11}\quad \lambda_1''=\lambda_1/A_{22}\quad \mu_1=\lambda_2/\lambda_1\quad \epsilon_1=(1+\mu_1)$$
$$\lambda_2'=\lambda_2/A_{11}\quad \lambda_2''=\lambda_2/A_{22}\quad \mu_2=\lambda_1/\lambda_2\quad \epsilon_2=(1+\mu_2)$$

$$L_1=(\lambda_1+\lambda_2)\qquad L_1'=\tfrac{1}{2}(\lambda_1'+\lambda_2')\qquad L_1''=\tfrac{1}{2}(\lambda_1''+\lambda_2'')$$
$$L_2=(\lambda_1-\lambda_2)/L_1\quad L_2'=\tfrac{1}{2}(\lambda_1'-\lambda_2')\quad L_2''=\tfrac{1}{2}(\lambda_1''-\lambda_2'')$$
$$L_3=\lambda_1\lambda_2/L_1$$

$$\left.\begin{array}{lll} A_{12}'=A_{12}/D & A_{12}''=\tfrac{1}{2}L_1A_{12}' & A'=(A_{11}A_{22}/D)^{\frac{1}{2}} \\ A_{11}'=A_{11}/D & A_{11}''=\tfrac{1}{2}L_1A_{11}' & A=(A'')^2 \\ A_{22}'=A_{22}/D & A_{22}''=\tfrac{1}{2}L_1A_{22}' & D'=(\lambda_1-\lambda_2)/2D^{\frac{1}{2}} \\ & & D''=A''D' \end{array}\right\}\text{, where } A''=A_{12}/D^{\frac{1}{2}}.$$

$$a_1=(A_{22}/A_{11})^{\frac{1}{2}}\quad E=[(A')^2-(A''/L_2)^2]^{\frac{1}{2}}\quad E'=EL_2'\quad E''=EL_2''$$
$$a_2=A_{12}/A_{11}\qquad F=[(A')^2-(A''L_2)^2]^{\frac{1}{2}}\quad F'=FL_1'\quad F''=FL_1''$$
$$a'=a_2/a_1{}^2$$

$$B_1=(A'+1)^2\quad C_1=(A''+1)^2\quad P_1=[1+(1/A')]^{-1}\quad Q_1=[1+(1/A'')]$$
$$B_2=(A'-1)^2\quad C_2=(A''-1)^2\quad P_2=[1-(1/A')]^{-1}\quad Q_2=[1-(1/A'')]$$
$$C=(C_1C_2)^{\frac{1}{2}}$$
$$K_1=[(A'-A'')/(A'+A'')]$$
$$K_2=(1/K_1)$$

Where there are alternative values for the force constants, but only one for any of the quantities in the last four columns, the latter is associated with the upper of the alternative signs in the expressions for the constants; the alternative values are obtained by interchanging the subscripts 1 and 2 in the quantities B, C, K, P, and Q.

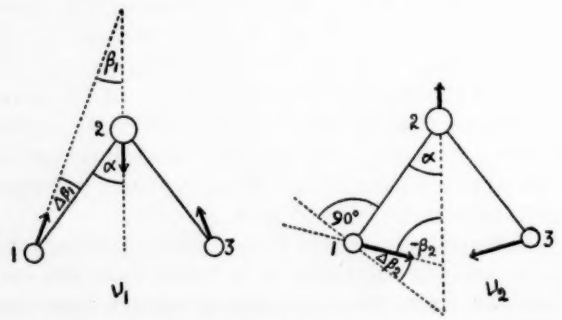

FIG. 2. Directions of displacement vectors in the class A_1 vibrations of the symmetrical triatomic molecule.

IV. PARTICULAR SOLUTIONS

It is required to find one or more particular sets of constants, giving satisfactory normal coordinates and potential energy distributions, which can be used whenever there is no evidence as to the nature of the magnitude of the interaction constant d_{12}. If we define ν_i as the mode whose normal coordinate is in practice determined by Δ_i (cf., the terms "C–H stretching," "CCl_2 bending," etc., used in the de-

TABLE II. Directions of displacement vectors in certain singular solutions for the symmetrical triatomic molecule.

	Minimum d_{22} (VII)	Minimum d_{11}	Maximum d_{11} (VIII)	Maximum d_{22}
$\tan\beta_1$	$\tan\alpha$	$-\cot\alpha$	$M\tan\alpha$	$-M\cot\alpha$
$\tan\beta_2$	$-M\cot\alpha$	$M\tan\alpha$	$-\cot\alpha$	$\tan\alpha$

$(M=[1+2(m_1/m_2)])$

scription of normal modes), and if the subscripts are ordered so that $\nu_1>\nu_2$, then those solutions corresponding to ν_i^-, as defined in Section III, can be immediately discarded, i.e., only half the total range of solutions need be considered. As a starting point we take the case $d_{12}=0$ (solution I in Table I), which corresponds to an idealized force field containing only square terms. This is not a general solution, as real values of the other constants cannot be obtained unless the condition (12) holds. But it may be possible to find some characteristic property of the normal modes associated with this solution which can be applied to determine a more general one, applicable to every case yet comparable with the ideal. Such a property has been found in the relation between the energy contributions from the two square terms in Eq. (1); they are mutually reciprocal in the two modes. If we impose this property as a necessary condition, we find that there is a solution II, corresponding to $d_{12}=-(2A_{12}/D)[\lambda_1\lambda_2/(\lambda_1+\lambda_2)]$ (see Section III). It is to be noted that here the fraction of the potential energy in the cross term in Eq. (1) is the same in both modes, i.e., the solution II is characterized by the relations $V_{11}(\nu_1)=V_{22}(\nu_2)$, $V_{22}(\nu_1)=V_{11}(\nu_2)$, $V_{12}(\nu_1)=V_{12}(\nu_2)$, holding simultaneously.

Where solution I is found to give complex values for the constants d_{11} and d_{22}, perhaps an obvious first alternative is solution III, with d_{12} a minimum. But this cannot be generally applicable, since here $V_{11}(\nu_i)=V_{22}(\nu_i)$. Where the frequency-difference $(\nu_1-\nu_2)$ is small, so that on general grounds it would be regarded as difficult to assign either frequency to a definite mode of vibration, the above energy relationship is clearly the ideal one with which to define the force constants. Where $(\nu_1-\nu_2)$ is small but there is sufficient evidence for a definite assignment to be made, one of the three solutions IV to VI, corresponding to mean values of the constants, may be used; in these solutions the ratios $(V_{ii}/V_{jj})(\nu_i)$ will be somewhat greater than unity, in agreement with the favored assignment.* In the general case, none of these solutions is as satisfactory as II. Solutions VII and VIII, in which d_{22} and d_{11} take minimum and maximum values, respectively, are of some interest, since they correspond to the secular determinant in Eq. (3) splitting into two linear factors. (See Section II.) In VII, the (unnormalized) normal coordinate η_1' is identical with Δ_1, and $V_{12}(\nu_1)=-2V_{22}(\nu_1)$, while in VIII η_2' is identical with Δ_2, and $V_{12}(\nu_2)=-2V_{11}(\nu_2)$. VIII cannot be generally applicable, since it leads to an unsatisfactory distribution of the potential energy in ν_2 when (λ_1/λ_2) is large; the fraction $V_{12}(\nu_2)$ would be expected to decrease with (λ_2/λ_1), as $V_{12}(\nu_1)$ does in VII, while here the reverse is true. (See Table I.) As an actual example, the results for the symmetrical vibrations of the chlorine monoxide molecule are given below,

$$d_{12}=1.809,\quad d_{11}=3.519,\quad d_{22}=1.213,\quad \times 10^5 \text{ dynes/cm},$$

$$V_{11}(\nu_2)=3.293,\quad V_{22}(\nu_2)=4.293,\quad V_{12}(\nu_2)=-6.585.$$

The fractional contributions to the potential energy are most unlikely, and the interaction constant d_{12} seems improbably large (cf., Tables VII and VIII). It will be shown that solution VII gives quite satisfactory results. The general relationship between the three solutions I, II, and VII is indicated below; the superscripts, here and subsequently, refer to

TABLE III. Solutions for the symmetrical triatomic molecule in which the displacement vectors of the terminal atoms have only x or y components.

	d_{12}	d_{11}	d_{22}	i	β_i	ρ_i	$V_{11}(\nu_i)$	$V_{22}(\nu_i)$	$V_{12}(\nu_i)$
$\beta_1^-=0$	$(\sigma_2''-\sigma_1')cs$	$c^2\sigma_1'+s^2\sigma_2''$	$c^2\sigma_2''+s^2\sigma_1'$	1	0	$-(1/t)$	$(c^2+s^2\sigma_1)c^2$	$(s^2+c^2\sigma_1)s^2$	$2(1-\sigma_1)c^2s^2$
				2	$(\pi/2)$	$(1/t)$	$[s^2+(c^2/\sigma_1)]s^2$	$[c^2+(s^2/\sigma_1)]c^2$	$2[1-(1/\sigma_1)]c^2s^2$
$\beta_2^+=0$	$(\sigma_1''-\sigma_2')cs$	$c^2\sigma_2'+s^2\sigma_1''$	$c^2\sigma_1''+s^2\sigma_2'$	1	$(\pi/2)$	t	$(s^2+c^2\sigma_2)s^2$	$(c^2+s^2\sigma_2)c^2$	$2(1-\sigma_2)c^2s^2$
				2	0	$-t$	$[c^2+(s^2/\sigma_2)]c^2$	$[s^2+(c^2/\sigma_2)]s^2$	$2[1-(1/\sigma_2)]c^2s^2$

$(\sigma_{1,2}'=\lambda_{1,2}/[2\{2+(m_2/m_1)\}],\quad \sigma_{1,2}''=\lambda_{1,2}/2(m_2/m_1),\quad \sigma_1=(\sigma_2''/\sigma_1'),\quad \sigma_2=(\sigma_2'/\sigma_1''),\quad c=\cos\alpha,\quad s=\sin\alpha,\quad t=\tan\alpha.)$

*The situation in mind would resemble that in the vinyl halides (H. W. Thompson and P. Torkington, Proc. Roy. Soc. A 184, 1, 21 (1945); Trans. Faraday Soc. 41, 236 (1945); J. Chem. Soc., 303 (1944)) where there is a pair of Class A'' fundamentals with frequencies ~900 and 940 cm^{-1}; evidence from related molecules suggests that they are essentially CH_2 and CH bending modes, respectively. But here there is a third Class A'' (twisting) mode. There seems to be no example of a similar situation arising where the secular equation is only of the second degree; an ideal case would be the pair of parallel vibrations of the linear molecule BAB^i, where B and B^i are isotopes, but there are no certain data available.

TABLE IV. Fundamental vibration frequencies and angles of symmetrical triatomic molecules.

	H_2O	D_2O	ClO_2	SO_2	O_3	NO_2	F_2O	Cl_2O	
ν_1	[a]3652	[b]2666	[c]954	[e]1151.2	[g]1043.4	[i]1320	[k]830	[l]680	
ν_2	1595	1179	529	519	710	648	490	330	
ν_3	3756	2789	1105	1358	1740	1621	1110	973	cm^{-1}
α	*52° 30′	*52° 30′	[d]68° 30′	[f]60° 30′	[h]63° 30′	[j]65° 0′	[d]52° 0′	[d]55° 30′	

* G. Herzberg, *Infrared and Raman Spectra of Polyatomic Molecules* (D. van Nostrand Company, Inc., New York 1945), gives $2\alpha = 105° 3'$, for the lowest vibrational level.

[a] Earle K. Plyler, Phys. Rev. **39**, 77 (1932); Rank, Larsen, and Bordner, J. Chem. Phys. **2**, 464 (1934); Harold H. Nielsen, Phys. Rev. **62**, 422 (1942).

[b] E. F. Barker and W. W. Sleator, J. Chem. Phys. **3**, 660 (1935); B. T. Darling and D. M. Dennison, Phys. Rev. **57**, 128 (1940).

[c] C. R. Bailey and A. B. D. Cassie, Proc. Roy. Soc. **A137**, 622 (1932); **140**, 605 (1933); **142**, 129 (1933); Z. W. Ku, Phys. Rev. **44**, 376 (1933); T. Y. Wu, *Vibrational Spectra and Structure of Polyatomic Molecules* (Edwards Brothers, Inc., Ann Arbor, 1946).

[d] L. O. Brockway, Rev. Mod. Phys. **8**, 231 (1936).

[e] Earnest F. Barker, Rev. Mod. Phys. **14**, 198 (1942); H. Gerding and W. J. Nijveld, Nature, **137**, 1070 (1936); Bailey, Cassie, and Angus, Proc. Roy. Soc. **130**, 142 (1930).

[f] V. Schomaker and D. P. Stevenson, J. Am. Chem. Soc. **62**, 1267 (1940).

[g] Hettner, Pohlman, and Schumacher, Zeits. f. Physik **91**, 372 (1934); S. L. Gerhard, Phys. Rev. **42**, 622 (1932).

[h] W. Shand and R. A. Spurr, J. Am. Chem. Soc. **65**, 179 (1943).

[i] C. R. Bailey and A. B. D. Cassie, Nature **131**, 239, 910 (1933); Roland Schaffert, J. Chem. Phys. **1**, 507 (1933); G. B. B. M. Sutherland and W. G. Penney, Proc. Roy. Soc. **A156**, 678(1936).

[j] L. R. Maxwell and U. M. Mosley, J. Chem. Phys. **8**, 738 (1940).

[k] Hettner, Pohlman, and Schumacher, Zeits. f. Physik **96**, 203 (1935). G. B. B. M. Sutherland and W. G. Penney, Proc. Roy. Soc. **A156**, 678 (1936).

[l] C. R. Bailey and A. B. D. Cassie, Proc. Roy. Soc. **142**, 129 (1933); G. B. B. M. Sutherland and W. G. Penney, Proc. Roy. Soc. **A156**, 678 (1936); R. Pohlman and H. J. Schumacher, Zeits. f. Physik **102**, 678 (1936).

particular solutions.

$|d_{12}^{II}| > |d_{12}^{VII}| > |d_{12}^{I}| (=0)$;
(sign opposite to that of A_{12}).

$d_{11}^{II} > d_{11}^{VII} > d_{11}^{I}$; $d_{22}^{I} > d_{22}^{II} > d_{22}^{VII}$.

$|\rho_1^{II}| > |\rho_1^{VII}| > |\rho_1^{I}|$;
(sign the same as that of A_{12}).

$|\rho_2^{VII}| > |\rho_2^{II}| > |\rho_2^{I}|$; $(\rho_2^{VII} = \infty$,
ρ_2^{II} same sign as A_{12}, ρ_2^{I} of opposite sign).

For ν_i,

$$V_{ii}^{II} > V_{ii}^{VII} > V_{ii}^{I}; \quad V_{ij} \lesssim 0.$$

It is noteworthy that in all the solutions for which explicit expressions are given for $\rho_{1,2}$ in Table I, these are independent of λ_1 and λ_2, i.e., the vibrational forms are determined solely by the geometry of the system under consideration, and the atomic masses. This is not so for solutions I and II; in these cases the parameters ρ_1 and ρ_2 take the following values

$$\rho_{1,2}^{I} = \{\tfrac{1}{2}(\epsilon_{1,2}'/a_2)[1 \pm \{(A/L_2)+E\}/(A')^2]\}^{\pm 1}, \quad (17)$$

$$\rho_{1,2}^{II} = \{\tfrac{1}{2}(\epsilon_{1,2}/a_2)[1 \pm (AL_2+F)/(A')^2]\}^{\pm 1}, \quad (18)$$

where the notation of Table I is used, with the addition $\epsilon_{1,2}' = (1-\mu_{1,2})$, and in each case the positive signs refer to ν_1 and the negative to ν_2. It seems unlikely that the form of vibration would be quite independent of the vibration frequencies, so solution II must be regarded as more satisfactory than VII in this respect. It should also be observed that in VII the constants d_{12} and d_{22} are independent of ν_1, while in I and II both frequencies enter into the expressions for all three constants. VII can therefore be regarded as an approximation to II, which only holds rigidly when the frequency-difference $(\nu_1 - \nu_2)$ is large; since it corresponds to factorization of the secular equation, it enables a complete solution to be obtained very rapidly. Solutions with maximum d_{22} and minimum d_{11}, which also lead to factorization, correspond to a reversed assignment of the vibration frequencies.

Recapitulating, we have shown that there is a solution, II, of the second-degree secular equation in which the fractional contributions to the potential energy from the two square terms are mutually reciprocal in the two modes of vibration, as in the solution for the case of no cross term, I; and a solution, VII, in which the (unnormalized) normal coordinate for the higher frequency is identical with the corresponding valence-type coordinate in the potential energy expression. Both are in principle universally applicable. For the special case of small frequency-difference $(\nu_1 - \nu_2)$, it is suggested that the solution III, corresponding to minimum d_{12} and to equal potential energy fractions V_{11} and V_{22}, would be most satisfactory where the two observed fundamental frequencies cannot be definitely assigned, and solutions IV, V, or VI, corresponding to mean values of the constants, where there is evidence for an assignment one way or the other.

V. THE SYMMETRICAL TRIATOMIC MOLECULE

We shall apply the above general results to the class A_1 (symmetrical) vibrations of the non-linear triatomic system AB_2. The coordinates and various coefficients defined in Eqs. (2) and (4) take the following values. (See Fig. 1.)

$$\left.\begin{aligned} z_1 &= x_3 - x_1 \\ z_2 &= 2y_2 - y_1 - y_3 \end{aligned}\right\} \quad (19)$$

$$\left.\begin{aligned} m_{z1} &= (m_1/2) \\ m_{z2} &= [m_1 m_2/2(m_2+2m_1)] \end{aligned}\right\}. \quad (20)$$

$$\left.\begin{aligned} a_{11} &= -a_{22} = \sin\alpha \\ a_{12} &= a_{21} = \cos\alpha \end{aligned}\right\}. \tag{21}$$

$$\left.\begin{aligned} A_{11} &= 2[(m_2/m_1) + 2\cos^2\alpha] \\ A_{22} &= 2[(m_2/m_1) + 2\sin^2\alpha] \\ A_{12} &= -2\sin 2\alpha \\ M &= m_2 \end{aligned}\right\}. \tag{22}$$

$\Delta_1 = (\Delta r_{12} + \Delta r_{23})$ is the coordinate for stretching of the $A-B$ bonds, and $\Delta_2 = r\Delta\theta$ the coordinate for deformation of the angle $\widehat{BAB}$. A convenient parameter for the description of the geometrical form of the normal modes in a triatomic molecule is the ratio of the Cartesian displacements of the terminal atoms. This quantity can be expressed as follows:

$$\left.\begin{aligned} (x_1/y_1)^{\nu_{1,2}} = [1 + 2(m_1/m_2)](z_1/z_2)^{\nu_{1,2}} &= \frac{\{2[2 + (m_2/m_1)](d_{22}\sin\alpha - d_{12}\cos\alpha) - \lambda_{1,2}\sin\alpha\}}{\{2(m_2/m_1)(d_{12}\sin\alpha + d_{22}\cos\alpha) - \lambda_{1,2}\cos\alpha\}} \\ &= \frac{\{2[2 + (m_2/m_1)](d_{12}\sin\alpha - d_{11}\cos\alpha) + \lambda_{1,2}\cos\alpha\}}{\{2(m_2/m_1)(d_{11}\sin\alpha + d_{12}\cos\alpha) - \lambda_{1,2}\sin\alpha\}} \end{aligned}\right\}, \tag{23}$$

where the constants are any set satisfying Eqs. (6) and (8). We shall define angles

$$\beta_{1,2} = \tan^{-1}(x_1/y_1)^{\nu_{1,2}}, \tag{24}$$

and two derived angles,

$$\left.\begin{aligned} \Delta\beta_1 &= (\alpha - \beta_1) \\ \Delta\beta_2 &= [\alpha - \{(\pi/2) + \beta_2\}] \end{aligned}\right\}. \tag{25}$$

$\Delta\beta_1$ is the angle made by the displacement vector of atom 1 with the valence bond $A-B$, and $\Delta\beta_2$ that between the displacement vector of atom 1 and the normal to the valence bond, the signs of the two angles being such that the vectors in the two modes are mutually perpendicular when $\Delta\beta_1 = \Delta\beta_2$. Clearly, $\Delta\beta_{1,2} = 0$ correspond to idealized stretching and bending modes respectively (see Fig. 2). $\rho_{1,2}$ and

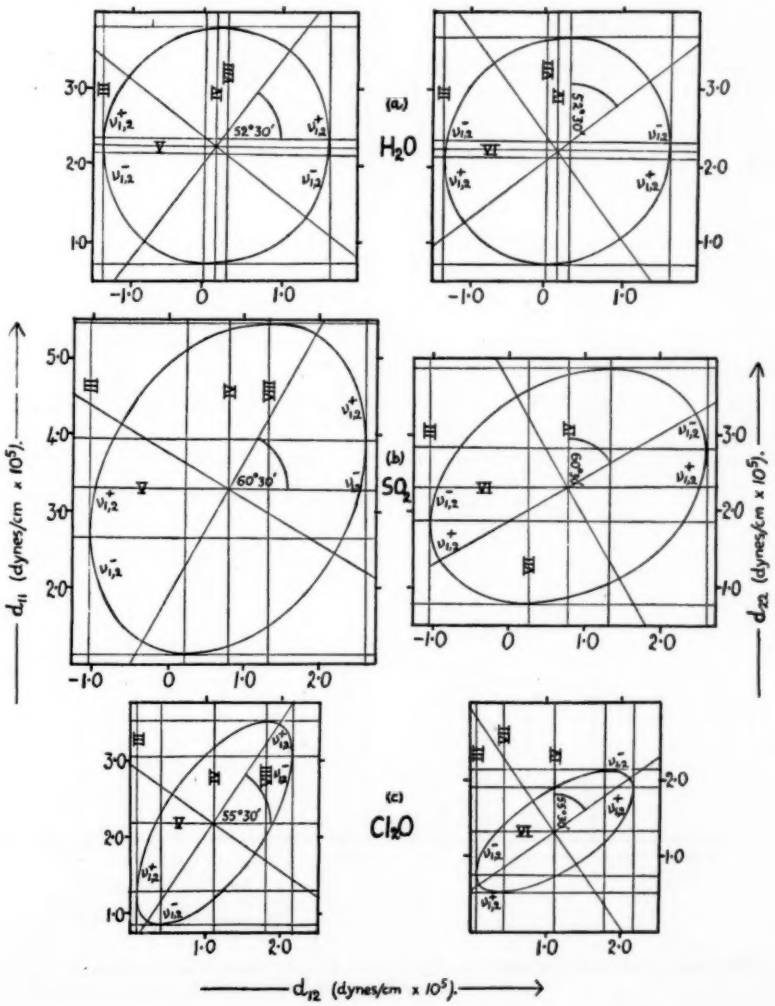

FIG. 3. Allowed solutions for the force constants for the class A_1 vibrations of typical symmetrical triatomic molecules.

$\tan\beta_{1,2}$ are mutually related as follows:

$$\rho_{1,2}=\left\{\frac{\tan\alpha\,\tan\beta_{1,2}+[1+2(m_1/m_2)]}{\tan\beta_{1,2}-[1+2(m_1/m_2)]\,\tan\alpha}\right\}^{\pm 1}, \quad (26)$$

$$\tan\beta_{1,2}=[1+2(m_1/m_2)]\frac{\{(\rho_{1,2})^{\pm 1}\tan\alpha+1\}}{\{(\rho_{1,2})^{\pm 1}-\tan\alpha\}}, \quad (27)$$

where in each case the positive sign refers to ν_1, the negative to ν_2. It is found that in the four solutions corresponding to maximum and minimum values of the constants d_{11} and d_{22}, the angles $\beta_{1,2}$ are simply related to the angle α, as shown in Table II. It will be observed that the simple normal coordinates for ν_1 and ν_2 in solutions VII and VIII, respectively, are associated with idealized displacement vectors. ($\Delta\beta_1^{\rm VII}=0$, $\Delta\beta_2^{\rm VIII}=0$.) In solution VII, $\tan\Delta\beta_2=\{\tan\alpha/[1+(m_2/2m_1)\sec^2\alpha]\}$; in the limits $(m_1/m_2)=0$ and ∞ $\Delta\beta_2$ takes values 0 and α, respectively. It can be shown that $\Delta\beta_1^{\rm I}>0>\Delta\beta_1^{\rm II}$, and that $\Delta\beta_2^{\rm I}>\Delta\beta_2^{\rm VII}>\Delta\beta_2^{\rm II}>0$. It follows from Eqs. (26) and (27) that the plot of $\beta_{1,2}$ against d_{12}, for all possible solutions, is symmetrical about $d_{12}=-(A_{12}/2D)(\lambda_1+\lambda_2)$; reflection of the segments for ν_1^+ and ν_1^- (which lie on one continuous curve), give those for ν_2^- and ν_2^+, respectively. For $\nu_{1,2}^+$, $(\partial\beta/\partial d_{12})>0$, and for $\nu_{1,2}^-(\partial\beta/\partial d_{12})<0$, while at the extreme values of d_{12}, $(\partial\beta/\partial d_{12})=\infty$. Where the curves cross the d_{12} axis, the displacement vectors of the terminal atoms in ν_1 and ν_2 are mutually perpendicular; the data for these solutions are summarized in Table III.

It is found that the angle θ giving the gradient of the major axis of the ellipse (6) is $[(\pi/2)-\alpha]$, and that the semi-axes (7) are as follows:

$$\left.\begin{aligned} a^2&=(A_{22}/8D)(m_1/m_2)(\lambda_1-\lambda_2)^2\\ b^2&=(A_{22}/8D)[m_1/(2m_1+m_2)](\lambda_1-\lambda_2)^2\end{aligned}\right\}. \quad (28)$$

Hence, the ratio of the semi-axes for both ellipses (6) and (8) is $(a/b)=[(m_2+2m_1)/m_2]^{\frac{1}{2}}$, and the eccentricity is $e=[(m_2+2m_1)/2m_1]^{-\frac{1}{2}}$. At the limits $(m_1/m_2)=0$ and ∞, each ellipse degenerates into a circle and a straight line, respectively.

To obtain numerical results, a series of eight symmetrical triatomic molecules representing a convenient range of (m_1/m_2) has been taken. The

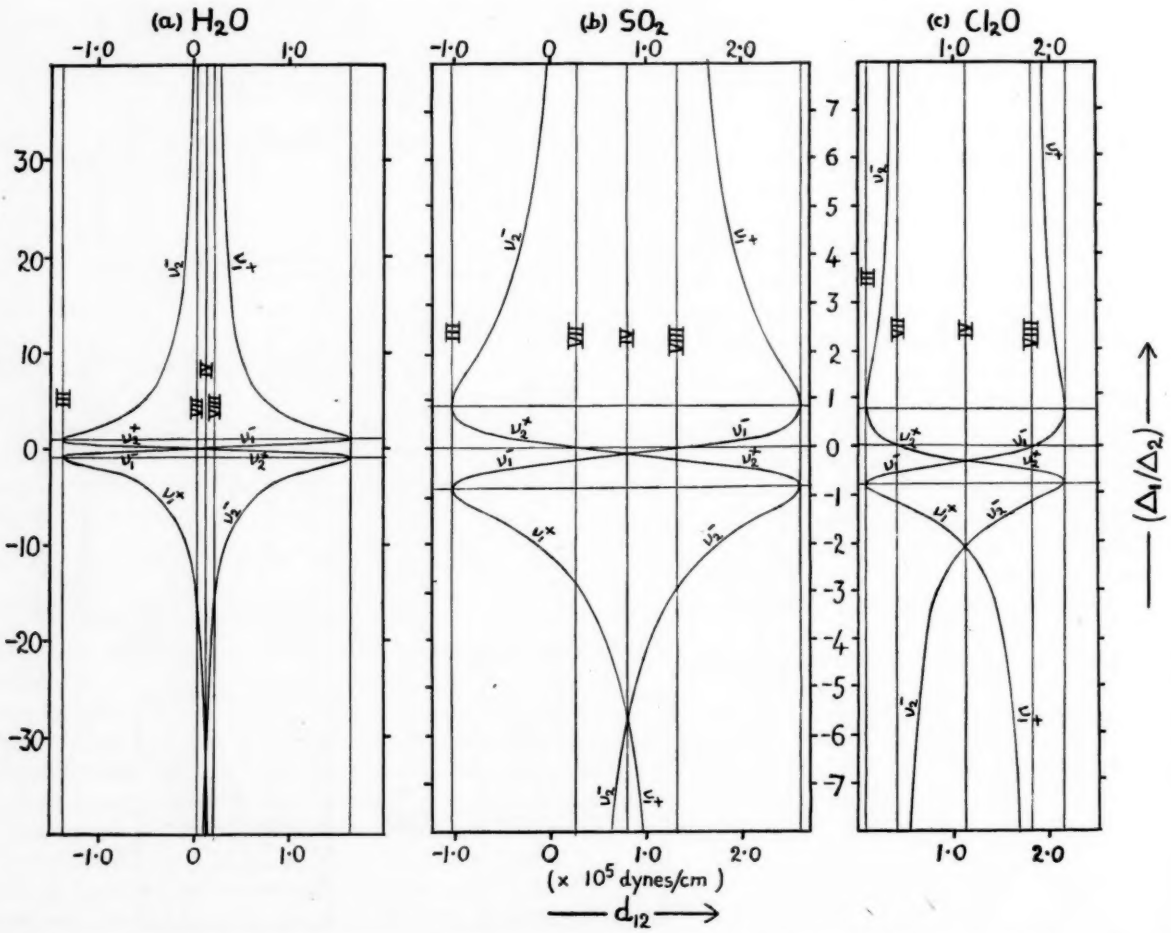

FIG. 4. The composition of the normal coordinates for the class A_1 vibrations of typical symmetrical triatomic molecules, for all allowed solutions of the force constants.

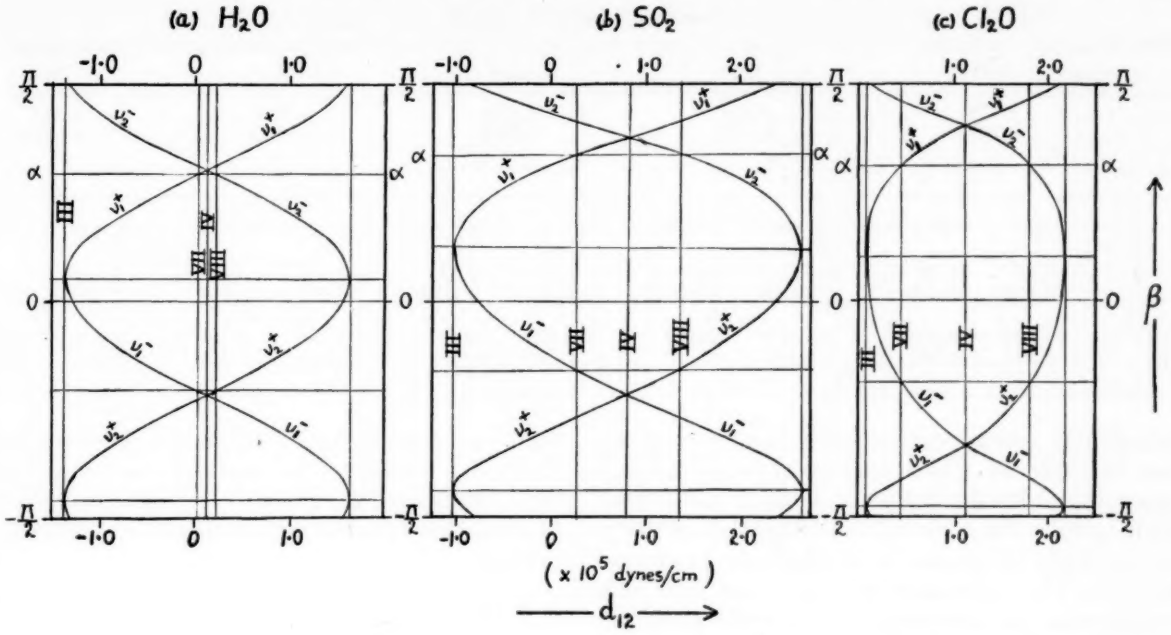

FIG. 5. The direction of the displacement vectors of the terminal atoms in the class A_1 vibrations of typical symmetrical triatomic molecules, for all allowed solutions of the force constants.

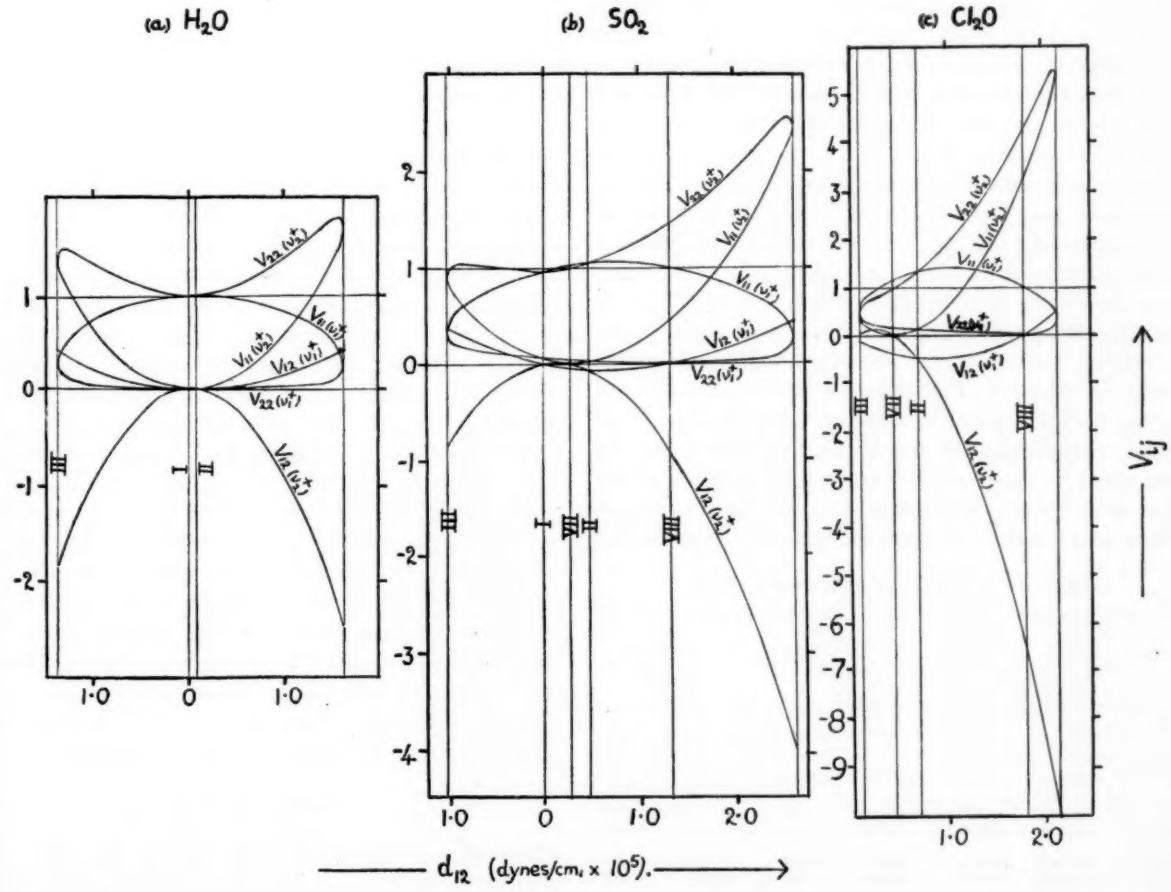

FIG. 6. The distribution of the potential energy in the class A_1 vibrations of typical symmetrical triatomic molecules, for all allowed solutions of the force constants.

TABLE V. Solution I. ($d_{12}=0.$)

	H_2O		D_2O		ClO_2		SC_2		NO_2	
d_{11}	3.779		3.845		3.729		4.903		5.345	
d_{22}	0.7025		0.7223		0.7916		0.8078		0.9249	
i	1	2	1	2	1	2	1	2	1	2
$\Delta\beta_i$	0° 46′	4° 7′	1° 29′	7° 53′	4° 55′	22° 4′	4° 6′	23° 33′	8° 18′	40° 8′
ρ_i	−13.92	74.86	−7.226	38.47	−2.466	11.62	−2.294	13.92	−1.186	6.855
N_i	0.1724	0.04911	0.2808	0.08092	0.4920	0.1688	0.5076	0.1383	0.9649	0.2812
$V_{11}(\nu_i)$	99.904	0.096	99.642	0.358	96.628	3.372	96.965	3.035	89.049	10.951
$V_{22}(\nu_i)$	0.096	99.904	0.358	99.642	3.372	96.628	3.035	96.965	10.951	89.049

fundamental vibration frequencies and angles are given in Table IV. No attempt has been made to correct for anharmonicity; it seemed more consistent to take the observed fundamentals in every case, since the correction to be applied is in general unknown. The constants for H_2O and D_2O will therefore not be comparable with those given by Dennison,[4] who includes cubic and quartic terms. In the case of the chlorine oxides, the calculations were carried out for $Cl^{35}O_2$ and $Cl_2{}^{35}O$, using the observed frequencies. This seemed the best procedure, since we are interested here in the normal coordinates for a given model, and the frequencies cannot be accurately corrected without knowing the force field; the error in any case is small, and does not detract from the use of these molecules as illustrations of the general theory.

The ellipses (6) and (8) are given in Fig. 3 for the three molecules H_2O, SO_2, and Cl_2O; the increase of the eccentricity as (m_1/m_2) increases is an obvious feature. Plots of (Δ_1/Δ_2), β and V_{ij} for the same three molecules are shown in Figs. 4, 5, and 6. It is seen that the general form of each curve is the same in all three cases, as would be expected from the analysis in Section III. The changes encountered in the (Δ_1/Δ_2) and V_{ij} plots in passing from H_2O to Cl_2O can be correlated with the general tendency for the cross term in the potential energy expression to become of increasing importance as (m_1/m_2) increases from a small value. It may be observed that in the limit $(m_1/m_2)=0$ the V_{ij} curves are all symmetrical about $d_{12}=0$. Points for some of the general solutions discussed previously are indicated on the figures. These particular solutions are dealt with as follows:

I. (for the five molecules which satisfy Eq. (12),) in Table V;
III. (for the three molecules which do not satisfy Eq. (12),) in Table VI;
II. (all cases), in Table VII;
VII. (all cases), in Table VIII.

In the tables, force constants are given in units of 10^{-5} dyne/cm, to four significant figures, the angles $\Delta\beta_i$ to the nearest minute, and the relative energy components V_{ij} as percentages of the total potential energy, to three decimal places. The quantity N_i is a normalizing factor for the amplitudes in the first vibrational level: $N_i\rho_i=\Delta_i{}^{\nu_i}$ (i.e., $N_i=\Delta_j{}^{\nu_i}$), in tenths of an Angstrom; except for the case $\rho_2{}^{\text{VII}}$, $(=\infty)$, when the actual magnitude of $\Delta_2{}^{\nu_2}$ is given, in the same units. For completeness, the constant d_{33} for the class B_1 (asymmetrical stretching), mode, and the corresponding normal coordinate, normalized as above, is given in Table IX; and the solution, IX, of the symmetrical vibrations, in which $d_{11}=d_{33}$, in Table X, for all cases which allow of a real solution. In solution IX, the interaction constant d_{13} associated with the interaction term $\Delta r_{12}\Delta r_{23}$ in the general valence force potential energy function for the triatomic molecule takes the value nought; IX can therefore be regarded as an analog of I (for which $d_{12}=0$), for the special case of the triatomic molecule. The symmetry coordinate for the class B_1 vibration, corresponding to Δ_1, is $\Delta_3=\Delta r_{12}-\Delta r_{23}$ (see Eqs. (2) and (21)), and the force constant d_{33} is given by the linear equation

$$A_{33}d_{33}-\lambda_3=0, \tag{29}$$

where A_{33} is identical with A_{22} in Eq. (22). The normal coordinate is identical with Δ_3 except for a normalizing factor. It may be observed that solution VII for ν_1 is the geometrical analog of ν_3.

TABLE VI. Solution III. (d_{12} a minimum.)

	O_3		F_2O		Cl_2O	
d_{12}	0.1223		0.08065		0.07123	
d_{11}	2.754		1.417		1.285	
d_{22}	1.480		1.088		0.7778	
i	1	2	1	2	1	2
$\Delta\beta_i$	36° 15′	53° 45′	41° 14′	48° 46′	37° 53′	52° 7′
ρ_i	−0.7331	1.364	−0.8762	1.141	−0.7780	1.285
N_i	1.496	0.8507	1.559	0.9836	1.674	0.8450
$V_{11,22}(\nu_i)$	53.253	47.121	53.474	46.950	53.836	46.675
$V_{12}(\nu_i)$	−6.507	5.758	−6.949	6.101	−7.671	6.651

[4] David M. Dennison, Rev. Mod. Phys. **12**, 175 (1940).

TABLE VII. Solution II. ($V_{11}(\nu_1) = V_{22}(\nu_2)$, $V_{11}(\nu_2) = V_{22}(\nu_1)$, $V_{12}(\nu_1) = V_{12}(\nu_2)$.)

	H_2O		D_2O		ClO_2		SO_2	
d_{12}	0.06856		0.1340		0.3285		0.4521	
d_{11}	3.788		3.876		3.934		5.232	
d_{22}	0.7022		0.7211		0.7779		0.7961	
$\backslash i$	1	2	1	2	1	2	1	2
$\Delta\beta_i$	−0° 31′	2° 48′	−1° 0′	5° 19′	−2° 25′	12° 2′	−2° 30′	16° 3′
ρ_i	−20.48	−110.4	−10.74	−57.75	−4.694	−23.73	−3.478	−22.85
N_i	0.1171	0.03333	0.1889	0.05417	0.2596	0.08595	0.3355	0.08787
$V_{11}(\nu_i)$	100.133	0.044	100.485	0.162	102.734	0.922	103.855	1.307
$V_{22}(\nu_i)$	0.044	100.133	0.162	100.485	0.922	102.734	1.307	103.855
$V_{12}(\nu_i)$	−0.177		−0.647		−3.656		−5.162	
	O_3		NO_2		F_2O		Cl_2O	
d_{12}	0.8643		0.8494		0.6803		0.6898	
d_{11}	4.249		6.514		2.534		2.732	
d_{22}	1.131		0.8698		0.7881		0.5382	
$\backslash i$	1	2	1	2	1	2	1	2
$\Delta\beta_i$	−6° 3′	21° 42′	−3° 51′	26° 47′	−8° 9′	24° 42′	−7° 53′	35° 7′
ρ_i	−2.512	−9.434	−1.981	−14.83	−2.174	−6.990	−1.422	−7.217
N_i	0.5131	0.2184	0.5840	0.1495	0.7101	0.3043	0.9941	0.3074
$V_{11}(\nu_i)$	113.604	4.793	110.819	3.772	122.128	8.038	134.725	13.130
$V_{22}(\nu_i)$	4.793	113.604	3.772	110.819	8.038	122.128	13.130	134.725
$V_{12}(\nu_i)$	−18.397		−14.591		−30.166		−47.854	

TABLE VIII. Solution VII. ($\rho_2 = \infty$.)

	H_2O		D_2O		ClO_2		SO_2	
d_{12}	0.04082		0.08012		0.2148		0.2720	
d_{11}	3.785		3.865		3.878		5.118	
d_{22}	0.7020		0.7202		0.7731		0.7882	
$\backslash i$	1	2	1	2	1	2	1	2
$\Delta\beta_i$	0	3° 20′	0	6° 21′	0	15° 32′	0	19° 2′
ρ_i	−17.20	∞	−8.989	∞	−3.600	∞	−2.898	∞
N_i	0.1395	(3.679)	0.2258	(3.123)	0.3389	(2.019)	0.4032	(1.981)
$V_{11}(\nu_i)$	100.063	0	100.231	0	101.563	0	101.868	0
$V_{22}(\nu_i)$	0.063	100	0.231	100	1.563	100	1.868	100
$V_{12}(\nu_i)$	−0.125	0	−0.462	0	−3.125	0	−3.737	0
	O_3		NO_2		F_2O		Cl_2O	
d_{12}	0.6322		0.5270		0.4587		0.4261	
d_{11}	4.029		6.158		2.307		2.344	
d_{22}	1.107		0.8481		0.7564		0.5017	
$\backslash i$	1	2	1	2	1	2	1	2
$\Delta\beta_i$	0	29° 44′	0	31° 52′	0	31° 14′	0	40° 21′
ρ_i	−1.751	∞	−1.609	∞	−1.649	∞	−1.177	∞
N_i	0.7435	(1.955)	0.7217	(2.134)	0.9468	(1.964)	1.214	(1.980)
$V_{11}(\nu_i)$	109.844	0	105.618	0	113.714	0	118.262	0
$V_{22}(\nu_i)$	9.844	100	5.618	100	13.714	100	18.262	100
$V_{12}(\nu_i)$	−19.689	0	−11.235	0	−27.429	0	−36.525	0

TABLE IX. d_{33}. (Class B_1 mode.)

	H_2O	D_2O	ClO_2	SO_2	O_3	NO_2	F_2O	Cl_2O
d_{33}	3.880	3.983	3.210	4.942	5.482	4.304	2.786	2.456
Δ_3	2.401	2.040	1.432	1.279	1.375	1.498	1.541	1.536

The data summarized in the tables illustrate most of the points dealt with in the general case. Here the coefficient A_{12} is negative, so the interaction constant d_{12} is positive in solutions I, II, and VII. The tendency of the system to reach a minimum potential energy conventionally requires that ρ_1 and ρ_2 be both negative or both positive according as d_{12} is positive or negative; if d_{12} is zero, then ρ_1 and ρ_2 may be either positive or negative. Solutions I, II, and VII satisfy these conditions in all cases. The three cases given for solution III are all unsatisfactory in ν_2, while in solution IX only F_2O and Cl_2O satisfy the required conditions in both normal modes. Solution IX is in any case not generally applicable; it gives a negative value of d_{12} for ClO_2 and NO_2, and a large positive one for F_2O; for SO_2 and Cl_2O it differs only slightly from II and VII, while for H_2O, D_2O, and O_3, $d_{33}>d_{11}$(max.) and there is no real solution. The interaction constant d_{13} is given in Table XI for solutions I, II, and VII. With respect to d_{11}^{II}, it is small and negative for H_2O, D_2O, and F_2O, small and positive for SO_2 and Cl_2O, large and negative for O_3, and large and positive for NO_2 and ClO_2. The energy principle does not necessarily require d_{13} to be negative because the product term $\Delta r_{12}\cdot\Delta r_{23}$ is positive in class A_1 modes, or positive because the product term is negative in the class B_1 mode; d_{13} is a subsidiary constant which occurs in the general valence force field, but which is eliminated when the secular equation is reduced to a product of symmetry factors, and the minimum number of constants employed.

Differences between the solutions I, II, and VII in general increase with (m_1/m_2); for H_2O they are very small. For this reason, the molecules H_2S, D_2S, H_2Se, and D_2Se were not included in the series studied. The maximum difference in the constants is $(d_{11}^{II}-d_{11}^{I})$ for NO_2, (1.169×10^5 dynes/cm = 21.9 percent); but NO_2 only just satisfies Eq. (12). For Cl_2O, the maximum difference is 16.5 percent, and in all other cases much less. This, of course, is excluding solution III, which will not be satisfactory for any of the cases dealt with here (see Section IV, and the energy principle discussed above), and is given merely to illustrate the general theory in those cases where there is no real solution permitted with $d_{12}=0$.

A general solution for the force constants of the triatomic molecule has been given by Glockler and Tung,[2] who extended the results to apply to other second-degree systems. They concluded that at singular points $(\partial d_{13}/\partial d_{22})=(\partial d_{13}/\partial d_{12})=0$ satisfactory sets of constants were obtained. They attempted no analysis of the normal coordinates, but claimed that the results for the isotopic molecules H_2O, D_2O; H_2S, D_2S, supported their choice. Since $d_{13}\equiv(d_{11}-d_{33})$, their solution is identical with the solution VIII of this paper, which corresponds to the singularity $(\partial d_{11}/\partial d_{12})=0$, and which, in the limit $(m_1/m_2)=0$, (more generally $(A_{12}/D)=0$), is identical with VII ($(\partial d_{22}/\partial d_{12})=0$), but becomes less satisfactory as (m_1/m_2) increases. (cf. Section

TABLE X. Solution IX. ($d_{11}=d_{33}$.)

	ClO_2		SO_2		NO_2		F_2O		Cl_2O	
d_{12}	−0.4136		0.04453		−0.4069		1.095		0.4950	
d_{11}	3.210		4.942		4.304		2.786		2.456	
d_{22}	0.9729		0.8018		1.187		0.9814		0.5046	
i	1	2	1	2	1	2	1	2	1	2
$\Delta\beta_i$	17° 38′	35° 48′	3° 24′	22° 49′	19° 58′	48° 3′	−19° 28′	10° 32′	−2° 25′	38° 58′
ρ_i	−1.386	3.145	−2.378	16.82	−0.8990	2.753	−5.378	−2.829	−1.237	−23.63
N_i	0.8281	0.5549	0.4903	0.1151	1.207	0.5907	0.2662	0.8105	1.155	0.08684
$V_{11}(\nu_i)$	74.426	31.368	97.932	2.118	64.443	38.906	115.475	62.687	123.702	0.942
$V_{22}(\nu_i)$	11.739	94.055	2.810	97.240	22.000	81.349	1.406	176.756	16.614	108.030
$V_{12}(\nu_i)$	13.835	−25.423	−0.742	0.642	13.557	−20.255	−16.881	−139.442	−40.316	−8.972

TABLE XI. Values of the interaction constant d_{13}.

	H_2O	D_2O	ClO_2	SO_2	O_3	NO_2	F_2O	Cl_2O
Solution I	−0.101	−0.138	0.519	−0.039		1.041		
Solution II	−0.092	−0.107	0.724	0.290	−1.233	2.210	−0.252	0.276
Solution VII	−0.095	−0.118	0.668	0.176	−1.453	1.854	−0.479	−0.112

IV.) Solution VIII can be used when (m_1/m_2) is small, as in H_2O, D_2O, H_2S, and D_2S, but is not a general one.

APPENDIX

The following approach to the second-degree equation may be of interest.

In place of the two valence-type coordinates Δ_1 and Δ_2, we use two linear combinations defined as below.

$$\Delta_1' = \Delta_1 + p_1\Delta_2,$$
$$\Delta_2' = \Delta_2 + p_2\Delta_1,$$

where p_1 and p_2 are arbitrary parameters. With these coordinates, the secular equation can be written

$$|d'A' - \lambda I| = 0,$$

where I is the unit matrix, d' is the force constant matrix for the coordinates Δ_1', Δ_2', and the elements of A' are

$$A_{11}' = A_{11} + 2p_1A_{12} + p_1^2A_{22},$$
$$A_{22}' = A_{22} + 2p_2A_{12} + p_2^2A_{11},$$
$$A_{12}' = A_{21}' = A_{12}(1 + p_1p_2) + p_2A_{11} + p_1A_{22},$$

the A_{ij} referring to the initial coordinates Δ_1 and Δ_2. The condition for reduction to canonical form is

$$A_{12}' = 0.$$

With values of p_1 and p_2 satisfying this equation, Δ_1' and Δ_2' are the (unnormalized) normal coordinates for the problem. p_2 may be expressed in terms of p_1, the latter replaced by p, and the solution given in terms of this single parameter. The results, referring to the initial coordinate system, are given by

$$d_{12} = d_{11}'[p - (RS/D)\mu_1],$$
$$d_{11} = d_{11}'[1 + (R^2/D)\mu_1], \qquad p_1 = (S/R),$$
$$d_{22} = d_{11}'[p^2 + (S^2/D)\mu_1], \qquad p_2 = -(1/p),$$

$$V_{11}(\nu_1) = (S/A_{11}')^2[1 + (R^2/D)\mu_1],$$
$$V_{22}(\nu_1) = (R/A_{11}')^2[p^2 + (S^2/D)\mu_1],$$
$$V_{12}(\nu_1) = [2RS/(A_{11}')^2][p - (RS/D)\mu_1],$$

$$V_{11}(\nu_2) = (p/A_{11}')^2[D\mu_2 + R^2],$$
$$V_{22}(\nu_2) = (1/A_{11}')^2[p^2D\mu_2 + S^2],$$
$$V_{12}(\nu_2) = -[2p/(A_{11}')^2][pD\mu_2 - RS],$$

where

$$d_{11}' = (\lambda_1/A_{11}'),$$
$$R = A_{12} + pA_{22},$$
$$S = A_{11} + pA_{12},$$

and other quantities are as defined previously. Solutions VII and VIII correspond to $p = 0$ and $-(A_{12}/A_{22})$, (i.e., to $p_1 = 0$, $p_2 = 0$), respectively.

THE JOURNAL OF CHEMICAL PHYSICS VOLUME 17, NUMBER 4 APRIL, 1949

Temperature Variation of Ultrasonic Velocity in Liquids

R. T. LAGEMANN, D. R. MCMILLAN, JR., AND W. E. WOOLF
Department of Physics, Emory University, Emory University, Georgia

(Received September 1, 1948)

Measurements have been made of the ultrasonic velocity in thirty-four organic liquids over a temperature range of 0–60°C by use of a variable-path ultrasonic interferometer operating at 500,000 cycles per second. For all of the liquids studied the relation between velocity and temperature was found to be essentially linear. Values of density, adiabatic compressibility, and temperature coefficient $(\Delta V/\Delta T)$ are also reported. It was found that the successive substitution of a heavier atom in a molecule leads to successively smaller temperature coefficients. It is pointed out that the temperature coefficient of ultrasonic velocity appears to be inversely proportional to the square root of the molecular weight, to a fair degree of accuracy.

THE variation of the velocity of ultrasonic waves in liquids with changes in temperature has been studied by various workers. Perhaps the earliest work of precision was that of Freyer, Hubbard, and Andrews,[1] who showed that the relation was essentially a linear one for the organic liquids studied by them. Other workers[2] have confirmed and added to their results, so that we find for all substances studied, with the exception of water below a certain temperature, that the ultrasonic velocity decreases with increasing temperature; that is, liquids possess a negative temperature coefficient which is of the order of -3×10^{-3} C^{-1}. Over short ranges of temperature, say 50 centigrade degrees, the velocity-temperature curves appear essentially linear for the substances studied.

On the other hand, Rao[2,3] proposes the relation

$$V = V_0(1 - \theta/\theta_c)^{9/10},$$

where V is the ultrasonic velocity at temperature θ, and θ_c is the critical temperature. This is, of course, very nearly a linear relation. No analysis of the available data was made by Rao to determine whether this relation fits better than one assuming

[1] E. B. Freyer, J. C. Hubbard, and D. H. Andrews, J. Am. Chem. Soc. **51**, 759 (1929).

[2] W. Busse, Ann. d. Physik **75**, 657 (1924); W. Schaaffs, Zeits. f. Physik **105**, 658 (1937); N. Seifen, Zeits. f. Physik **108**, 681 (1938); E. Schreuer, Akustische Zeits. **4**, 215 (1939); S. Bhagavantam and C. V. J. Rao, Proc. Ind. Acad. Sci. **9A**, 312 (1939); M. R. Rao, Ind. J. Phys. **14**, 109 (1940); V. Suryaprakasam, Proc. Ind. Acad. Sci. **12A**, 341 (1940); G. Suryan, Curr. Sci. **10**, 489 (1941); J. R. Pellam and J. K. Galt, J. Chem. Phys. **14**, 608 (1946); G. W. Willard, J. Acous. Soc. Am. **19**, 235 (1947); R. T. Lagemann, D. R. McMillan, Jr., and M. Woolsey, J. Chem. Phys. **16**, 247 (1948).

[3] M. R. Rao, J. Chem. Phys. **9**, 682 (1941).

TABLE I. Experimental values of ultrasonic velocity and temperature coefficient.

Compound	Ultrasonic velocity (m/sec.) 0°	10°	20°	30°	40°	50°	60°	Temperature coefficient (m/sec.-deg.)
Fluorobenzene, C_6H_5F	1275	1231	1189	1147	1108	1065		−4.174
Chlorobenzene, C_6H_5Cl	1364	1326	1289	1249	1213	1176	1141	−3.732
Bromobenzene, C_6H_5Br	1234	1202	1170	1139	1108	1077	1047	−3.118
Iodobenzene,* C_6H_5I	1170	1142	1114	1087	1060	1034	1008	−2.700
n-butyl chloride, C_4H_9Cl	1223	1182	1140	1100	1059	1020	978	−4.071
n-butyl bromide, C_4H_9Br	1087	1053	1019	985.6	952.8	919.2	887.0	−3.335
n-butyl iodide, C_4H_9I	1029	1001	971.5	943.6	915.8			−2.838
Methylene chloride, CH_2Cl_2		1132	1093	1054	1015			−3.900
Methylene bromide, CH_2Br_2	1015	989.1	963.2	937.8	912.4	887.2	861.8	−2.551
Methylene iodide,* CH_2I_2		991.9	973.3	954.6	936.5	918.2	899.4	−1.845
Ethylene chloride, $C_2H_4Cl_2$	1294	1253	1216	1174	1135	1097		−3.946
Ethylene bromide, $C_2H_4Br_2$		1035	1009	983.2	957.6	931.9	905.8	−2.580
Propylene chloride, $C_3H_6Cl_2$	1242	1202	1162	1127	1091	1053	1014	−3.761
Propylene bromide, $C_3H_6Br_2$	1049	1022	994.9	967.6	940.9	914.9	889.9	−2.663
Chloroform, $CHCl_3$	1073	1037	1001	967.7	933.4	899.9	867.7	−3.420
Bromoform,* $CHBr_3$		953	931	910	888	866	845	−2.163
Carbon tetrachloride, CCl_4	1002	969.8	937.8	907.0	876.0	845.3	815.3	−3.110
o-chlorotoluene, C_7H_7Cl	1394	1357	1319	1283	1246	1211	1176	−3.639
p-chlorotoluene, C_7H_7Cl		1345	1308	1272	1235	1200	1165	−3.603
m-chlorotoluene, C_7H_7Cl	1392	1355	1316	1280	1245	1208	1174	−3.639
o-bromotoluene, C_7H_7Br	1268	1236	1205	1173	1143	1113	1084	−3.071
p-bromotoluene, C_7H_7Br				1164	1133	1103	1073	−3.030
Benzene,* C_6H_6		1374	1327	1280	1234	1184	1143	−4.657
Ethyl bromide,* C_2H_5Br	968	935	900	866				−3.410
Ethyl iodide, C_2H_5I	932	905	876	848	820	795	768	−2.743
Pyridine, C_5H_5N	1526	1488	1441	1403	1361	1321	1278	−4.136
Methyl ethyl ketone, C_4H_8O	1306	1262	1217	1176	1132	1091	1048	−4.289
o-nitrotoluene, $C_7H_7O_2N$	1548	1510	1473	1436	1401	1364	1329	−3.646
m-nitrotoluene,* $C_7H_7O_2N$			1481	1445	1408	1373	1337	−3.600
Acetonitrile,* C_2H_3N	1387	1345	1305	1264	1224	1184	1144	−4.043
p-methyl cyclohexyl bromide,* $C_7H_{13}Br$	1259	1223	1189	1156	1123	1090	1062	−3.296
m-methyl cyclohexyl bromide,* $C_7H_{13}Br$	1263	1229	1194	1160	1128	1095	1063	−3.336
s-tetrachloroethane, $C_2H_2Cl_4$	1232	1203	1170	1138	1107	1074		−3.171
s-tetrabromoethane, $C_2H_2Br_4$	1086	1066	1041	1021	999.5	979.2	955.8	−2.160

* Not redistilled.

linear dependence of velocity on temperature. It is interesting to note that a relation similar to that of Rao is proposed by Guggenheim[4] for the dependence of surface tension on temperature.

The case of water[5] (including D_2O) is exceptional, however. It possesses a positive coefficient from its freezing point to about 74°C, above which its temperature coefficient is negative, as for normal liquids. Heavy water[6] behaves similarly, but its inversion temperature appears to occur at a slightly higher temperature. The data for water are fitted quite well by a relation of parabolic form. The relation of association to velocity of sound in water has been discussed by Weissler.[7]

Although most of the work on temperature effects has been concerned with the more common organic liquids, some results[8] are available on liquids of the so-called permanent gases at low temperatures. Considerable work has also been done on the temperature coefficient of velocity of liquid mixtures having water as one component.[9]

It is the purpose of the present report to give precise data on the variation of ultrasonic velocity with temperature in some organic liquids, particularly organic halides, and then to point out the influence of molecular weight on the temperature coefficient. While some of the data presented extend

[4] E. A. Guggenheim, J. Chem. Phys. **13**, 253 (1945).

[5] J. C. Hubbard and A. L. Loomis, Nature **120**, 189 (1927); J. C. Hubbard and A. L. Loomis, Phil. Mag. **5**, 1177 (1928); R. W. Boyle, J. F. Lehmann, and S. C. Morgan, Trans. Roy. Soc. Can. **22**, 371 (1928); L. G. Pooler, Phys. Rev. **35**, 832 (1930); E. B. Freyer, J. Am. Chem. Soc. **53**, 1313 (1931); C. R. Randall, Bur. Stand. J. Research **8**, 79 (1932); R. Bar, Helv. Phys. Acta **11**, 472 (1938); K. Yosioka, Inst. Phys. and Chem. Research, Tokyo, Sci. Pap. **34**, 843 (1938); P. Prosorov and V. Nozdrev, J. Exper. Theor. Phys. (U.S.S.R.) **9**, 625 (1939); E. Schreuer, see reference 2; B. K. Singh, Nature **156**, 569 (1945); P. L. F. Jones and A. J. Gale, Nature **157**, 341 (1946); G. W. Willard, see reference 2.

[6] R. Bar, Helv. Phys. Acta. **8**, 500 (1935); K. Yosioka, see reference 5; D. R. McMillan, Jr. and R. T. Lagemann, J. Acous. Soc. Am. **19**, 956 (1947).

[7] A. Weissler, J. Chem. Phys. **15**, 210 (1947).

[8] A. Pitt and W. J. Jackson, Can. J. Research **12**, 686 (1935); E. Hirschlaff, Proc. Cam. Phil. Soc. **34**, 296 (1938); Findley, Pitt, Smith, and Wilhelm, Phys. Rev. **54**, 506 (1938); **56**, 122 (1939); H. W. Liepmann, Helv. Phys. Acta **11**, 381 (1938); **12**, 421 (1939); J. R. Pellam and C. F. Squire, Phys. Rev. **72**, 1245 (1947); J. H. Galt, J. Chem. Phys. **16**, 505 (1948).

[9] J. C. Hubbard and A. L. Loomis, see reference 5; E. B. Freyer, see reference 5; C. R. Randall, see reference 5; A. Giacomini, J. Acous. Soc. Am. **19**, 701 (1947); G. W. Willard, see reference 2.

the velocity measurements of certain liquids to new temperatures, some are for liquids on which no previous measurements have been made. In what follows we will refer more often to a temperature coefficient which we define as $\Delta V/\Delta T$ than to the usual coefficient which is defined as $(1/V)(\Delta V/\Delta T)$. The coefficient, $\Delta V/\Delta T$, if we assume that the velocity is a linear function of temperature, is a constant characteristic of each liquid. On the other hand, the temperature coefficient, as it is customarily defined, suffers from the shortcoming that it varies with the temperature at which the measurement is made.

EXPERIMENTAL

The ultrasonic velocities were measured with a moving-reflector ultrasonic interferometer described previously,[10] employing a frequency of 500,000±20 cycles per second. For each measurement about 40 ml of liquid was studied in a gold-lined cup. The interferometer, except for the reading micrometer, was completely submerged in a thermostatically controlled water bath. The temperature was observed with a Bureau of Standards calibrated thermometer. Temperatures below that of the room were obtained by circulating cold water from a refrigerator through the bath and maintaining equilibrium by means of the usual thermostatically controlled heating coils. In no case did the temperature during a run deviate more than ±0.05°C from the stated value.

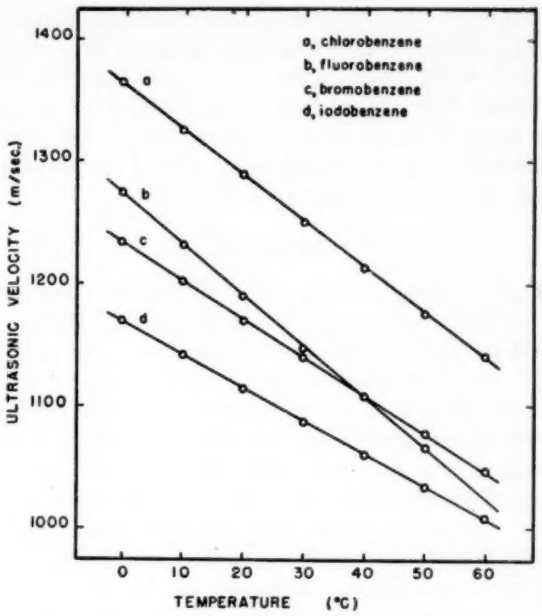

FIG. 1. Ultrasonic velocity *versus* temperature for four monohalogenated benzenes.

Eastman White Label compounds were used

TABLE II. Measured values of density and computed values of adiabatic compressibility.

Compound	Density (g/cc) 10°	20°	30°	40°	50°	Adiabatic compressibility (atmos.$^{-1}$ ×10^6) 10°	20°	30°	40°	50°
Fluorobenzene		1.0249	1.0130	1.0008	0.9888		69.93	76.03	82.47	90.35
Chlorobenzene	1.1146	1.1042	1.0947			51.70	55.23	59.33		
Bromobenzene	1.5075	1.4953	1.4819	1.4681	1.4535	46.52	49.50	52.71	56.22	61.10
Iodobenzene*	1.8431	1.8280	1.8125	1.7977	1.7822	42.15	44.66	47.31	50.16	53.18
n-butyl chloride		0.8851	0.8740	0.8621	0.8514		88.09	95.81	104.8	114.4
n-butyl bromide		1.2741	1.2599	1.2454	1.2308		76.59	82.79	89.62	97.43
n-butyl iodide		1.6144	1.5973	1.5805	1.5647		66.50	71.25	76.44	
Methylene bromide		2.4843	2.4587	2.4322	2.4063		43.96	46.86	50.04	53.50
Ethylene chloride		1.2524	1.2379	1.2230	1.2090		54.72	59.39	64.31	69.64
Ethylene bromide		2.1777	2.1574	2.1354	2.1153		45.70	48.59	51.75	55.16
Propylene chloride		1.1554	1.1428	1.1295	1.1169		64.95	69.81	75.37	81.82
Propylene bromide		1.9405	1.9221	1.9037	1.8852		52.75	56.31	60.12	64.21
Chloroform		1.4870	1.4674	1.4485	1.4290		68.01	73.74	80.29	87.56
Bromoform*	2.9159	2.8904	2.8639	2.8377	2.8118	38.26	40.44	42.72	45.28	48.05
Carbon tetrachloride		1.5942	1.5748	1.5550	1.5352		72.27	78.21	84.92	92.37
o-chlorotoluene		1.0826	1.0728	1.0633	1.0532		53.80	57.38	61.38	65.60
p-chlorotoluene		1.0697	1.0596	1.0503	1.0401		55.37	59.10	63.25	67.65
m-chlorotoluene	1.0824	1.0728	1.0628	1.0531	1.0433	50.99	54.54	58.19	62.07	66.55
o-bromotoluene		1.4237	1.4115	1.3994	1.3873		49.02	52.17	55.42	58.97
p-bromotoluene			1.3934	1.3815	1.3691			53.67	57.14	60.83
Ethyl bromide*	1.4803	1.4606	1.4398			78.30	85.65	93.84		
Ethyl iodide	1.9578	1.9357	1.9122	1.8896	1.8661	63.19	68.21	73.69	79.75	85.91
Pyridine	0.9938	0.9832	0.9727	0.9626	0.9526	46.05	49.63	52.92	56.83	60.96
Methyl ethyl ketone	0.8157	0.8053	0.7946	0.7843	0.7732	78.00	84.95	92.20	100.8	110.1
o-nitrotoluene	1.1728	1.1629	1.1535	1.1438	1.1342	37.89	40.16	42.60	45.13	48.02
m-nitrotoluene*		1.1570	1.1478	1.1382	1.1288		39.93	42.28	44.91	47.62
p-methyl cyclohexyl bromide*	1.2780	1.2670	1.2550	1.2438	1.2326	53.01	56.57	60.42	64.60	69.19
m-methyl cyclohexyl bromide*	1.2697	1.2587	1.2470	1.2364	1.2251	52.83	56.47	60.38	64.41	68.98
s-tetrachloroethane	1.6101	1.5947	1.5789	1.5632	1.5473	43.49	46.42	49.56	52.89	56.77
s-tetrabromoethane	2.9881	2.9666	2.9445	2.9213	2.8989	29.84	31.52	33.01	34.72	36.45

* Not redistilled.

[10] D. R. McMillan, Jr. and R. T. Lagemann, see reference 6.

throughout. Before the interferometer measurements, all but a few were refractionated in a column packed with glass helices and equipped with a standard Penn State head. The distillation column was equivalent to about twelve theoretical plates. Densities were measured using a 5-ml pycnometer[11] of the double capillary arm type.

RESULTS

The measured values of the ultrasonic velocity in thirty-four compounds, mostly organic halides, are listed in Table I for the temperature range 0° to 60°C. Some of the values at 20°C have appeared earlier.[12] A few of the measurements have been reported by other workers, but the variation in results warrants new measurements. In the last column are given the respective temperature coefficients. These were calculated from the original data by the method of least squares on the assumption that velocity was a linear function of the temperature over the range studied. On the assumption of a linear relation, the calculated values of velocity agree with the observed ones within our error of measurement.

The relation of velocity and temperature over the 60-degree range is illustrated as an example in Fig. 1 for the monohalogenated benzenes. This graph illustrates also that care must be taken when one states such rules as the one by Parshad,[13,14] namely, that "introduction of a heavier atom in the molecule decreases the velocity." It may be seen that at about 75°C the fluorobenzene will have the lowest velocity, and at temperatures above 75°C Parshad's rule is violated with regard to the other three benzenes. Clearly the difference in temperature coefficients among compounds demands that any rule of this kind be accompanied by a statement concerning the temperature involved.

From Table I it may be noted that the successive substitution of a heavier atom in a molecule results in a lowered numerical value of the temperature coefficient ($\Delta V/\Delta T$). This is illustrated, for example, by the successive substitution of a halogen in the same position in benzene to form the monohalogenated benzenes, and in the successive substitution of chlorine for hydrogen atoms in methane to form the series, CH_2Cl_2, $CHCl_3$, CCl_4.

Table II gives measured values of the densities of the liquids and values of the adiabatic compressibilities calculated by use of the well-known relation $V=1/(\rho B_{ad})^{\frac{1}{2}}$.

TEMPERATURE COEFFICIENT AND MOLECULAR WEIGHT

In this section we wish to point out the usefulness of the molecular weight in predicting values of the temperature coefficient. When all the available data on the change of ultrasonic velocity with temperature in liquids are considered, one notes a general tendency for the numerical value of the temperature coefficient to decrease with increase in molecular weight of the liquid, omitting water from consideration. This trend is shown in Fig. 2. In the cases of hydrogen, helium, argon, oxygen, and nitrogen an average coefficient is used, since for them velocity and temperature are not strictly linear. For all the other compounds the data on temperature coefficients are taken from Table I. From a large scale plot, such as that of Fig. 2, a good estimate can be made of the temperature coefficient for a com-

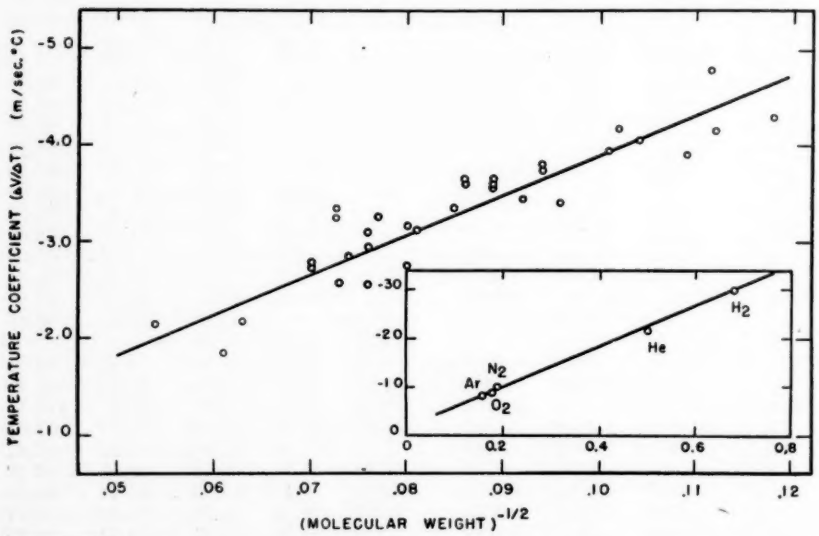

FIG. 2. Temperature coefficient of ultrasonic velocity *versus* molecular weight$^{-\frac{1}{2}}$. The principal curve represents the data of Table I, omitting only acetonitrile, which lies off to the right, and whose behavior is due to association. The data for the insert are taken from the following sources: hydrogen, Pitt and Jackson, and Galt (see reference 8); helium, Findley *et al.* (see reference 8); nitrogen, Hirschlaff (see reference 8); oxygen, Galt (see reference 8); argon, Liepmann (see reference 8). The slopes of the two curves are approximately the same.

[11] Lipkin, Davison, Harvey, and Kurtz, Jr., Ind. Eng. Chem. (Anal. Ed.) **16**, 55 (1944).
[12] R. T. Lagemann, J. S. Evans, and D. R. McMillan, Jr., J. Am. Chem. Soc. **70**, 2996 (1948).
[13] R. Parshad, Ind. J. Phys. **19**, 47 (1945).
[14] S. Parthasarathy, Curr. Sci. **7**, 322 (1938).

pound of known molecular weight. That this estimate cannot be of high accuracy may be illustrated by *o*-, *m*-, *p*-isomers which, while possessing the same molecular weight, have slightly different temperature coefficients. It will be seen that certain associated compounds for which data are available, such as methyl and ethyl alcohol, for example, and acetonitrile, lie to the right of the curve of Fig. 2. However, if it is recalled that actually these liquids have an effective molecular weight greater than that of the monomer (which is the molecular weight used in the plot), their points on the plot should rightfully be shifted to the left along the molecular weight axis, bringing them into better alignment with the normal compounds.

It might be expected that the proportionality between temperature coefficient and $M^{-\frac{1}{3}}$ might hold best for similar molecules, and indeed it is so. Figure 3 shows a plot for the monohalogenated benzenes, where a single heavier atom is successively substituted in the same position. Rather than substitute for the same atom, we may substitute Cl for H in succession in methane derivatives, with a similar result. If, in the benzene series, a radical is substituted, such as in $C_6H_5NO_2$, the point falls off the curve.

Certainly the relation suggested by Figs. 2 and 3 can be helpful in estimating the temperature coefficient of a liquid of known molecular weight. A rough rule which, for the liquids of Table I, leads to an average deviation of only about 6 percent, is

$$(\Delta V/\Delta T)M^{\frac{1}{3}} = 39.0 \text{ m sec.}^{-1}{}^{\circ}\text{C}^{-1} \text{ g}^{\frac{1}{3}}.$$

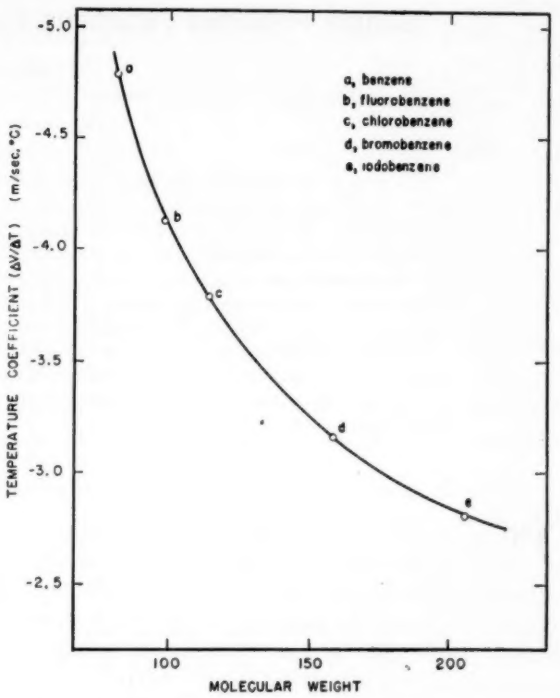

FIG. 3. Temperature coefficient of ultrasonic velocity *versus* molecular weight for a series of related compounds.

ACKNOWLEDGMENTS

It is a pleasure to acknowledge gratefully the generous assistance of the Research Corporation and of the Society of the Sigma Xi through Grants-In-Aid to one of us. To Mr. John Evans and Mrs. Martha Woolsey we are grateful for assistance in making the measurements.

Simple Potential Functions and the Hydrogen Halide Molecules

MANSEL DAVIES
The Edward Davies Chemical Laboratories, University College, Aberystwyth, Wales
(Received August 24, 1948)

Five simple molecular potential functions have been tested by comparison with spectroscopic data for the hydrogen halides. It is shown that when plotted on a "reduced" distance scale (r/r_e), the potential curves for these molecules coincide closely up to $\Delta(r)=0.10r_e$. Two electrostatic functions indicate β/r^n as the more satisfactory form of the repulsive term. Significant values of the effective polarizability and "fractional ionic character" are deduced. The latter are higher and more nearly constant than the uncorrected values currently quoted as showing changing bond type in these molecules. The results conform with Kirkwood's very successful treatment of HCl as a polarizable ion pair.

Of purely empirical functions, the Pöschl-Teller provides a slight improvement upon the simple Morse relation, and is only a little more cumbersome than the latter. The Rosen-Morse function is less satisfactory for these molecules. Simple expressions are given for evaluating the three parameters in these functions from spectroscopic data.

ONE of the central problems in molecular structure is the correct representation of the potential field binding the atoms in the molecule. The problem assumes its simplest form in the case of diatomic molecules where r, the distance apart of the nuclei, is the one independent variable. As yet, specific indications of the most appropriate general form of potential function are not provided by theory, as only for the simplest molecules, such as H_2, has quantum-mechanical theory been applied with precision. Further, it is more than likely that the type of potential function required for an accurate representation of the conditions, from equilibrium to dissociation, will vary with the nature of the molecule: the degree of polarity in the bond will clearly be one of the features leading to such variations. Currently quoted estimates[1] of the "percentage ionic character" give this as 43 percent in HF and 5 percent in HI, the former value being almost coincident with the figure for KI. With this point in mind the hydrogen halides would appear to provide reasonably wide ground for the testing of simple potential functions. These functions will be at least partly empirical.

The basis of the treatment lies in the expansion of $U(r)$ near the equilibrium value $U(r_e)$ as follows:

$$U(r)=\tfrac{1}{2}!\cdot U''(r_e)(r-r_e)^2+\tfrac{1}{3}!\cdot U'''(r_e)(r-r_e)^3 +\tfrac{1}{4}!\cdot U^{\mathrm{iv}}(r_e)(r-r_e)^4\cdots. \quad (1)$$

TABLE I.

Molecule	$U''(r_e)10^{-6}$	$U'''(r_e)10^{-14}$	$U^{\mathrm{iv}}(r_e)10^{-22}$	$D_e\cdot10^{12}$	μ	$\alpha_{X^-}\cdot10^{24}$
HF	0.967	−7.53	57.8	10.65	1.91	0.96
HCl	0.515_5	-2.84_6	13.7_2	7.41	1.03	3.57
HBr	0.409_0	-2.07_3	8.7_9	6.34	0.78	4.99
HI	0.314_8	-1.55_3	6.8_5	5.21	0.38	7.57

[1] L. Pauling, *The Nature of the Chemical Bond* (Cornell University Press, Ithaca 1939), p. 46; C. P. Smyth, *Frontiers in Chemistry*, Vol. 5 (Interscience Publishers, Inc., New York, 1948), p. 31.

$U'(r_e)$, the value of the first derivative at r_e, is, of course, zero. Relations first deduced by Kratzer and modified for the above form of expansion[2] provide values of these derivatives in terms of the spectroscopic constants as follows:

$$U''(r_e)=(2\pi c\omega_e)^2\cdot m,$$
$$U'''(r_e)=-(3U''(r_e))/(r_e)[(\alpha\omega_e/6B_e^2)+1],$$
$$U^{\mathrm{iv}}(r_e)=5/3\cdot([U'''(r_e)]^2)/(U''(r_e)) -(8x_e\cdot\omega_e)/(B_e\cdot r_e^2)\cdot U''(r_e).$$

In addition, there are available the energies of dissociation, $D_e=D_0+\frac{1}{2}\cdot hc\omega_e(1-x_e/2)$, and such factors as the dipole moments (μ), and polarizabilities of the halide ions (α_{X^-}).[3] The spectroscopic data have been taken from Herzberg[4] with the corrections to the D_0 values for HBr and HI pointed out by Gaydon.[5] The dipole moments listed in Table I (see, for instance, reference 1) are in Debyes; the other items are in c.g.s. units, i.e., D_e in erg./molecule, etc. An accuracy of at least one percent has been aimed at in most of the subsequent numerical work. $U''(r_e)$, of course, is identical with the force constant, the units above being dynes/cm. An interesting calculation is that of the work needed to increase the internuclear distance by, say, 1 percent or 10 percent of its equilibrium value. With the latter value of $(r-r_e)$, the third term in Eq. (1) is, at most, 5 percent of the first, so that the absence of higher terms is not serious at that extension. The work of stretching is given in Table II in units of 10^{-14} erg/molecule, and then as the percentage of

[2] See, for instance, Jevons, *Report on Band Spectra of Diatomic Molecules* (Physical Society, London, 1932), p. 27.
[3] K. Fajans, Zeits. f. physik. Chemie **B24**, 118 (1934); O. K. Rice, *Electronic Structure and Chemical Binding* (McGraw-Hill Book Company, Inc., New York, 1940), p. 178.
[4] G. Herzberg, *Molecular Spectra and Molecular Structure: Vol. I: Diatomic Molecules* (Prentice-Hall, Inc., New York, 1939), p. 482 *et seq.*
[5] Nature **161**, 731 (1948). The correction arises from the non-gaseous standard state to which the thermal data for Br_2, and I_2 are referred (Gaydon, private communication).

the dissociation energy D_e. The degree of equality in the energy values measures the coincidence in the potential curves for these molecules near their minima when the curves are plotted in energy units against a "reduced" distance scale, i.e., in terms of r/r_e. An alternative numerical expression of the same result is found in the approximate constancy of $U''(r_e)\cdot r_e^2$. The markedly different values of D_e show that this coincidence occurs only in the neighborhood of r_e.

The subsequent calculations accept the values of the derivatives in Table I as being correct. This is only so within certain limits, depending upon the adequacy of the representation of the spectroscopic terms by the constants employed in calculating them. This, and other relevant points, are critically discussed in the work of Coolidge, James, and Vernon on the potential function for H_2.[6] In the present instance the approximations involved are quite adequate for the comparisons to be made.

ELECTROSTATIC POTENTIAL FUNCTIONS

The first quantitative treatment of the hydrogen halide bonding[7] suggested on simple physical grounds the potential function

$$U(r) = -e^2/r - e^2\cdot\alpha_{eff}/2r^4 + \beta e^2/r^n \cdots. \qquad (2)$$

Writing $a=(2n-8)e^2\cdot\alpha_{eff}/r_e^3$, $b=(n-1)e^2$; $U'(r_e)=0$, $U''(r_e)=1/r_e^3(a+b)$, $U'''(r_e)=-3/r_e^4(2a+b)$, $U^{iv}(r_e)=6/r_e^5(7a+2b)$. This corresponds to electrostatic binding between ions of charge e, the sum of whose effective polarizabilities is α_{eff}. β and n are adjustable or arbitrary parameters in the form assumed for the repulsive term. Apart from the latter, Eq. (2) is precisely the form arrived at by Kirkwood[8] in his quantum-mechanical calculations of the molecular constants of the hydrogen halides. He was able to make very successful estimates of what are here adjustable parameters. Other calculations[7,9] have taken $e=\epsilon=$electronic charge $=4.80\cdot10^{-10}$ e.s.u. Even in the most polar molecule, HF, reasons can be advanced which suggest that at equilibrium the conditions may depart appreciably from those of a polarizable ion pair.[10] Thus, a more general approach to the conditions obtaining is to use the observed dipole moment to determine e.

$$\mu_{observed} = er_e(1-\alpha_{eff}/r_e^3) = er_e(1-s).$$

Three other relations are then needed to define α_{eff}, β and n. These can be taken as $U'(r_e)=0$, $U''(r_e)=(2\pi c\omega_e)^2 m$, and $U(r_\infty)-U(r_e)=D_e$.

[6] A. S. Coolidge, H. M. James, and E. L. Vernon, Phys. Rev. **54**, 726 (1938).
[7] M. Born and W. Heisenberg, Zeits. f. Physik **23**, 388 (1924).
[8] J. G. Kirkwood, Physik. Zeits. **33**, 259 (1932).
[9] G. Briegleb, Zeits. f. physik. Chemie **B51**, 9 (1941).
[10] L. Pauling, J. Am. Chem. Soc. **54**, 998 (1932).

TABLE II.

Molecule		HF	HCl	HBr	HI
$r_e\cdot10^8\cdot$cm		0.917	1.275	1.414	1.604
1 percent extension	$\times10^{14}$ erg per molecule	0.396	0.410	0.400	0.395
10 percent extension	$\times10^{14}$ erg per molecule	32.6	33.6	32.6	31.7
1 percent extension	percentage of D_e	0.037	0.055	0.063	0.076
10 percent extension	percentage of D_e	3.06	4.54	5.15	6.08
$U''(r_e)\cdot r_e^2\cdot10^{10}$		0.813	0.839	0.818	0.811

Sufficient consistency with these equations is readily obtained by assuming a reasonable value for n, say $n=8.0$, solving for $s=\alpha_{eff}/r_e^3$ from $U''(r_e)$, and then calculating D_e. A few successive approximations will define n adequately. The resulting $U(r)$ correctly reproduces r_e, ω_e, D_e, and μ. Further tests of the function are then provided by a comparison of the values calculated for $U'''(r_e)$ and $U^{iv}(r_e)$ with those in Table I; the latter, being based on spectroscopic data, are designated $U_s'''(r_e)$ and $U_s^{iv}(r_e)$.

The summary in Table III shows the ratios of the calculated to the spectroscopic values of the higher derivatives. It is seen that the calculated derivatives, and hence the values of the further spectroscopic functions related to them, are only some 60 percent of the observed. This is not a satisfactory result. Briefly, two reasons can be advanced for these deficiencies. The assumed form of the potential function is not, of course, throughout consistent with the physical facts, as in the ground state these molecules dissociate into atoms. Secondly, the adjustment of the curve to give the correct D_e, i.e., to extrapolate to the correct asymptote at r_∞, gives rise to slight departure from the true curvature at r_e which makes itself felt in the values of the third and fourth derivatives. An alternative mode of choosing the constants in (2), i.e., by equating to the "observed" values of $U'(r_e)$, $U''(r_e)$, $U'''(r_e)$, and μ, leads to physically meaningless values of the constants—e.g., for HCl, $a=144\cdot10^{-20}$, $b=-37\cdot10^{-20}$.

TABLE III.

Molecule	HF	HCl	HBr	HI
$e\cdot10^{-10}$ e.s.u.	3.27	2.98	2.88	2.69
e/ϵ	0.68	0.62	0.60	0.56
$\alpha_{eff}\cdot10^{24}$ cm^3	0.280	1.51	2.28	3.77
α_{eff}/α_X-	0.292	0.423	0.457	0.499
n	6.3	7.6	8.3	9.3
β	$6.9\cdot10^{-44}$	$2.55\cdot10^{-53}$	$1.57\cdot10^{-58}$	$6.1\cdot10^{-66}$
$U'''(r_e)/U_s'''(r_e)$	0.52	0.61	0.63	0.58
$U^{iv}(r_e)/U_s^{iv}(r_e)$	0.39	0.58	0.63	0.50

TABLE IV.

Molecule	HF	HCl	HBr	HI
α_{eff}: Table III	0.28	1.51	2.28	3.77
α_{eff}: Kirkwood	0.6	1.5	2.3	3.9
α for inert gas	0.394	1.65	2.54	4.11
$\alpha_{eff}/\alpha_{inert\ gas}$	0.71	0.92	0.90	0.92

These provide a better value for $U^{iv}(r_e) = 1.21 U_s^{iv}(r_e)$, but give a worthless figure for D_e.

Returning to Table III, the values deduced for n, $\alpha_{eff}/\alpha_{X^-}$ and e/ϵ are all physically acceptable. If the ratios $\alpha_{eff}/\alpha_{X^-}$ are divided by the corresponding ionic radii in angstroms,[11] the following figures result: 0.215; 0.233; 0.235; 0.231. The significance of this apparent constancy is not clear; it might mean that α_{eff} is proportional to α_{X^-} and inversely proportional to the electrostatic potential which can be ascribed to the electrons at the "surface" of the ions: $\alpha_{eff} = \text{const.}\ \alpha_{X^-}/r^{-1}$. But this is merely the simplest, and not a very helpful, hypothesis. Even if the quantitative agreement in this factor is regarded as accidental, it nevertheless serves to emphasize the reasonableness in the trend of $\alpha_{eff}/\alpha_{X^-}$.

A further feature of the above α_{eff}'s is their concurrence with those values calculated by Kirkwood and given, in units of 10^{-24} cm^3, in Table IV. With the exception of HF, the coincidence is practically complete, although it should be noted that Kirkwood's α_{eff}'s are based on older values of α_{X^-} which have all now been increased by about 10 percent. Debye pointed out many years ago[12] that to account for the observed dipole moments of the hydrogen halides in terms of an ionic structure, an effective polarizability only slightly different from that of the inert gas with the same number of electrons as X^- is needed. This relation is retained by the present values of α_{eff}, as is shown by the last row in Table IV. The reason for this relation is also unknown.

The ratio e/ϵ can be taken as an estimate of the "fractional ionic character" derived from the dipole moment after correction for polarizability. A small but reasonable trend is seen. Without discussing the significance of the "fractional ionic character" (a term which arises in the resonance treatment of the molecular bond), it is certain that these figures provide far more reliable estimates of this factor than those[13] having no correction for polarizability. These uncorrected values are, from HF to HI, 0.43, 0.17, 0.11, 0.05—showing a different order of variation from that suggested here and tending to give an entirely false impression of changes in the nature of the hydrogen halide bonds. The present much higher and roughly constant values of this factor are in conformity with the fact that Kirkwood's quantitative treatment of the bond in HCl on the basis of purely ionic character met with considerable success.

An electrostatic potential function of the type treated here has proved satisfactory in calculating the energy of interaction leading to $[F\cdots H-F]^-$.[14]

The repulsive term in (2) is of the arbitrary power form. It has been known since the work of Born and Mayer[15] that better results are found for ionic lattices by using a repulsive term of an exponential form which is also indicated by quantum mechanics. The simplest version of this type, $b\cdot e^{-r/\rho}$, contains the two constants b and ρ which now replace β and n of Eq. (2). It seemed of interest to examine whether the new function, Eq. (3), provided any improvement upon Eq. (2).

$$U(r) = -e^2/r - e^2\cdot\alpha_{eff}/2r^4 + b\cdot e^{-r/\rho}\cdots, \qquad (3)$$

$$U'(r_e) = 0 \quad \text{gives} \quad (b/\rho)\cdot e^{-r_e/\rho} = e^2/r^2(1+2s),$$

$$U''(r_e) = e^2/r_e^2\{(1/\rho) - (2/r_e) + 2s((1/\rho) - (5/r_e))\},$$

$$U'''(r_e) = -2e^2/r_e^3\{(1/\rho) - (3/r_e) + 5s((1/\rho) - (6/r_e))\},$$

$$U^{iv}(r_e) = 6e^2/r_e^4\{(1/\rho) - (4/r_e) + 10s((1/\rho) - (7/r_e))\},$$

$$D_e = e^2/r_e\{1 - (\rho/r_e) + (s/2)(1 - (4\rho/r_e))\}.$$

$U'(r_e)$, $U''(r_e)$, D_e, and μ are used to evaluate the constants, a process which is again effected most readily by successive approximations from a value of ρ near $0.15\cdot 10^{-8}$ cm. The results are summarized in Table V.

Comparison of the last two rows with the similar entries in Table III shows that the new form of the repulsive term has caused a marked deterioration in the calculated values of $U'''(r_e)$ and $U^{iv}(r_e)$. However, the values of e/ϵ and $\alpha_{eff}/\alpha_{X^-}$ are practically unchanged, so that the comments previously made on the basis of these ratios need no modification. It is not a justifiable conclusion that in such potential functions the power form of the repulsive term will generally be the more acceptable, even when the attractive energy is written as a power series, for the exponential form is superior in ionic lattice calculations. Solution of (3) from the spectroscopic values of $U'(r_e)$, $U''(r_e)$, $U'''(r_e)$, $U^{iv}(r_e)$ leads, for HF, to

TABLE V.

Molecule	HF	HCl	HBr	HI
$e\cdot 10^{10}$ e.s.u.	3.21	2.96	2.83	2.67
e/ϵ	0.67	0.62	0.59	0.56
$\alpha_{eff}\cdot 10^{24}$ cm^3	0.27_1	1.51	2.27	3.76
$\alpha_{eff}/\alpha_{x^-}$	0.28_2	0.42_4	0.45_6	0.49_7
$\rho\cdot 10^8$ cm	0.122_5	0.145	0.149	0.155
$b\cdot 10^8$ erg	0.454	1.26	2.04	3.78
$U'''(r_e)/U_s'''(r_e)$	0.275	0.37_0	0.39_6	0.37_6
$U^{iv}(r_e)/U_s^{iv}(r_e)$	0.086	0.53	0.245	0.217

[11] See reference 1, L. Pauling, p. 326.
[12] P. Debye, *Polar Molecules* (The Chemical Catalogue Company, New York, 1929), p. 62.
[13] See reference 1, Pauling and Smyth.
[14] Mansel Davies, J. Chem. Phys. **15**, 739 (1947).
[15] P. M. Morse, Phys. Rev. **34**, 57 (1929).

$\rho=0.530\cdot10^{-8}$, $s=0.160$, but a negative value for e^2 and a similarly impossible value of D_e.

MORSE FUNCTION

A remarkably simple and successful general potential function is the well-known one of Morse.[15] This may be written as

$$U(r)=D_e\cdot[1-\exp(-a(r-r_e))]^2.$$

Both the attractive and repulsive terms are now of an exponential character. The function expresses $U'(r_e)=0$ implicitly and has the two constants a and D_e. The derivatives take the very simple forms:

$$U''(r_e)=2a^2\cdot D_e,\quad U'''(r_e)=-6a^3\cdot D_e,$$
$$U^{\mathrm{iv}}(r_e)=14a^4\cdot D_e.$$

To test the adequacy of this relation in the same manner as the earlier one, we take the values of D_e and $U''(r_e)$ from Table I and then calculate a and the other derivatives. These results are collected in Table VI. The Morse curve reproduces $U'''(r_e)$ and $U^{\mathrm{iv}}(r_e)$ a good deal more accurately than the simple electrostatic functions. One of the associated factors in its satisfactory performance is the fact that the Morse function when inserted in the Schrödinger equation leads to the explicit form

$$E_{\mathrm{vib}}=h\omega_e(v+\tfrac{1}{2})-x_eh\omega_e(v+\tfrac{1}{2})^2$$

for the vibrational energy levels. This relation is the exact expression used to represent the results for low vibrational quantum numbers, and from it the experimental values of ω_e, x_e are deduced. Thus, any divergence between the true and the spectroscopic values of the derivatives $U'''(r_e)$ and $U^{\mathrm{iv}}(r_e)$ is the less likely to appear in testing the Morse function.

Some adjustment or extension of the Morse curve is a likely line of improvement for these empirical potential functions. An extended form of the function with an arbitrary number of terms can be used where the data warrant it,[6] but there are obvious practical advantages in restricting the number of adjustable parameters. This restriction is maintained in the two following alternative and somewhat generalized forms of the Morse expression; no more data are required for their definition than for the simple Morse equation.

ROSEN-MORSE FUNCTION

The first of these is the Rosen-Morse function,[16] which we take in the simple version:

$$U(r)=A\cdot\tanh(r/d)-C\cdot\mathrm{sech}^2(r/d)\cdots. \quad (4)$$

TABLE VI.

Molecule	HF	HCl	HBr	HI
$a\cdot10^{-8}$	2.13_2	1.86_6	1.79_7	1.73_9
$U'''(r_e)/U_s'''(r_e)$	0.82_2	1.01_2	1.06_5	1.06_0
$U^{\mathrm{iv}}(r_e)/U_s^{\mathrm{iv}}(r_e)$	0.53_2	0.91_6	1.05_1	0.97_3

[16] N. Rosen and P. M. Morse, Phys. Rev. **42**, 210 (1932).

TABLE VII.

Molecule	HF	HCl	HBr	HI
$d\cdot10^8$	0.84_2	0.99_2	1.04_9	1.10_2
$(-A)\cdot10^{12}$	413	629	730	872
$C\cdot10^{12}$	259	367	417	486
$U'''(r_e)/U_s'''(r_e)$	0.73	0.95	1.01	0.98
$U^{\mathrm{iv}}(r_e)/U_s^{\mathrm{iv}}(r_e)$	0.36	0.72	0.86	0.96

This leads to:

$$\tanh(r_e/d)=-A/2C.$$

And writing

$$1/C^2\cdot(4C^2-A^2)^2=f,$$
$$U''(r_e)=f/8d^2C,$$
$$U'''(r_e)=3Af/8d^3C^2,$$
$$U^{\mathrm{iv}}(r_e)=(9A^2-8C^2)f/8d^4C^3,$$
$$D_e=(A+2C)^2/4C.$$

As previously, the constants are chosen to fit $U'(r_e)$, $U''(r_e)$, and D_e. A and C have the dimensions of erg/molecule, and d is in cm. Table VII summarizes the constants and their testing. Except for HI and possibly HBr, the curvature in the neighborhood of r_e is reproduced no better than by the Morse function. There is, however, a steady improvement in the accuracy of the function in going to the molecules of smaller apparent polarity, and the degree of agreement for HI is probably not far short of the accuracy of testing. The evaluation of the constants can also be made on the basis of $U'(r_e)$, $U''(r_e)$, and $U'''(r_e)$, but this method is particularly unsatisfactory in practice, because of the very slow variation and closeness to unity of $\tanh(r_e/d)$, when $r_e/d\sim2$. Thus for HF and HI, respectively, it yields values of D_e calc./D_e obs. $=0.17$ and 0.25, and for $U^{\mathrm{iv}}(r_e)/U_s^{\mathrm{iv}}(r_e)$ 2.7 and 3.5, i.e., widely divergent from the results of alternative methods. Even more direct is the evaluation of A, C, and d from $U''(r_e)$, $U'''(r_e)$, and $U^{\mathrm{iv}}(r_e)$, using the relations

$$(C/A)^2=9/8\{1-U^{\mathrm{iv}}(r_e)\cdot U''(r_e)/[U'''(r_e)]^2\},$$
$$d=3A/C\cdot U''(r_e)/U'''(r_e).$$

This latter is virtually the method described by Kronig[17] for fitting the Rosen-Morse curve, but the above relations are far more convenient for numerical evaluation. They do not, however, lead to satisfactory parameters. The ratios D_e calc./D_e obs. for the same two molecules, HF and HI, now have the values 1.74 and 1.60, for which the most that can be said is that they are an improvement on those deduced via $U'(r_e)$, $U''(r_e)$, and $U'''(r_e)$. Whilst not improbable values of d are given by this method, the ratio $-A/2C$, which should equal $\tanh(r_e/d)$, assumes the impossible values of 3.98 and 1.47. Incidentally, the Kronig version of the Rosen-Morse

[17] R. de L. Kronig, *The Optical Basis of the Theory of Valency* (Cambridge University Press, Cambridge, England, 1935), p. 88.

TABLE VIII.

Molecule	HF	HCl	HBr	HI
D_{Morse}/D_e	0.88	1.16	1.21	1.21
D_{Lotmar}/D_e	1.73	1.35	1.32	1.56
D_{RM}/D_e	0.53	0.70	0.73	0.77

curve, i.e., in Kronig's notation,

$$U(\rho) = -a\cdot\tanh((\rho+c)/d) - b\cdot\mathrm{sech}^2((\rho+c)/d),$$

which has four adjustable parameters, is no improvement, in the present circumstances, upon Eq. (4). Solved on the basis of $U'(r_e)$, $U''(r_e)$, $U'''(r_e)$, and $U^{iv}(r_e)$, it leads to precisely the same results as the latter, with the meaningless equation for c, $\tanh((0.917+c)/3.08) = 3.98$.

Lotmar[18] has discussed the use of the Rosen-Morse curve and has given the solutions for A, C, and d on the basis of $U''(r_e)$, $U'''(r_e)$, and D_e. This, then, is a fourth way of fitting the constants. That it is not a suitable treatment for the present cases is shown by the results for HF where it leads to $\tanh(r_e/d) = 1.56$; thus, it fails to define a real value for r_e, the equilibrium internuclear distance. Lotmar also gives an independent formula for D_e; this is based on the value obtained for $\omega_e x_e$ when the Rosen-Morse potential is inserted in the Schrödinger equation for a vibrator. Although it is a somewhat clumsy expression, it appeared of interest to test it and, in particular, to compare it with the value of D_e calculated in the same way from the Morse function, i.e., $D_{Morse} = \omega_e/4x_e$. Lotmar indicates too an empirical expression for D_e which arose from Rosen and Morse's solution of the Schrödinger equation but which was in error by a numerical factor. This empirical value, D_{RM}, whilst better than D_{Lotmar}, is not, contrary to what Lotmar suggests, any improvement upon D_{Morse}. These values are compared in Table VIII by their ratios to the correct D_e.

PÖSCHL-TELLER FUNCTION

From the alternative approaches explored here it appears that the Rosen-Morse function is no improvement upon the simpler Morse equation for these molecules. The clearest expression of this unsuitability is the tendency for $\tanh(r_e/d) > 1$. Lotmar indicates that this will occur when the real potential curve is more unsymmetrical than that given by the Morse function. In such instances, the appropriate hyperbolic form is that given by Pöschl and Teller.[19] Thus we write

$$U(r) = M\cdot\mathrm{csch}^2(r/d) - N\cdot\mathrm{sech}^2(r/d).$$

And the following relations are found:

$$\tanh^4(r_e/d) = M/N = y^4, \text{ (say)}.$$

$$U''(r_e) = 8N/d^2\cdot(1-y^2)^2,$$
$$U'''(r_e) = -24N/yd^3\cdot(1-y^2)(1-y^4),$$
$$U^{iv}(r_e) = 8/d^4\cdot\{15(MN)^{\frac{1}{2}}\cdot((1-y^4)/y^2)^2 - 32N(1-y^2)^2\},$$
$$D_e = N(1-y^2)^2.$$

In terms of the observed r_e, $U''(r_e)$, and D_e, explicit solution follows readily from

$$d^2 = 8D_e/U''(r_e),$$
$$y = \tanh(r_e/d),$$
$$N = D_e/(1-y^2)^2.$$

The values thus calculated are given in Table IX. Apart from those for HBr, the figures in the last two rows show, on the average, slightly better concordance than is obtainable with the simple Morse equation. This suggests that the Pöschl-Teller function is able to represent the spectroscopic constants, up to the stage considered, somewhat more accurately than any of the other relations tested here. It should be emphasized that the function contains no more arbitrary constants than the simple Morse equation and, although its higher derivatives are more cumbersome, its numerical handling is not difficult. Substituted in the Schrödinger equation it leads to practically the same satisfactory solution for the vibrational energy levels as the simple Morse function. Thus it would scarcely be distinguishable from the latter by the test made in Table VIII. In this respect again it is nearer the experimental relations than the Rosen-Morse function, for which the expansion of E_v in terms of $(v+\frac{1}{2})$—see Lotmar—does not close with the $(v+\frac{1}{2})^2$ term.

TABLE IX.

Molecule	HF	HCl	HBr	HI
$d\cdot10^8$	0.93_8	1.07_2	1.11_0	1.15_2
$M\cdot10^{12}$	18.03	36.6_4	46.5_4	66.1
$N\cdot10^{12}$	56.4	77.0	87.2	108.3
$U'''(r_e)/U_e'''(r_e)$	0.86	1.03_1	1.09	1.06
$U^{iv}(r_e)/U_e^{iv}(r_e)$	0.63	0.98_3	1.12	0.99

Although the foregoing is numerically the easiest and, partly for that reason, the most satisfactory means of fitting the simple version of the Pöschl-Teller function to the present data, the results of an alternative method may also be given. With the values of d quoted in Table IX as a first approximation, successive adjustment of that factor can be made to provide values of the parameters which satisfy the observed $U'(r_e)$, $U''(r_e)$, and $U'''(r_e)$. The two terms D_e and $U^{iv}(r_e)$ then provide independent tests of the constants so chosen. The same process can, of course, be applied to the simple Morse function itself, i.e., a and D_e can be calcu-

[18] W. Lotmar, Zeits. f. Physik **93**, 528 (1935).

[19] G. Pöschl and E. Teller. Zeits. f. Physik **83**, 143 (1933).

lated from $U''(r_e)=2a^2\cdot D_e$: $U'''(r_e)=-6a^3\cdot D_e$. The first five rows in Table X refer to the Pöschl-Teller function treated in this way, and the last three rows to the Morse function. Compared on this basis, the Pöschl-Teller function reproduces $U^{iv}(r_e)$, and, hence, the curvature near r_e the more accurately, but there is the suggestion (HCl and HBr) that it extrapolates to a slightly poorer value of D_e than the simple Morse equation. Part of this second result is probably due to the poorer self-consistency of the $P-T$ curve constants when determined by the (at most two) successive approximations used here, but some of the superiority of the Morse D_e's based on $U'(r_e)$, $U''(r_e)$, and $U'''(r_e)$ in HCl and HBr is real.

Nearly all the spectroscopic constants for these molecules are based on limited series of rotational and vibrational features in the infra-red; the D_e values are derived via a number of thermal measurements and may possibly be in error by some parts per thousand, if not by more than one percent. Thus a more detailed comparison of the present or of more elaborate potential functions is probably not justified in these instances by the over-all accuracy of the data or of the assumptions involved in the treatment. It is clear that the simple Morse and the Pöschl-Teller functions are far the most satisfactory, with the latter holding a slight advantage.

TABLE X.

Molecule	HF	HCl	HBr	HI
$d\cdot 10^8$	0.78_2	1.10_6	1.21_0	1.22_6
$M\cdot 10^{12}$	33.4	32.4	33.7	51.6
$N\cdot 10^{12}$	72.3	72.2	73.1	92.4
D_e(calc)/D_e(obs.)	0.70	1.06	1.18	1.13
$U^{iv}(r_e)/U_e^{iv}(r_e)$	0.83	0.94	0.97	0.91
a(Morse)$\cdot 10^{-8}$	2.59_5	1.84_1	1.69_0	1.64_5
D_e(Morse)/D_e(obs.)	0.67	1.03	1.13	1.12
$U^{iv}(r_e)/U_e^{iv}(r_e)$	0.79	0.89	0.93	0.87

THE JOURNAL OF CHEMICAL PHYSICS VOLUME 17, NUMBER 4 APRIL, 1949

Hydrogen Peroxide in the Thermal Hydrogen Oxygen Reaction
I. Thermal Decomposition of Hydrogen Peroxide

C. K. McLANE*
Lyman Laboratory of Physics, Harvard University, Cambridge, Massachusetts
(Received September 13, 1948)

The decomposition of hydrogen peroxide (at partial pressures of one to two millimeters of mercury) was studied in the presence of one atmosphere of oxygen or nitrogen by the use of a flow system. The concentration of H_2O_2 was measured photometrically, using the continuous ultraviolet absorption of this compound. Determination by this means was more rapid, and offered less chance for errors of manipulation than conventional chemical analysis. A first order reaction with an activation energy of 40 kcal./mole was found in the neighborhood of 520°C. Evidence is presented to support the conclusion that the reaction is partly, at least, homogeneous in boric acid treated vessels at temperatures in the 470 to 540°C range.

I. INTRODUCTION

HYDROGEN peroxide was first found as one of the products of combustion of hydrogen in 1882 by Schuller.[1] In 1930, Pease[2] showed that this compound appeared among the frozen-out products of the near third limit steady reaction of hydrogen and oxygen, and in 1947, Holt and Oldenberg[3] detected it spectroscopically in the smoothly reacting mixture of these gases at temperatures near 540°C. This was surprising in view of the low thermal stability of this compound, and hence it aroused interest in a determination of the lifetime of hydrogen peroxide at these temperatures. It also became desirable to find out as much as possible about the reaction of hydrogen peroxide with hydrogen gas and to see whether decomposing hydrogen peroxide could initiate chains in the near third limit hydrogen oxygen reaction as suggested by von Elbe and Lewis.[4] Papers on the last two topics will be submitted in the near future.

A search of the literature revealed a considerable amount of work done on the thermal decomposition of hydrogen peroxide vapor; however, in no case was any homogeneous reaction observed. Baker and Ouellet,[5] Mackenzie and Ritchie,[6] and Giguère,[7] who did the most recent and extensive work, confirmed the reports of other investigators that this reaction showed an extreme sensitivity to the character of the surface of the reaction vessel, and found

* Present address: Department of Physics, University of Wisconsin, Madison 6, Wisconsin.
[1] A. Schuller, Chem. Centr. (1882), p. 281.
[2] R. N. Pease, J. Am. Chem. Soc. **52**, 5106 (1930).
[3] R. B. Holt and O. Oldenberg, Phys. Rev. **71**, 479 (1947).
[4] G. von Elbe and B. Lewis, J. Chem. Phys. **10**, 366 (1942).
[5] Baker and Ouellet, Can. J. Research **23B**, 167 (1945).
[6] Mackenzie and Ritchie, Proc. Roy. Soc. **A185**, 207 (1946).
[7] Giguère, Can. J. Research **25B**, 135 (1947).

that it was difficult, if not impossible, to prepare two reaction vessels which gave the same rate constants.

A process for commercial synthesis of hydrogen peroxide from the elements, patented by G. A. Cook,[8] utilized reaction vessels coated with boric acid or borates to improve yields by decreasing the rate of surface decomposition of peroxide. This suggested that more reproducible surfaces, or possibly even the elimination of surface reaction, might be achieved by applying some such coating. The best coatings for the present purpose were obtained by rinsing the clean, dry vessel with a saturated solution of reagent grade crystalline boric acid in 95 percent ethyl alcohol, then drying with air. After ten minutes to one hour in an oven at 200°C to remove the balance of the solvent, the vessel was allowed to remain overnight at 500–520°C in the electric furnace in which the experimental runs were to be made. A stream of oxygen or nitrogen, saturated with the vapor of 90 percent hydrogen peroxide at room temperature, was then passed at 0.5 *l*/min. for a period of one to four hours, until the concentration of hydrogen peroxide in the effluent gas reached its maximum value and remained constant there.

With such coatings, the decomposition of hydrogen peroxide was found to be far less rapid than in uncoated Pyrex, and the reproducibility of rates was found to be far better. In fact, it was found possible to obtain consistent results with different vessels or with the same vessel upon cleaning and recoating by this procedure. The reproducibility of surfaces thus achieved made it possible to study the reaction in a flow system in which concentrations were measured at room temperature, before and after the gas had passed through the reaction vessel in the furnace.

II. EXPERIMENTAL METHOD

It was evident from the beginning that the decomposition of hydrogen peroxide at the high temperatures of interest to this study would be too fast to employ any sort of static system such as those used by previous workers. It was therefore decided to use a flow system. A discussion of the applicable rate equations, and of the problem of diffusion in a reaction vessel will be given in the following section.

In the system employed, a stream of tank oxygen or nitrogen, measured with a capillary flowmeter, was passed through a loose plug of fine glass wool to filter out any possible dust particles, then saturated with hydrogen peroxide. The latter was accomplished by passing the gas twice through 90 percent aqueous H_2O_2 kept at room temperature. The partial pressure of hydrogen peroxide in the saturated gas was about 1.5 mm Hg. This was determined by freezing out the condensible fraction of a known volume of gas in a trap cooled to dry ice temperature and titrating the condensate with permanganate according to the accepted procedure.

For routine work, it was found that this analytical procedure was far too slow to permit obtaining even a moderately sufficient amount of data. Consequently, the saturated gas stream was passed through a six-foot absorption cell in a photometer which measured the concentration of hydrogen peroxide by determining the optical density at 2536A. At this wave-length, the continuous ultraviolet absorption by this compound was found to follow Beer's law quite exactly, and the absorption coefficient determined with this apparatus was within 1.5 percent of the value published by Holt, McLane, and Oldenberg.[9]

The photometer source was a germicidal lamp (low pressure, low temperature discharge through mercury vapor) from which the unwanted wavelengths were removed by filtering the light through ten centimeters of chlorine gas at one atmosphere pressure,[10] and three centimeters of a nickel and cobalt sulfate solution.[11] The latter effectively removes the visible and infra-red, beginning at 3660A, hence overlapping the chlorine filter.

This source was operated from a Sola voltage regulating transformer, which greatly reduced, but did not entirely eliminate the effects of line voltage variation. The optical transmissions of the gaseous mixtures could be measured with this photometer to an estimated accuracy of at least one percent. Translated into terms of concentration error by the use of Beer's law, this one percent error means a possible error in concentration of 3 to 10 percent in the range employed in this work. Though such an error seems large, it is of about the same order of magnitude as the largest scatter experimentally observed due to imperfections in the boric oxide coatings.

Measurement of intensities was made in the photometer with an ultraviolet sensitive photomultiplier (RCA type 1P28). Radio 'B' batteries were used to supply 90 volts per stage and 135 volts, which resulted in saturation, on the anode. The dark current, which was about 1–2 percent of the full scale deflection of about one microampere, was subtracted from all readings. The light aperture in the photomultiplier housing was normally closed by

[8] U. S. 2,368,640 and 2,368,806.

[9] Holt, McLane, and Oldenberg, J. Chem. Phys. 16, 225 (1948).

[10] Designed according to absorption coefficient data in Landolt-Börnstein (Physikalische-Chemische Tabellen, 5. Auflage, Springer, Berlin, 1923, Hw II, 893) to transmit better than 75 percent at 2536A, about 25 percent at 2650A, which is already very weak in this source, and to completely remove the lines from 2800A to and including 3660A.

[11] F. Daniels, J. H. Mathews, and J. W. Williams, *Experimental Physical Chemistry* (McGraw-Hill Book Company, Inc., New York, 1941), p. 396.

a magnetic shutter, so that fatigue effects would be minimized.

From the first absorption tube, where the concentration of the hydrogen peroxide in the saturated gas was determined, the gas flowed through the reaction vessel in the furnace. The furnace temperature could be controlled by its phase-shift thyratron regulator[12] to within 0.1–0.2°C at the operating temperatures of 470 to 540°C; in practice, however, variations of 0.5 degree during a run, caused by starting and stopping the gas flow through the reaction vessel, were common. Over the several months during which the experiments were done, the maximum variation in temperature corresponding to any particular bridge setting was not more than 1–2°C. Temperatures were measured by chromel-P alumel thermocouples which were standardized at the freezing point of zinc by the method recommended by the National Bureau of Standards.

In order that some indication of the extent of surface reaction might be obtained, two sets of reaction vessels with different surface to volume ratios were used. All vessels had identical inlet and outlet tubes of 5-mm O. D. Pyrex tubing, in order that the effect of reaction occurring in these tubes could be eliminated from the final results by the method to be outlined in the next section. A test with an inserted thermocouple showed that the gas came to temperature equilibrium with the furnace after passing through the inlet tube ($15\frac{1}{2}$ inches in over-all length, of which 10 inches were within the furnace cavity).

In the first series of six vessels, the duration of the reaction time was varied by using reaction volumes of various lengths of 8-mm O. D. Pyrex tubing, connected by U-bends and nested together compactly so that the whole could be inserted through the $1\frac{1}{8}$-inch opening in the top of the furnace. The volumes, which were measured by filling the vessels from a calibrated pipet, or by weighing the contained water, were between 9.5 and 31.2 ml. In this series of vessels, as will be shown in the next section, longitudinal diffusion can be neglected for all practical purposes. Therefore the element of reaction time can be calculated as the volume element divided by the volume rate of flow, and the rate equations for a reaction system in which no change of volume takes place assume their familiar form. This series of vessels had a surface to volume ratio of approximately 7 cm^{-1}.

It was next desirable to have a set of vessels with a smaller surface to volume ratio. The effect of diffusion is such that it can no longer be neglected in vessels of much larger diameter than those of the first set, described above. To produce well defined conditions in the lower surface vessel, it was therefore necessary to secure complete uniformity of composition of the gas in the reaction volume. (This called for the application of a different form of the rate equation.) The reaction volume of this vessel consisted of a bulb about 2.5 cm in diameter and 4.3 cm in length. The gases were admitted as a jet directed away from the outlet tube, such as to secure as nearly complete mixing as possible. This mixing aided diffusion in the approach to uniform composition in the reaction volume. The effect of reaction occurring in the inlet and outlet tubes was eliminated with the help of control experiments done in a vessel with identical inlet and outlet tubes, but with no reaction bulb (see discussion in the next section). The surface to volume ratio of the reaction bulb in the first of these vessels was approximately 3 cm^{-1}.

From the reaction vessel, the gases were led into a second absorption tube in the photometer, identical with the first, in which the concentration of peroxide in the effluent gas was measured. From this point back to and including the saturators, the entire system was constructed of Pyrex glass with the exception of the windows of the absorption tubes, which were of quartz, and which were held in place on the flanged absorption tubes with a minimum quantity of paraffin. There was only one stopcock in the system beyond the saturators, and this was used as a bypass around the reaction vessel in the furnace. It was lubricated with Apiezon *L* grease. Standard taper joints were used, unlubricated, to permit easy interchange of reaction vessels. No decomposition was observed when peroxide vapor was allowed to stand in the absorption tubes for a time long as compared with its time of flow through the entire system.

III. MATHEMATICAL PART

Three topics will be discussed in this section: (1) the effect of volume change in the reaction on the kinetic equations, (2) the effect of diffusion on the degree of reaction in a flowing system, and (3) the method used for eliminating the effect of reaction occurring in the inlet and outlet tubes of the reaction vessel, where the temperature is not uniform.

The 50 percent volume change in the reaction:

$$H_2O_2 = H_2O + \tfrac{1}{2}O_2$$

when carried out at constant pressure, is completely masked in the present work by the approximately 500 to 1 excess of inert gas which is always present. The effect of change of volume on the definition of concentration units may therefore be neglected here.

The treatment of longitudinal diffusion will be essentially the same as that given by H. M. Hulburt.[13] Radial diffusion will be of importance

[12] For design of regulator used, see D. Bancroft, Rev. Sci. Inst. **13**, 24, 114 (1942).

[13] H. M. Hulburt, Ind. Eng. Chem. **36**, 1012 (1944); **37**, 1063 (1945).

only if the reaction is occurring at the surface, and then only if such diffusion is rate limiting. Since in the higher surface vessels the time of diffusion, $R^2/2D$, is small compared to the half period of the reaction, $0.693/k$, it is not necessary to consider radial diffusion. If a heterogeneous reaction were being observed, and diffusion became rate limiting in the lower surface vessel, this would only enhance the dependence of rate constant on vessel size.

Anticipating the result to be obtained, that the reaction is of the first order, the treatment of a simultaneously flowing, diffusing, and chemically reacting system was made for this case. The solution of the general differential equation given by Hulburt is, then

$$\frac{c(x)}{c_0}=\exp\frac{v_0}{2D}\left\{1-\left(1+\frac{4kD}{v_0^2}\right)^{\frac{1}{2}}\right\}x \qquad (1)$$

where $c(x)$ is the concentration of peroxide at a distance x along the reaction tube, c_0 is the input concentration, v_0 is the linear velocity of the gas, k is the first order reaction rate constant, and D is the diffusion coefficient. Equation (1) differs from the corresponding equation obtained by Hulburt in that one boundary condition used here ($\lim_{x\to\infty} c(x)=0$) differs from that used by Hulburt ($(\partial c/\partial x)_l=0$, where l represents the value of x where the reaction tube is constricted to the size of the outlet tube). Neither condition is strictly correct, since the reaction neither stops completely nor continues at the same rate at this point. The second boundary condition in both cases is, of course, that $c(0)=c_0$.

Application of Eq. (1) to estimate the effect of longitudinal diffusion requires knowledge of the orders of magnitude of k, v_0, x, and D. The first three of these were taken from the experimental data obtained in preliminary runs, and values of D were calculated from Langevin's formula[14] using the molecular weight of hydrogen peroxide, and the cross section of water (this being smaller than the corresponding quantity for hydrogen peroxide, the diffusion coefficient will be too large; since an upper limit is sought, an error in this direction will not be serious). If D is assumed to vary as the 7/4 power of the absolute temperature, it may be extrapolated from 288°K, where cross section values are tabulated, to 800°K, the approximate temperature of this work. By this method, D for hydrogen peroxide diffusing through air at 800°K is calculated to be roughly 1.2.

TABLE I. Study of effect of gas flow rate on hydrogen peroxide decomposition in vessels with lowest S/V ratio. (Nitrogen used as inert diluent.)

Furnace temperature °K	Rate constant k, sec.$^{-1}$	Flow rate l/min.
774	0.46	0.31
774	0.46	0.40
774	0.44	0.50
774	0.48	0.57
794	1.17	0.31
794	1.02	0.40
794	0.98	0.50
794	0.95	0.57

[14] See, for example, E. H. Kennard, *Kinetic Theory of Gases* (McGraw-Hill Book Company, Inc., New York, 1938), pp. 190–194.

If diffusion were completely absent, the appropriate rate equation would be

$$c(x)/c_0=\exp(-kx/v_0). \qquad (2)$$

Using the value of D estimated above, and the experimental orders of magnitude for all other quantities appearing in Eqs. (1) and (2), it is found that these two equations give values of $c(x)/c_0$ which are the same to within 0.2 percent for the first series of vessels (those for which the surface to volume ratio is roughly 7 cm^{-1}). It follows that the effect of diffusion is entirely negligible in these particular vessels.

A calculation of the Reynolds number for the conditions of flow in the first series of vessels (surface to volume ratio approximately 7 cm^{-1}) showed that this quantity was far below its critical value (by a factor of 20 or more). It was concluded that turbulence of flow could not be a very important factor, even though these vessels are not the long straight tubes required for accurate application of the Reynolds criterion.

Quite different, however, is the case of the lower surface vessel. Here the effect of diffusion is too large to be neglected, but insufficient to result in uniform composition within the bulb. Therefore, the mixing caused by the jet of incoming gas will be of importance. The extent of this mixing will depend on the velocity of flow, and hence examination of the dependence of the observed rate constant on flow velocity is indicated. The rate constant should be found to be independent of the flow velocity over the range in which uniform composition is achieved. In practice, the rate constant was independent of flow velocity except for a rapid reaction and low flow rate at high temperature (Table I). Hence it is probable that uniform composition was achieved.

The last topic of this section concerns the method of eliminating the effect of reaction in tubes leading into and out of the furnace. An expression for the amount of reaction occurring in these tubes will first be derived and this will be applied to two cases of the determination of the first order rate constant, i.e., with the vessels of higher and lower specific surface.

The rate equation for the first order is

$$dc/c=-kAT_R dx/T_x F_0. \qquad (3)$$

Here the element of time, dt, has been expressed in terms of the cross-sectional area of the inlet tube, A, the distance along this tube, x, the room temperature, T_R, and the temperature at the point x, T_x. The temperature dependence of the concentrations on the left side, being a factor common to dc and c, will cancel, and (3) may be integrated along the inlet tube to give

$$\ln(c_i'/c_i) = -\phi_i \tag{4}$$

where ϕ_i is a constant for constant flow rate and temperature conditions, and with the same construction of the inlet tube maintained through the series of vessels. c_i and c_i' are the concentrations of peroxide at the beginning and end, respectively, of the inlet tube.

It is obvious that an exactly similar equation can be derived for the outlet tube. If the two equations are added and rearranged, the result is

$$\ln(c_f/c_i) - \ln(c_f'/c_i') = \text{constant} \tag{5}$$

where subscripts 'f' indicate concentrations in the outlet tube. This equation is very useful, in that it shows that $\ln(c_f/c_i)$, which consists only of measurable quantities, differs from $\ln(c_f'/c_i')$, which is simply and directly related to the rate constant, by a constant.

We shall consider first the application of Eq. (5) to the higher surface vessels, in which longitudinal diffusion has been shown to be negligible and the reaction time is varied by varying the length of tubing constituting the reaction volume. For this case

$$\ln(c_f'/c_i') = -kt_r' \tag{6}$$

$$= -kt_r + \text{constant} \tag{6'}$$

where t_r' is the time of residence of the gas in the reaction volume enclosed between the end of the inlet, and beginning of the outlet, tubes. But this volume differs from the total volume of the reaction vessel only by the constant volume of the inlet and outlet tubes. Hence the second form, (6'), where t_r is a defined time of reaction given by the total volume of the reaction vessel divided by the volume rate of flow, corrected from room temperature, where it is measured, to the temperature of the furnace. Substituting (6') in (5), we obtain the desired rate equation for use with the series of reaction vessels in which diffusion is negligible:

$$\ln(c_f/c_i) = -kt_r + \text{constant}. \tag{7}$$

It is now necessary to obtain the rate equation for use with the lower surface vessel, in which uniform composition in the reaction volume is assumed. This is obtained by setting up a material balance on the peroxide entering, decomposing in, and leaving the reaction bulb of volume, V. The result is

$$c_f'/c_i' = (1 + VkT_R/F_0T_F)^{-1} \tag{8}$$

where T_R and T_F are room and furnace temperatures, respectively, k is the first order rate constant, and F_0 is the volume rate of flow, measured at T_R. In this case, it is not possible simultaneously to vary the reaction volume, keep the surface to volume ratio constant, and retain a shape in which uniform composition can be readily obtained. Therefore, a vessel was constructed which had no reaction bulb, i.e., in which $V=0$, but which had inlet and outlet tubes identical to those in the previously mentioned vessel. For this vessel, $c_f'/c_i' = 1$, and the constant in Eq. (5) will be the same as for the vessel in which $V \neq 0$, because of the identical construction of inlet and outlet tubes. Letting c_f/c_i as measured with the vessel in which $V=0$ be designated by subscript "0", we obtain by use of (5) and (8):

$$(c_f/c_i)(1 + VkT_R/F_0T_F) = (c_f/c_i)_0. \tag{9}$$

Solving for k:

$$k = (c_f/c_i)^{-1}[(c_f/c_i)_0 - (c_f/c_i)]F_0T_F/VT_R. \tag{10}$$

TABLE II. Summary of rate constants for hydrogen peroxide decomposition (gas flow rate, 0.5 l/min.).

Furnace temp. °K	Gas	Rate constant, k Higher surface	Lower surface
740	N_2	0.184	0.11
758	N_2	0.349	0.27
762	N_2	0.324	—
773	N_2	0.502	0.50
782	N_2	0.80	—
794	N_2	1.19	1.11
762	O_2	0.308	—
773	O_2	0.383	0.21
782	O_2	0.62	—
794	O_2	0.89	0.71
815	O_2	1.61	3.0

IV. EXPERIMENTAL RESULTS

As explained in Section I, an effort is being made here to minimize surface reaction by a suitable coating procedure. Since any inferior coating gives large deviations in the direction of too much decomposition, it is apparent that the errors will be largely one sided in nature and that least squares treatment of the data would give far from the "best fit." It was noticed that the results obtained with any one vessel tended to converge toward a common limit in the direction of least decomposition. Examination of the results as obtained with the higher surface vessels will show that these "upper points" tend to approach a straight line in the plot of *$\log c_f/c_i$ versus the time* (cf. Eq. (7)). This vindicates the assumption made in deriving this equation that the decomposition is of the first order. Error incurred in drawing the lines in by sight is undoubtedly

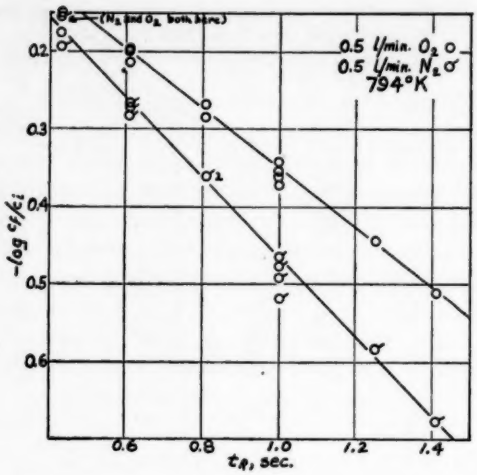

FIG. 1. Typical first order rate plots of the experimental data on the decomposition of hydrogen peroxide vapor.

smaller than experimental errors due to such causes as inferior coatings.

Space limitations do not permit inclusion of all the plots of Eq. (7) which were made, but Fig. 1 may be taken as typical. All the data used in plotting Fig. 1, and in obtaining the rate constants summarized in Table II were taken with a gas flow rate of 0.5 *l*/min., measured at room temperature. That this specialization did not seriously impair the validity of the results may be seen from Fig. 2, which includes data taken at several different flow rates. Figure 2 also shows that the effect of flow rate on the additive constant in Eq. (7) cannot be very large.

The rate constants summarized in Table II show that the reaction may be somewhat accelerated by the surface, but the rate is not strongly dependent on the surface to volume ratio. The results with the lower surface vessel cannot be regarded as being so reliable as those with the higher surface vessels, since really complete uniformity of composition in the reaction volume of the former cannot be unequivocally proven, and since the results depend on data taken with only two vessels. Some early results with very narrow vessels (surface to volume ratio of about 12 cm^{-1}) gave rate constants very nearly equal to those obtained with the higher surface vessels of Table II, but since at the time, difficulty was experienced in obtaining reproducible boric oxide coatings, the data so obtained are not deemed sufficiently reliable for inclusion here.

The logarithms of the constants obtained with the higher surface vessels are plotted against $1000/T$ in Fig. 3. The straight lines were calculated by the method of least squares, and are given by the following equations:

$$\textit{Oxygen:} \quad \log k = -8760/T + 10.961; \qquad (11)$$

$$\textit{Nitrogen:} \quad \log k = -8660/T + 11.150. \qquad (12)$$

Within experimental error, the slopes of both these lines correspond to an activation energy of 40 kcal./mole, and hence it may be concluded that the same rate controlling step is operative in both cases, even though the rates are somewhat higher in nitrogen.

This activation energy is too small by 13 kcal./mole for the reaction:

$$H_2O_2 + M = 2OH + M \quad \Delta H = 53 \text{ kcal.}^{7}$$

Therefore, if this is the important reaction, it must be assumed that there is enough surface reaction of considerably lower activation energy occurring simultaneously to lower the activation energy to the observed value. The curvature of the *logk versus 1000/T* plot which would occur with two simultaneous reactions of different activation energy might well be unobservable in the relatively small temperature range available here and with the rather large experimental errors involved. It does not seem to be reasonable in view of the observed rather small surface effect to conclude that the reaction is taking place exclusively at the surface with a heat of adsorption effect of at least 13 kcal./mole.

If a *logk versus 1000/T* plot is made of the results obtained with H_2O_2 in nitrogen in the lower surface vessel, a rather good straight line is obtained with a slope corresponding to an activation energy of 50 kcal./mole. This agrees with the suggested decomposition of the peroxide molecule into two hydroxyl radicals. In the low surface vessels, relatively more of the reaction would take place in the gas phase, thus causing a higher activation energy to be observed. Insufficient data were collected with H_2O_2 in oxygen in the lower surface vessel to warrant a similar treatment.

The observed activation energy was larger than the endothermic heat of reaction for:

$$H_2O_2 + M = H_2O + O + M \quad \Delta H = 35 \text{ kcal.}^{15}$$

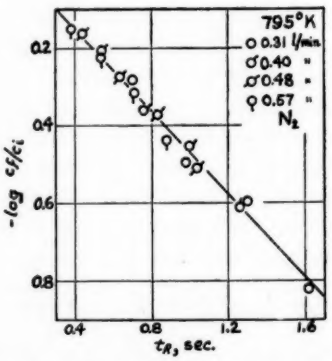

FIG. 2. Effect of flow rate on the rate of decomposition of hydrogen peroxide in the higher surface vessels.

[15] Calculated from the thermochemical data summarized by Giguère, see reference 7.

This mechanism, however, would require a considerable distortion of the peroxide molecule to reach an activated state which might decompose to the indicated products.[16] The result would be an activation energy higher than the endothermic heat of reaction, and possibly a small frequency factor in the rate equation.

V. CONCLUSIONS

The decomposition of hydrogen peroxide vapor at temperatures of 470 to 540°C was found to be of the first order with an activation energy of 40 kcal./mole. The dependence of rate on surface area indicates that the reaction is *not* occurring exclusively at the surface. The higher activation energy (50 kcal./mole) observed in the lower surface vessel indicates that a greater proportion of a volume reaction with higher activation energy must be occurring there. Previous investigators have found a reaction of low activation energy occurring exclusively at the surface. The present observations seem to show a transition to the volume reaction occurring at higher temperatures when reaction vessels with lower surface activities are used.

I wish to thank Professor O. Oldenberg for suggesting this problem and for his continuing interest and helpful advice on numerous points. I also wish to express my appreciation to the National Research Council for the grant of a predoctoral fellowship, which made this work possible. The financial support of the Rumford Fund of the American Academy of Arts and Sciences is gratefully acknowledged. The Buffalo Electrochemical Company generously supplied the 90 percent hydrogen peroxide used, and provided valuable information on the properties and safe handling of this material.

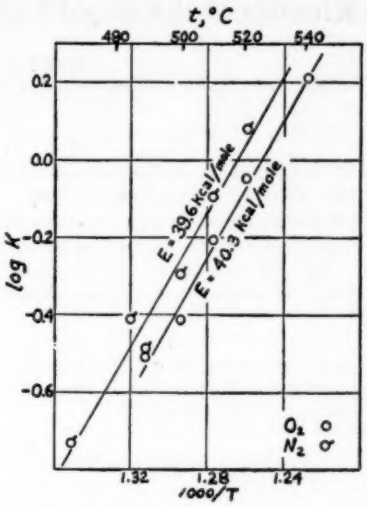

FIG. 3. Temperature dependence of rate of decomposition of hydrogen peroxide vapor in higher surface vessels.

[16] This conclusion assumes the structure of the H_2O_2 molecule given by Penney and Sutherland, J. Chem. Phys. **2**, 492 (1934).

The Kinetics of the Rapid Gas Reaction between Ozone and Nitrogen Dioxide*

HAROLD S. JOHNSTON** AND DON M. YOST
Gates and Crellin Laboratories of Chemistry, California Institute of Technology, Pasadena, California
(Received September 7, 1948)

An apparatus has been designed and constructed which will rapidly mix two gaseous reactants, isolate them in a reaction cell, and, by means of light absorption, follow the course of the reaction photoelectrically in one-tenth of a second or less. The output of the photoelectric tube is recorded by a time-exposure photograph of the screen of an oscilloscope.

The kinetics of the fast reaction between ozone and nitrogen dioxide was studied over a tenfold range of concentration of each reactant. The rate law was found to be

$$-d(O_3)/dt = k(NO_2)(O_3)$$

over the entire course of the reaction. From the temperature coefficient of the rate of reaction the energy of activation was found to be 7.0±0.6 kilo-calories per mole. A mechanism is proposed to account for the observations.

INTRODUCTION

THE rates of very rapid, non-explosive gas reactions have received attention in the recent past, but the cases studied were so rapid, for example the dissociation of nitrogen tetroxide, that very indirect and theoretically complicated methods of experimentation were required. It was deemed of interest, therefore, to study less extreme cases, and thus lay a firmer foundation for any further investigations. To this end it was decided to measure the rate of the reaction between ozone and nitrogen dioxide, which has been shown by Wulf, Daniels, and Karrer[1] to proceed quantitatively according to the equation

$$2NO_2(g)+O_3(g)=N_2O_5(g)+O_2(g). \qquad (1)$$

As an additional aspect of interest is the possibility that this reaction may be involved in the atmosphere immediately following a thunder clap.

EXPERIMENTAL METHOD

a. Method Summarized

Three streams of oxygen flowing at known rates from calibrated flowmeters were used (1) to pick up NO_2 from a saturator containing cold, liquid N_2O_4, (2) to dilute the NO_2 stream to the desired final concentration, and (3) to make ozone by passing through a silent electrical discharge tube. The two resulting streams were combined in about 0.01 sec. in a mixing chamber, and the resulting mixture was then passed immediately into a reaction cell of small, 2 mm diameter.

Through the reaction cell passed a filtered, chopped beam of light which fell on an electron multiplier photoelectric tube. The output of the photoelectric tube was put across the deflection plates of an oscilloscope which, however, was not firing its beam. After a steady state was obtained, a weight was dropped which threw a lever which, in turn, closed a stainless steel stop gate and stopped the flow of the gases; the reacting mixture was thus isolated in the reaction cell. When the stop gate closed it made electrical contact with a brush which caused the oscilloscope to give a single sweep of its beam. During this single sweep the shutter of a camera was open and caught the full sweep on one film. The final data appeared on the photographic negative as a modulated wave packet whose width was simply related to the NO_2 concentration, and whose wave-period was known precisely from the speed of the synchronous motor.

Temperature of the reacting gases was measured by a fine copper-advance thermocouple just below the outlet of the reaction cell.

b. Apparatus

Materials used in this study were compressed oxygen supplied by the Lindé Corporation, and a tank of nitrogen dioxide sold by the Matheson Company.

The flowmeter system, including ozonizer and saturator, is shown schematically in Fig. 1. Flow rates of the oxygen streams were measured by capillary flowmeters using dibutylphthalate as manometer fluid. To remove suspected impurities in the oxygen stream, it was passed through a charcoal trap and a one-liter flask full of P_4O_{10} and glass chips. Even though the vapor pressure of dibutylphthalate is extremely low, an additional charcoal and P_4O_{10} tube was placed between the flowmeter and saturator.

Reservoir bulbs were included to smooth out any instantaneous fluctuations in the output of the ozonizer or saturator and to cushion the effect of

* Contribution No. 1242.
** Present address: Chemistry Department, Stanford University, California.
[1] O. R. Wulf, F. Daniels, and S. Karrer, J. Am. Chem. Soc. 44, 2398 (1922).

suddenly stopping the flow as readings were being made. In order to make calibrations, it was necessary to bypass the ozonizer and ozone reservoir bulb, or the saturator and the nitrogen dioxide bulb.

A large water-cooled ozonizer was calibrated for various flow rates and voltages by absorbing the ozone in a neutral solution of potassium iodide, which was then acidified with sulfuric acid and titrated with standardized sodium thiosulfate solution. For flow rates below 100 cc per min. the yield was 5.5 percent, essentially independent of flow rate.

The N_2O_4 saturator was an all-glass apparatus which consisted of nine tubes, each six inches long and 12 millimeters in internal diameter, mounted parallel to each other and in a horizontal plane. They were connected from below by tubes which permitted liquid N_2O_4 to flow freely from one to another. Above the ends the tubes were alternately joined in such a manner that the oxygen flowed from tube to tube over the surface of the liquid for a total distance of $4\frac{1}{2}$ feet without bubbling. A well-stirred mixture of water and ice was used as a thermostat for the saturator.

Nitrogen dioxide was passed through P_4O_{10} into the ice-cooled saturator until it was half full of liquid. At first the liquid had a trace of greenish color due to N_2O_3. This color changed to straw orange at 0°C after the liquid had been exposed to an atmosphere of oxygen for a few hours during which time the N_2O_3 was oxidized to N_2O_4. In the calibration of the saturator a stream of oxygen was blown over the liquid N_2O_4, and the vapors picked up were absorbed completely by a known volume of standardized base in a washing column which provided agitated vapor-liquid contact for about 30 seconds. The excess base was titrated with acid to the phenolphthalein end point.

Assuming the perfect gas law to apply inside the saturator, and extrapolating the work of Verhoek and Daniels[2] to get the equilibrium constant for NO_2-N_2O_4 at 0°C, the partial pressure of NO_2 plus N_2O_4 was found to be 0.356 ± 0.003 atm. in nine determinations. Giauque and Kemp[3] found 0.346 atm. as the vapor pressure of N_2O_4 at 273.1°A. Although the difference between 0.356 and 0.346 lies outside the experimental error of the analysis, this difference could easily be due to gas imperfections or to an error in extrapolation of the equilibrium constant.

As an aid to calculation, nomographs were prepared which allow immediate translation to be made from flow rates to equilibrium pressures of NO_2 and N_2O_4 at any temperature between 0°C and 35°C.

A mixing chamber shown in Fig. 2 was designed after those of Hartridge and Roughton.[4] It was of all-glass construction with four tangential jets on the perimeter of the cylinder, which was 1-mm high and 18 mm in diameter. Mixed gases flowed out of a 2-mm diameter tube co-axial with the mixing cylinder. From the weight of mercury required to fill the mixing chamber and exit tube, the total volume was found to be 0.20 cc. By means of an experiment devised to measure the very fast rate of dissociation of N_2O_4[5] upon dilution with oxygen by this method, it was shown that mixing was at least 99.5 percent complete by the time the gases reached the 2-mm diameter reaction cell.

The two-holed stainless steel stop gate was such that, on suddenly moving it about 3/16 inch by means of a falling weight and a shock cushioning lever, the input and exit channels of flow were simultaneously cut off. The external synchronization circuit for the oscilloscope was a battery which charged a condenser when a key was pressed. When the plunger in the stop gate was closed, it touched a phosphor bronze brush permitting the condenser to discharge through a resistor and thereby initiate the single sweep of the oscilloscope.

The glass reaction cell was *2 mm in internal diameter* and 37 mm long. Its ends were covered with black tygon paint before the windows were sealed on, in order to prevent light from traversing the glass walls and hitting the photoelectric tube, and the light was made slightly convergent in the cell to avoid reflections from the walls. Windows of the cell, consisting of a small lens of 13 mm focal length on one end and a small square of microscope cover glass on the other, were secured by several

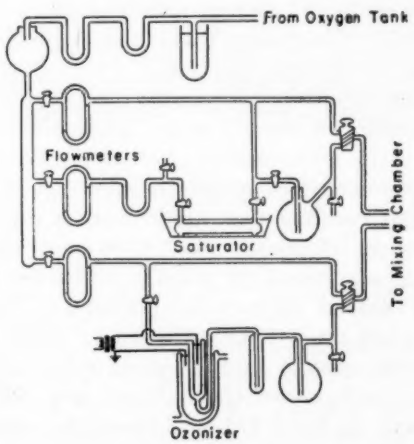

FIG. 1. Flowmeter system including saturator and ozonizer.

[2] F. H. Verhoek and F. Daniels, J. Am. Chem. Soc. **53**, 1250 (1931).
[3] W. F. Giauque and J. D. Kemp, J. Chem. Phys. **6**, 40 (1938).
[4] H. Hartridge and F. J. W. Roughton, Proc. Camb. Phil. Soc. **23**, 450 (1926).
[5] P. D. Brass and R. C. Tolman, J. Am. Chem. Soc. **54**, 1003 (1932).

layers of tygon paint. The reaction cell was fastened to the stop gate by squaring and polishing the ends of the lead-in tubes until they conformed to the countersunk portion of the stop gate, and then sealing wax was applied around the outside.

The flow system was of all-glass construction from the flowmeters to the stop gate. The only material except glass and stainless steel exposed to the corrosive action of the reactants was Dow-Corning silicone stopcock grease and tygon paint, which were attacked only slowly by these gases, very

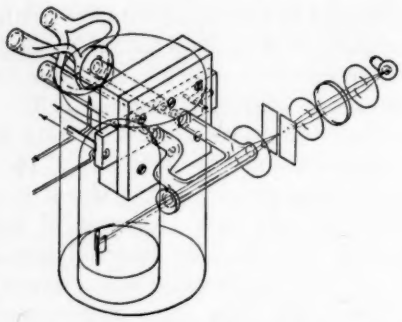

FIG. 2. Isometric projection of mixing chamber, stop gate, and 2-mm diameter reaction cell with schematic drawing of the light source, filters, and lenses.

much slower than the rate of reaction studied and also much slower than the rate of production of fresh quantities of the gases in the flow system.

The light source, shown schematically in Fig. 2, is a 500 watt General Electric projection bulb operated from storage batteries at 80.0 volts. Light was roughly collimated by a pair of condensing lenses and brought away from the hot source. It was filtered by a 1 cm path of 6 percent cupric sulfate solution in order to take out the heat rays, and by a pair of glass filters which transmitted a sharp, photochemically inactive peak between 4400 and 4800A. The beam was then focussed by a second pair of lenses on a hole 0.2 mm in diameter in a securely mounted, small piece of aluminum foil. An image of the 0.2 mm "point" source was formed by the lens-window about a cm beyond the light sensitive surface of the photoelectric tube.

The light chopper was made from a dural disk, 9½ inches in diameter and 1/16-inch thick, in which was machined 10 holes and 10 teeth equiangularly spaced around the perimeter. This disk was mounted on a 1/15 horsepower, 1800 r.p.m., synchronous motor, and it interrupted the light beam just in front of the 0.2-mm hole 300 times each second. An RCA 931-A photoelectric multiplier tube was used to measure the light emerging from the reaction cell. It was powered by a bank of 18 mini-max batteries rated at 67½ volts each. Selected pairs of 50,000-ohm wire wound resistors were combined to make a voltage divider of 10 equal steps. A 200,000-ohm potentiometer was adjusted so that at all times during the experiments the ammeter in series with the voltage divider read 0.920 ma when no light fell on the photoelectric tube. No more than a few hundredths of a milliampere flowed through the tube itself. A resistor and condenser were put in parallel across the output of the photoelectric tube in order to short out the high frequency components of the "noise" from the photoelectric tube, which was completely unusable at the low intensities employed without this filter. At these low intensities the amplitude of the wave packet on the oscilloscope screen was proportional to the intensity of the light, and this was proved in an experiment in which calibrated wire screens were put in the collimated beam of light. The oscilloscope was a DuMont type 247 with a 5-inch screen, which gave a blue light to which photograph film is quite sensitive. An Argus A-2 camera with its lens remounted and set forward was used for this work.

In this study temperature was measured rather than controlled. Temperature of the gases leaving the reaction cell was measured with a thermocouple made of 36 gauge copper and 30 gauge advance wire, protected by three coats of wire enamel. A reference junction was immersed in a well-stirred ice bath, and the potential developed by the thermocouple was read with a Leeds and Northrup portable precision potentiometer, No. 8662.

Special precautions had to be taken to reduce mechanical vibrations.

RESULTS OF THE RATE MEASUREMENTS

a. Computation of the Pressure of Reactants

From a knowledge of the flow rates of the oxygen streams, the calibrations of the saturator and the ozonizer, and the temperature, streams of different known NO_2 concentration were made up for calibration purposes and for rate experiments. The system was calibrated by trapping streams of known NO_2 concentration in the reaction cell, and the light transmission which was registered on the oscilloscope was photographed. Before and after such tests, pure oxygen was similarly analyzed to give a measure of the light intensity I_0. An example of a photograph of the oscilloscope screen for an O_2 blank and an NO_2 blank is shown in Fig. 3. Values of the logarithm of I/I_0 obtained for various pressures are plotted in Fig. 4 against one-half the NO_2 pressure, one-half pressure being used to simplify stoichiometric calculations. It can be seen that, with the filters and pressures of NO_2 used, Beer's law is obeyed. From the calibration curve, Fig. 4, the sensitivity of the apparatus can be seen to be about 1×10^{-4} atmosphere of NO_2, and the most efficient working range is between 1 and 10 milliatmospheres.

In a rate experiment, pictures were made respectively of (1) pure O_2 alone, (2) NO_2 diluted by the full amount of O_2 used in the experiment, (3) three or more actual runs with O_2, NO_2, and O_3 with different velocities of the oscilloscope beam across the screen, and finally (2) and (1) again. Examples of the form of the data obtained are shown in Fig. 3. Temperature of the thermocouple junction was read at each stage of the run. The film, plus X, was developed in Defender 777 fine grain developer to a gamma of 1.2.

The traces on the film were projected by a microfilm reader on a sheet of white paper, details of the upper and lower edges were drawn, and the time scale marked and labeled. Upon removal of the paper, a smooth curve was drawn through the slightly ragged edges, and the width of the envelope was measured for each 1/300 sec. The edges were ragged in some cases due to mechanical vibrations from the falling weight, and some scatter was due to random variation in the output of the photoelectric tube.

From an analysis of the O_2 and NO_2 blanks, a portion of the data was found to have as much as two percent distortion. Correction curves for distortion were made from the O_2 and NO_2 blanks, and in view of the fact that these correction curves were reproduced almost identically for different blank runs, it can be stated that distortion was not an important source of error in the final results. A less satisfactorily handled source of error in this work was the drift of I_0 with time. An arbitrary procedure of linear interpolation with respect to the time was used. It was noted that the value of the rate constant which was calculated for a given experiment is very sensitive to the value of I_0 used, and greater precision might be attained if this source of uncertainty were reduced.

The pressure of NO_2, divided by two, was obtained from the value of I/I_0 and Fig. 4. A knowledge of the pressure of NO_2 and the temperature —and thus the equilibrium constant—permitted the calculation of the actual pressure of N_2O_4, and the total formal pressure of N_2O_4. The pressure of O_3 was found from its known initial value and by difference in the total formal N_2O_4 pressure from its initial value, for Wulf, Daniels, and Karrer[1] showed that the reaction between ozone and nitrogen dioxide is given quantitatively by the chemical equation

$$2NO_2+O_3=N_2O_5+O_2. \qquad (1)$$

Thus, for each experiment, there was tabulated opposite the time from the start of observations a column for the pressures of $NO_2/2$, N_2O_4, $(NO_2/2+N_2O_4)$, and O_3. An abbreviated but illustrative example is presented in Table I.

b. Differential Rate Equation

The following abbreviations are defined, all pressure units being milliatmospheres; x=pressure of NO_2, y=pressure of N_2O_4, z=pressure of O_3, c=total formal pressure of $N_2O_4=x/2+y$. The subscript zero will refer to the initial pressure at the start of the reaction upon mixing, not to the first observation.

The rate of the reaction was calculated by the differential method between two values of the O_3 pressure 1/300 sec. or in some cases 1/60 sec. apart. One column in Table I illustrates this procedure for one experiment, and in a similar fashion the average rate of reaction was computed for the other 42 runs made in this study. An inspection of the tables of the reaction rate lead to the hypothesis that the rate law is

$$-dz/dt=kxz, \qquad (2)$$

that is, the rate of disappearance of O_3 is proportional to the product of the pressures of NO_2 and O_3. To test this hypothesis the average rate obtained for a short interval was divided by the average value of x and z observed at the beginning

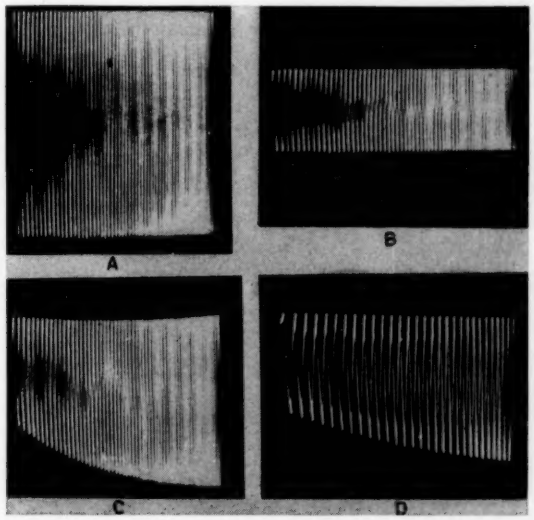

FIG. 3. Examples of photographs of the oscilloscope screen. Respectively, A to D, O_2 blank, NO_2 blank, and two actual runs.

and end of the interval, as is illustrated in the last column on Table I.

Though the individual, instantaneous values scatter fairly seriously, there is no trend in the values of k down the column. Similarly the values of k for the other experiments were computed, and these are tabulated as group averages in Table II-A which summarizes the runs made at room temperature, 21±1°C, and in Table II-B which shows the rate constants found at different temperatures. The initial values of c and z each vary over a factor of

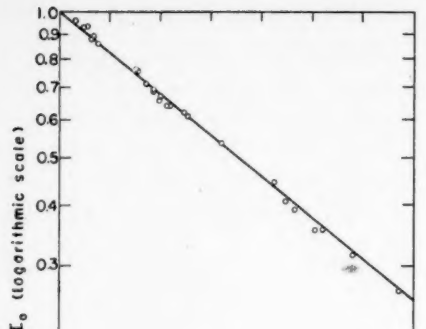

FIG. 4. Calibration of the reaction cell and the photoelectric circuit.

about 10, and the ratio of c_0 to z_0 similarly covers about a 10-fold range.

At one temperature it can be seen that, with some scatter, essentially the same value of the rate constant is obtained for the various concentrations. At 21°C the average value is 3.66×10^7 cm³/mole-sec.; the standard deviation for 27 cases is 0.34 in the same units, and thus the standard error of the mean is 0.07. Hence it is seen that this method has, for a kinetic study, a high degree of precision largely by virtue of the ease of producing a large number of data. In one night, for instance, data for 500 differential rate constants were collected. The deviation of values of k from the mean were not significantly correlated with any of the variables listed in Table II. Inspection of the data showed that no other product of integral powers of the pressures of the reactants gives a satisfactory rate law, and in experiments in which a large excess of NO_2 was present it was possible to decide between kxz and $2kcz$ in favor of the former.

c. Integrated Equation

Using the observed rate equation

$$-dz/dt=kxz,$$

the equilibrium equation between NO_2 and N_2O_4

$$K=x^2/y,$$

and the stoichiometry of the reaction with respect to O_3

$$z=c+(z_0-c_0),$$

the differential equation can be expressed in terms of the initial conditions and the pressure of NO_2

$$\frac{(\frac{1}{2}+2x/K)dx}{[(z_0-c_0)+x/2+x^2/K]x}=-kdt. \qquad (3)$$

This integrates, for $(4/K)(z_0-c_0)$ less than 1/4, to give

$$kt=C-\left[\frac{1}{4(z_0-c_0)}\log\frac{x^2}{z_0-c_0+x/2+x^2/K}+\frac{[\frac{1}{4}-(4/K)(z_0-c_0)]^{\frac{1}{2}}}{2(z_0-c_0)}\times\log\frac{2x/K+\frac{1}{2}+[\frac{1}{4}-(4/K)(z_0-c_0)]^{\frac{1}{2}}}{2x/K+\frac{1}{2}-[\frac{1}{4}-(4/K)(z_0-c_0)]^{\frac{1}{2}}}\right], \qquad (4)$$

where C is the value of the terms in the brackets when x is replaced by x_0, and the other terms have been defined above. Data from the experiment, which are summarized in Table I, were substituted in the integrated equation, and the expected linear relationship was found as is seen in Fig. 5. The slope of the line is 1.32 (milliatm. sec.)$^{-1}$ which is in satisfactory agreement with the average value of k, 1.29 in the same units, found from the same data by use of the differential equation.

The integrated equation gives a check on the completeness of mixing of the reactants. The intercept on the time axis of the line found by the integrated equation is −0.032 second, and the flow rate through the reaction cell for this experiment was 9.8 cc per sec. These facts imply a volume of 0.31 cc in front of the cell after mixing has occurred. Since the volume from the center of the reaction cell to the jets of the mixing chamber was 0.35 cc, it appears that mixing was essentially complete early in the stage of the mixing process.

d. Effect of Temperature Changes

Measurement of temperature was somewhat uncertain because of the temperature rise resulting from the heat of reaction. At 18°C the reaction as written above liberates 50 kilocal per mole of O_3,[6] and if the reaction occurred adiabatically, the temperature would rise 8°C when one milliatm. of O_3 reacted in the presence of one atm. of O_3. Actually the reaction occurred neither adiabatically nor isothermally. It required from 10 to 20 minutes for the temperature of the thermocouple to reach its steady state value when the reactants flowed through the reaction cell, and the maximum temperature rise observed was only about 10 percent of

[6] F. R. Bichowsky and F. D. Rossini, *The Thermochemistry of Chemical Substances* (Reinhold Publishing Corporation, New York, 1936).

that calculated on the assumption of adiabatic conditions.

In order to eliminate some of these uncertainties in the study of the effect of temperature on the rate of the reaction, these runs were made with low pressures of the reactants. A summary of the values of the rate constant for different temperatures is given in Table II-B for two different values of the initial pressures of reactants. The maximum temperature rise observed for the first set of conditions was less than 1°C, and that for the second set of conditions was about 2½°C. In all cases the temperature of the air thermostat around the mixing chamber and reaction cell was within two degrees of that of the thermocouple inside the glass line. Thus, though the temperature control was far from ideal, the errors in the temperature reported in Table II should be no more than about 2°C, and there is no reason to think that the errors are systematic in the sense of giving too great or too small a range of temperature which would invalidate the measurement of the energy of activation.

Rate constants were expressed in terms of moles per cubic centimeter rather than the temperature dependent pressure units, and the energy of activation was computed from the 22 experiments summarized in Table II-B by evaluating the constants in the Arrhenius equation

$$\ln k = -E/RT + \text{constant}$$

by that method of least squares which recognizes the possibility of error in both variables,[7] $\ln k$ and $1/T$. The value found for the energy of activation was 7.0 kilocal per mole, and the standard error of estimate was found to be 0.6 kilocal per mole.

To facilitate the comparison of these results with those of other kinetic studies the rate constant may be expressed in the following forms

$$k = 5.9\times10^{12}e^{-E/RT}$$
$$= 3.5\times10^{11}(T)^{\frac{1}{2}}e^{-E/RT}\ \text{cm}^3/\text{mole-sec.} \quad (5)$$

DISCUSSION OF RESULTS

a. A Mechanism

The mechanism proposed to account for the observation is

(1) $NO_2+O_3=NO_3+O_2$, rate determining
(2) $NO_2+NO_3+M=N_2O_5+M$, fast

where M represents any molecule including the walls of the vessels. The first step is in agreement with the observed second order rate equation; and the fact that two molecules of NO_2 react for each one of O_3 requires a reaction such as (2) to remove the second NO_2. Corrections were made for the equilibrium between NO_2 and N_2O_4 the rate of attainment of which is known[5] to be much more rapid than the rate determining step of this reacting system. Inclusion of M in the equations above does not imply that the three molecules collide at exactly the same time, and in fact these experiments gave no evidence as to how closely deactivating collision with M is associated in time with the initial encounter of an NO_2 and NO_3 molecule. NO_3 is a substance frequently postulated to explain the mechanism of reactions of the higher oxides of

[7] R. A. Fisher, *Statistical Methods for Research Workers* (Oliver and Boyd, Edinburgh, 1938), p. 139.

TABLE I. An example of the method used to analyze the data Experiment VI-9. Total flow rate 0.594 l per min., 12°C, $z_0=7.28$ milliatmospheres.

Time unit 1/300 sec.	I/I_0	Pressure of gases in milliatmospheres $NO_2/2$ $x/2$	N_2O_4 y	O_3 z	Δz	$\Delta z/\Delta t$ R	R/xz k
0	0.752	2.93	0.67	5.83			
					0.20	60	1.83
1	0.762	2.79	0.61	5.63			
					0.10	30	0.98
2	0.769	2.70	0.60	5.53			
					0.14	42	1.45
3	0.776	2.61	0.55	5.39			
					0.12	36	1.32
4	0.782	2.53	0.51	5.27			
					0.08	24	0.92
5	0.787	2.47	0.49	5.19			
					0.45	36	1.19
10	0.813	2.13	0.38	4.74			
					0.36	22	1.12
15	0.834	1.87	0.28	4.38			
					0.35	21	1.45
20	0.858	1.59	0.21	4.03			
					0.27	16	1.40
25	0.876	1.37	0.16	3.76			
					0.23	14	1.48
30	0.892	1.18	0.12	3.53			
					0.21	13	1.68
35	0.906	1.01	0.08	3.32			
					0.12	7	1.10
40	0.915	0.91	0.06	3.20			
					0.08	5	0.88
45	0.922	0.83	0.06	3.12			
					0.09	5	1.11
50	0.929	0.75	0.05	3.03			
		Average in $(\text{atm.}\times10^{-3}\times\text{sec.})^{-1}$					1.29

TABLE II. Summary of rate constants observed under various conditions. c_0 is the initial pressure of N_2O_4 plus $NO_2/2$. z_0 is the initial pressure of O_3.

Condition number	Temperature °C	c_0 milliatmospheres	z_0 milliatmospheres	Number of runs averaged	Average value of rate constant $\text{cm}^3/\text{moles sec.}\times10^{-7}$
A. Variation of initial pressures of reactants at one temperature					
1	20	1.23	1.92	3	3.7
2	20	1.28	3.68	2	3.5
3	20	1.21	5.70	3	3.5
4	21	5.35	4.69	2	3.9
5	20	5.00	7.52	4	3.9
6	21	4.55	11.35	4	3.3
7	22	13.4	5.60	4	3.4
8	22	14.9	18.0	2	4.1
9	20	12.3	23.8	3	3.6
B. Variation of temperature at constant ratio of initial pressure of reactants					
10	13	1.23	1.92	4	2.8
1	20	1.23	1.92	3	3.7
11	29	1.23	1.92	3	5.0
12	14	5.05	7.28	8	3.0
5	20	5.00	7.52	4	3.9

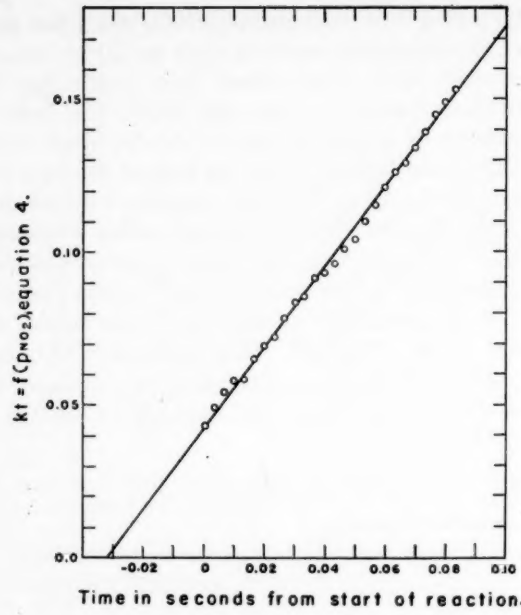

FIG. 5. Test of the integrated equation (Experiment VI-9)

nitrogen.[8–10] Since its absorption spectrum has been obtained (most recently by Jones and Wulf[11]), NO_3 is more nearly a substantiated compound than a hypothetical intermediate.

If simultaneous differential rate equations are written down for each step in the above mechanism, if the usual assumptions are made about the steady state concentration of NO_3, and if the second reaction is considered fast compared to the first, then it is found upon solution for the rate of disappearance of O_3 and of NO_2

$$-d(O_3)/dt = k_1(NO_2)(O_3) \quad (6)$$

$$-d(NO_2)/dt = 2k_1(NO_2)(O_3), \quad (7)$$

and the rate constant k tabulated above is k_1. Thus the mechanism given above is sufficient to account for the experimental facts found in this study.

b. Relations to Other Kinetic Studies

It should be noted that this reaction and its mechanism is related to and has interconnections with several other kinetic systems involving the higher oxides of nitrogen. The first step of this mechanism is identical with one step in the mechanisms proposed by Schumacher and Sprenger[8] to explain the N_2O_5 catalyzed decomposition of ozone. The second step of the mechanism proposed here is the reverse of the first step of the mechanism proposed by Smith and Daniels[9] for the reaction of NO and N_2O_5, and these two reactions together are the forward and reverse steps of the equilibrium proposed by Ogg[10] as one feature of a new mechanism for the first order decomposition of N_2O_5. It is believed that further work with these four kinetic systems will reveal quantitative interrelations among them.

ACKNOWLEDGMENTS

We wish to express here our sincere appreciation for the many constructive discussions with Doctor Oliver Wulf and Professors R. M. Badger and James H. Sturdevant. We are also deeply grateful to the Research Corporation for a grant in aid of this research.

[8] H. J. Schumacher and G. Sprenger, Zeits. f. physik. Chemie **B2**, 267 (1929); G. Sprenger, Zeits. f. Elektrochem. **37**, 674 (1931).
[9] J. H. Smith and F. Daniels, J. Am. Chem. Soc. **69**, 1735 (1947).
[10] R. A. Ogg, Jr., J. Chem. Phys. **15**, 337 (1947).
[11] H. J. Jones and O. R. Wulf, J. Chem. Phys. **5**, 873 (1937).

An Experimental and Theoretical Investigation of the Skeletal Frequencies of the Paraffin Hydrocarbons and the Far Infra-Red Spectrum of Carbon Tetrachloride

DAVID M. GATES
*Department of Physics, University of Michigan, Ann Arbor, Michigan**
(Received September 9, 1948)

The far infra-red spectra of the paraffin hydrocarbons and of carbon tetrachloride have been investigated. The following bands were located: propane at 370.6 cm^{-1}, *n*-butane at 215 cm^{-1}, and carbon tetrachloride at 315 cm^{-1}, the latter showing isotope structure. The contours of the following near infra-red bands for *n*-butane were surveyed, and some fine structure was revealed: 1342.9 cm^{-1}, 1295.6 cm^{-1}, 1135.6 cm^{-1}, 956.5 cm^{-1}, and 740.0 cm^{-1}. The assignment of the skeletal frequencies of vibration is made, and a theoretical analysis of the skeletal normal frequencies, assuming a valence potential for the molecules propane through pentane, is given.

I. INTRODUCTION

NUMEROUS investigations of the infra-red and Raman spectra of the normal paraffin hydrocarbons have been reported.[1] The complete assignment of the normal frequencies for ethane and propane have been made (references to these are given later), although the exact symmetry configuration of ethane is still in doubt. Eliashevich and Stepanov[2] have given the analysis of all the normal frequencies of *n*-butane. Two main difficulties plagued previous investigators—the absence of the low frequency infra-red data and the lack of knowledge concerning the structure of the infra-red bands, as well as the depolarization factors for the Raman bands. Kirkwood,[3] Whitcomb, Nielsen, and Thomas,[4] Pitzer,[5] Barriol,[6] and Kellner[7] have made use of the periodicity present in these molecules to treat them as finite segments of an infinite chain after the method of Born and Karman. This method could not convincingly identify the fundamental frequencies of the model with the observed bands, but may result in considerable usefulness after the shorter members of the series have been accurately analyzed. Recently Rasmussen,[8] Sheppard,[9] and Szasz, Sheppard, and Rank[10] have given analyses of the butanes and pentanes. Ahonen[11] gave a theoretical evaluation of the isomeric octanes. Kohlrausch and Köppl[12] gave a theoretical analysis of the hydrocarbons propane through heptane with experimental data listed through dodecane. The near infra-red prism spectra for the hydrocarbons all may be obtained from the American Petroleum Institute Research Project No. 44 through the National Bureau of Standards.

The purpose of the present investigation was to analyze only the skeletal frequencies of the normal paraffin hydrocarbons. Attention was concentrated on the skeletal motions as a result of the lack of fine structure data concerning the hydrogen bands enabling a classification of them and the complexity of the calculations when these are included. It became immediately clear that before one proceeded with the theoretical analysis of the normal modes of vibration the low frequency bending vibrations in the range 400 cm^{-1} to 200 cm^{-1} had to be established and some of the higher frequency skeletal bands further resolved.

II. EXPERIMENTAL

The far infra-red region of the spectrum has been studied relatively little and projects many difficulties, the greatest being the lack of transmitting materials for use as windows and prisms. The instrument used for these studies in the far infra-red was the large aperture grating instrument at the University of Michigan, described by Randall and Firestone.[13] The bending modes of the skeletal vibrations for the normal paraffin hydrocarbons are relatively weak, necessitating a long path length for the radiation through the gas. This was accomplished by filling the entire spectrometer case with the gas, except for the source and focusing mirror, yielding a path length of 460 centimeters. The source box, containing the electrically heated Chromel ribbon strip as a source and a mirror to focus the radiation on the entrance slit, was separated from the spectrometer proper by a thin window. Silver chloride was transparent to about 32 μ and beyond

* Now at the Department of Physics, University of Denver, Colorado.

[1] George Herzberg, *Infrared and Raman Spectra of Polyatomic Molecules* (D. Van Nostrand Company, Inc., New York, 1945).

[2] M. Eliashevich and B. Stepanov, Comptes Rendus U.R.S.S. 32, 481 (1941).

[3] J. G. Kirkwood, J. Chem. Phys. 7, 506 (1939).

[4] S. E. Whitcomb, H. H. Nielsen, and L. H. Thomas, J. Chem. Phys. 8, 143 (1940).

[5] K. S. Pitzer, J. Chem. Phys. 8, 711 (1940).

[6] J. Barriol, J. de phys. et rad. 10, 215 (1939).

[7] L. Kellner, Trans. Faraday Soc. 41, 217 (1945).

[8] R. S. Rasmussen, J. Chem. Phys. 16, 712 (1948).

[9] N. Sheppard, J. Chem. Phys. 16, 690 (1948).

[10] G. J. Szasz, N. Sheppard, and D. H. Rank, J. Chem. Phys. 16, 704 (1948).

[11] C. O. Ahonen, J. Chem. Phys. 14, 625 (1946).

[12] K. W. F. Kohlrausch and F. Köppl, Zeits. f. physik. Chemie B26, 209 (1934).

[13] H. M. Randall and F. A. Firestone, Rev. Sci. Inst. 9, 404 (1938).

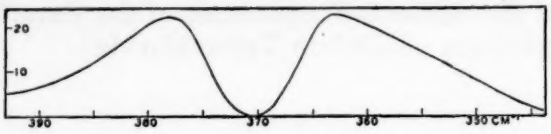

FIG. 1. *n*-Propane gas, 27-μ band.

this wave-length Nylon film 0.2 mil thick was extremely transparent, could withstand a $\frac{1}{3}$-atmosphere pressure differential, simultaneously being heated by the source. This Nylon film was far superior to any other material such as Pliofilm or cellulose nitrate by virtue of its ability to withstand heat. A further difficulty encountered was the dissolving of the stopcock grease sealing the thermopile by the hydrocarbon gases and carbon tetrachloride gas introduced into the spectrometer. The optical path through the spectrometer contained the following elements in this order: an adjustable entrance slit, a push-pull type shutter, a large aperture parabolic collimating mirror 24 inches in diameter and 35 inches in focal length, and a grating of the echelette type with an area of 10 inches by 20 inches ruled on a solder surface. After reflection from this grating, the radiation returned to the large mirror, then was reflected from a restrahlen plate, and focused upon the exit slit. The radiation from the exit slit diverged to an elliptical mirror and was then focused upon the thermopile receivers. The thermopile was of the Pfund type of tin-bismuth and tin-antimony coated with Aquadag. The four junctions were connected with the upper pair in series opposition with the lower pair. A single stage Firestone[14] amplifier with photographic recording was used.

Two methods of calibration of the instrument allowed an accurate measurement of the frequencies: the determination from the grating constant and position and the calibration by the rotation spectrum of water vapor, which has a great many lines throughout this wave-length region.[15] The water vapor spectrum was associated with each spectrum of the gases investigated, since the complete elimination of water in a gas is practically impossible. Only when the spectrometer was well evacuated and outgassed was the water vapor spectrum absent. For each of the following molecules studied the entire spectrum from 400 cm^{-1} to 170 cm^{-1} was carefully scanned, and only the bands shown here were found.

For propane it is known that a Raman line exists at 373 cm^{-1}. The symmetry type of this molecule allows the infra-red activity of this frequency and the band shown in Fig. 1 with center at 370.6 cm^{-1} was obtained. The propane was introduced into the spectrometer proper, giving a 460-cm path length at a gas pressure of 39 cm Hg. A grating with 900 lines per inch was used, 3.0-mm slits, KCl shutter, CaF_2 restrahlen plate, and AgCl entrance window. Only a single band was found in the region 25 μ to 50 μ.

For *n*-butane gas the spectrometer case was filled to a pressure of 46 cm and the source box with 47 cm of nitrogen gas. This was necessitated by the use of a Nylon entrance window for the investigation beyond 33 μ. A grating with 600 lines per inch was employed, 3.0-mm slits, KCl shutter, and CaF_2 restrahlen plate. For *n*-butane the far infra-red band at 215 cm^{-1} shown in Fig. 2 was found. Its general contour was that expected for a band with symmetry type B_u belonging to an asymmetric top molecule—that is, a hybrid band as a mixture of the usual type *A* and type *B* band, although no fine structure was observed. The entire spectrum from 400 cm^{-1} to 170 cm^{-1} was carefully scanned and only the single band was found. Normal pentane gas was introduced into the spectrometer at 24.4 centimeters pressure with a path length of 460 centimeters. No bands were found for pentane, probably because they were too weak.

The low frequency fundamental for carbon tetrachloride had been located in the Raman spectrum at 314 cm^{-1} (see Kohlrausch[16]). The present investigation located a band in the infra-red at 315 cm^{-1} shown in Fig. 3. Barchewitz and Parodi[17] found this band at 305 cm^{-1} and other additional bands at 217 cm^{-1}, 247 cm^{-1}, 370 cm^{-1}, and 529 cm^{-1}. These last few bands were not discovered in the present investigation, nor any evidence that they might be in the spectrum at those positions. The method of obtaining the carbon tetrachloride spectrum of Barchewitz and Parodi allows some suspicion as to

FIG. 2. *n*-Butane gas, 46.5-μ band.

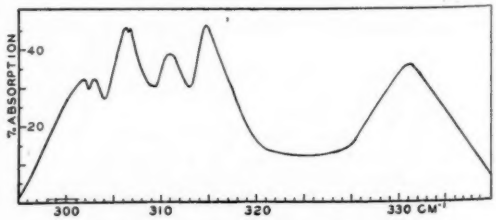

FIG. 3. Carbon tetrachloride gas, 32-μ band.

[14] F. A. Firestone, Rev. Sci. Inst. **3**, 163 (1932).
[15] Randall, Dennison, Ginsburg, and Weber, Phys. Rev. **52**, 160 (1937).
[16] K. W. F. Kohlrausch, *Der Smekal-Raman-Effect* (Verlag. Julius Springer, Berlin, 1931).
[17] P. Barchewitz and M. Parodi, J. de Phys. **10**, 143 (1939).

TABLE I. Interpretation of the infra-red frequencies.

Frequency in cm^{-1}		Symmetry type	Figure
1342.9	$(m)Q$	B_u	7
1295.6	$(m)Q$	B_u	7
1135.6	(m)	A_u	6
956.5	$(s)Q$	B_u	5
740.0	(m)	B_u	4
215.0	(w)	B_u	2

the occurrence of these bands. The Raman spectrum gives a band at 314.0 cm^{-1}.

The experimental difficulties encountered with CCl_4 were similar to those with the hydrocarbons, particularly the dissolving of the stopcock grease and the thermopile wax window. This dissolving eventually led to leaks in the thermopile housing which terminated the investigation. The maximum gas pressure attainable at room temperature is its vapor pressure of about 9.0 cm. Actually, 3.8 cm of pressure was used with a radiation path length in the CCl_4 of 460 centimeters, yielding the band shown in Fig. 3.

The fine structure apparent here was actually very real and is probably attributed to isotope effect. Wu and Sutherland[18] have discussed in detail the isotope effect in CCl_4 and have given quantitative results for the isotopic line separations of the fundamental bands. This band at 315 cm^{-1} is the low frequency triply degenerate fundamental vibration of symmetry type F_2, carbon tetrachloride belonging to the tetrahedral symmetry group. The abundance ratio of the isotopes of CCl_4 is

$$CCl_4^{35}:Cl^{37}CCl_3^{35}:Cl_2^{37}CCl_2^{35}:Cl^{35}CCl_3^{37}:CCl_4^{37} = 31.6:42.2:21.1:4.7:0.4.$$

Considering the first three isotopes to be the only ones intense enough to yield a noticeable contribution to the absorption spectrum, one obtains a six-line spectra. The quantitative agreement of Wu and Sutherland's calculations with the curve of Fig. 3 are incompatible. Further experimental investigation of this band should be undertaken. The "Michigan" instrument with the proper care is capable of resolving the "isotope" fine structure nicely.

The near infra-red high resolution studies were done on the prism-grating instrument originally described by Hardy.[19] A KBr fore prism and a grating with 2400 lines per inch was employed. The limit of resolution of the instrument was just less than the fine structure for the type A bands of n-butane. Propane had been previously studied by Wu and Barker[20] so that only the bands of n-butane and n-pentane were investigated here. The band contours for n-butane are shown in Figs. 4, 5, 6, and 7. The fine structure revealed here was not sufficiently reliable to give any more than a confirmation of the moments of inertia as obtained from other information but did allow one to classify the band as to its symmetry type. The center of each of these bands for n-butane occurred at 1342.9 cm^{-1}, 1295.6 cm^{-1}, 1135.6 cm^{-1}, 956.5 cm^{-1}, and 740.0 cm^{-1}. The contours of these bands allow the assignment of the frequencies given in Table I. The representation A_u is the usual type C band, due to a change in electric moment perpendicular to the plane of symmetry giving rise to bands with a Q branch, although not necessarily very distinct. The representation B_u is a mixture of type A and type B bands giving rise to a contour of a hybrid nature. Type A would exhibit a sharp Q branch and type B no Q branch at all, so that the combination may be almost anything. There is some doubt as to the proper interpretation

TABLE II. Distribution of the skeletal vibrations among the symmetry representations.

Molecule of symmetry (C_{2h})	Total number of skeletal vibrations	A_g	A_u	B_g	B_u
n-Butane (*trans*)	6	3	1	0	2
n-Hexane	12	5	2	1	4
Molecule of symmetry (C_{2v})	Total number of skeletal vibrations	A_1	A_2	B_1	B_2
Propane	3	2	0	0	1
n-Butane (*cis*)	6	3	1	0	2
n-Pentane	9	4	1	1	3
n-Heptane	15	6	2	2	5

TABLE II*a*.

C_{2v}	E	C_2	σ_x	σ_y	Activity
A_1	+1	+1	+1	+1	IR, R
A_2	+1	+1	−1	−1	R
B_1	+1	−1	+1	−1	IR, R
B_2	+1	−1	−1	+1	IR, R
C_{2h}	E	C_2	σ_h	i	Activity
A_g	+1	+1	+1	+1	R
A_u	+1	+1	−1	−1	IR
B_g	+1	−1	−1	+1	R
B_u	+1	−1	+1	−1	IR

TABLE III. Significance of the force constants for the skeletal frequency calculations for the paraffin hydrocarbons.

Parameter	Significance
k_{33}	Force constant between two CH_3 groups
k_{32}	Force constant between CH_3 and CH_2 groups
k_{22}	Force constant between two CH_2 groups
$k\beta_{323}$	Force constant for the valence angle deformation involving $CH_3-CH_2-CH_3$
$k\beta_{322}$	Force constant for the valence angle deformation involving $CH_3-CH_2-CH_2$
$k\beta_{222}$	Force constant for the valence angle deformation involving $CH_2-CH_2-CH_2$
β	Valence angle

[18] C. K. Wu and G. B. B. M. Sutherland, J. Chem. Phys. 6, 114 (1938).
[19] J. D. Hardy, Rev. Sci. Inst. 1, 429 (1930).
[20] V. Wu and E. F. Barker, J. Chem. Phys. 9, 487 (1941).

TABLE IV. Skeletal frequency assignments for the normal paraffin hydrocarbons.

Molecule	Experimental frequency in cm^{-1}		Assignment	References
Ethane	993		—	(21)
Propane	1053		B_1	(11) and this work
	870		A_1	
	370.6		A_1	
n-Butane*	1056	Raman	A_g	(12), (20) and this work
	956.4	*IR*	B_u	
	833	Raman	A_g	
	319	Raman	A_g	
	215	*IR*	B_u	
n-Pentane	1072		B_1	(12), (13) and this work
	1025		A_1	
	914		B_1	
	861		A_1	
	337		A_1	
	279		B_1	
	149		A_1	

* The choice of these frequencies will be discussed in more detail below

to be given to the band in the region of 740.0 cm^{-1}. It appears as if it may be of symmetry type B_u being considered as without a Q branch. On the other hand, it might be thought of as two bands each exhibiting a Q branch, at 747.8 cm^{-1} and at 733.2 cm^{-1}. This author had decided that if it were a single band at 740.0 cm^{-1} it should belong to the CH_3 rocking frequency, but this assignment appears inconsistent with other data indicating this frequency to be greater than 900 cm^{-1}.[8,10]

For *n*-pentane the bands with centers at 1167 cm^{-1}, 1141.4 cm^{-1}, 1072 cm^{-1}, and 914 cm^{-1} were surveyed. None of the bands could be resolved and each appeared to lack a Q branch consisting only of two absorption maxima separated by about 10 cm^{-1}. Often when the infra-red spectrum is given for pentane, there will be listed pairs of lines separated by about 10 cm^{-1}. Each of these pairs of lines should in most cases be considered as a single band.

III. ANALYSIS

Several articles have appeared recently on the vibrational frequency assignments for the paraffin hydrocarbons[8–11] with an attempt to systematize the spectra of the larger members of the paraffin series. This author has confined his attention to the analysis of the planar skeletal modes of vibration, neglecting the hydrogen vibrations and the out-of-plane motions. The paraffin hydrocarbon molecules forming the series, ethane, propane, butane, pentane, hexane, etc., are considered to be zigzag chains of methylene groups with a methyl group on each end. Ethane is formed of two methyl groups only. The carbon-carbon distance is taken as 1.54A from electron diffraction and the bond angle as 111° 30′ $\pm 2°$. The skeletal modes of vibration concern only the relative motions of the CH_3 and CH_2 groups.

The method of symmetry coordinates discussed by Herzberg[1] was used for setting up the secular determinants. The potential function was approximated with a valence force potential, each of which will be written down in the following discussion. These molecules will be considered to belong to either symmetry type C_{2v} or C_{2h}, except for ethane which may be either D_{3h} or D_{3d}. Table II gives the number of skeletal vibrations belonging to each representation.

The representations given in Table II have the meanings given in Table II*a*:

The procedure followed was to determine precisely the potential constants for the first molecule in the series, and then approximate the potential constants of the next larger molecule with these. This then gives an indication of where the skeletal frequencies will lie for the more complicated molecule. The most probable choice of frequencies was made from the experimental data and the parameters adjusted by a least squares method to obtain the best fit of the calculated frequencies with the experimental. This procedure was repeated for each molecule through *n*-pentane, the calculations becoming too cumbersome beyond that point. The valence angle, β, for the angle between a methyl and two methylene groups or between three methylene groups was considered an additional parameter which was adjusted by the least squares method for each molecule. No distinction in the angle with its position in the chain was considered. The angle was implicit in the potential functions as written below but appears explicitly after the transformation to symmetry coordinates is made.

Table III gives the meaning of the parameters chosen for the potential functions. The choice of experimental frequencies made for the determina-

TABLE V. Comparison of the calculated with the experimental frequencies for the skeletal vibrations of the paraffin hydrocarbons.

Molecule	Experimental frequency in cm^{-1}	Calculated frequency in cm^{-1} with β a parameter	Percent deviation	Calculated frequency in cm^{-1} with $\beta = 111° 30'$	Percent deviation
Ethane	993	993	0		
Propane	1053	1053	0	1053	0
	870	870	0	860	1.1%
	370.6	370.6	0	375	1.3%
n-Butane (*trans*-form) C_{2h}	1056	1092	3.4%	1045	1.04%
	956.4	941.9	1.5%	959.9	0.36%
	833	820.4	1.5%	846.7	1.64%
	319	306.4	3.9%	290	9.10%
	215	221.5	3.0%	231.8	7.80%
n-Pentane	1072	1091	1.8%		
	1025	1015.7	0.9%		
	914	883.6	3.3%		
	861	874.3	1.5%		
	337	334.3	0.8%		
	279	254.5	8.8%		
	143	143.2	0		

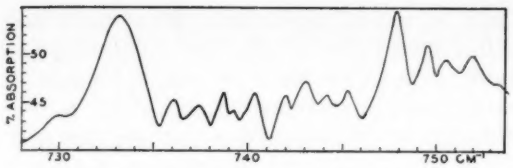

FIG. 4. *n*-Butane gas, 13.5-μ band.

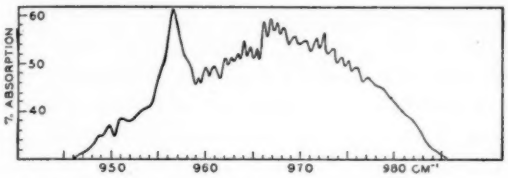

FIG. 5. *n*-Butane gas, 10.45-μ band.

tion of the parameters in each potential function is given in Table IV.

Ethane.—This molecule has been rather completely discussed by Crawford, Avery, and Linnett[21] and by Stitt.[22] It has a single skeletal frequency at 993 cm^{-1} and gives the force constant k_{33} to be 4.36×10^{-5} dynes/cm.

Propane C_3H_8.—This molecule has been investigated under high resolution by Wu and Barker.[20] They give for the fundamental frequencies 1053 cm^{-1}, 870 cm^{-1}, and stated that they failed to find a band in the region of 370 cm^{-1}. Kohlrausch and Köppl[12] reported a band at 373 cm^{-1} in the Raman spectrum. This investigation located a band in the infra-red for propane centered at 370.6 cm^{-1}. Each of the following references included the analysis of propane in their study: 1, 2, 3, 5, 8, 12, 16, 20, 23. The potential function chosen for this analysis is:

$$2V=2k_{32}(\Delta r_{32})^2+k_{\beta 323}l^2(\Delta\beta)^2.$$

n-Butane C_4H_{10}.—There is possibility for this molecule that a mixture of four forms may exist: the *trans-* (C_{2h}) form, the *cis-* (C_{2v}) form, and two identical optical isomers of form (C_2). Szasz, Sheppard, and Rank[10] give evidence for the presence of the *trans-* (C_{2h}) form and the optical isomer of form (C_2) in the liquid. For the infra-red spectrum of the gas it can be shown that all of the observed lines can be accounted for with the use of the C_{2h} model. The presence of another form in the gaseous state would give many more lines than have been observed. Information on *n*-butane has been given in each of these references: 1, 2, 3, 5, 8, 10, 12, 16, and 23. The reason for the choice of frequencies used in the calculation was twofold. First, the force constants determined for propane were used for the butane calculation giving an indication of the position of the frequencies. Second, the division of the modes of vibration into two distinct representations restricted one to choose two frequencies from the infra-red data and three from the Raman for the molecular form C_{2h}. The intensity of the lines aided further in the proper choice. The potential function for the C_{2h} and C_{2v} forms was taken as

$$2V=2k_{32}(\Delta r_{32})^2+k_{22}(\Delta r_{22})^2+2k_{\beta 322}l^2(\Delta\beta_{322})^2.$$

n-Pentane C_5H_{12}.—This molecule introduces the fourth and final new valence force constant necessary for the determination of the planar modes of vibration. Larger molecules in the series should involve the same type of four force constants, altered slightly to fit the particular molecule. The form of this molecule was chosen as C_{2v}. References to previous data on *n*-pentane are: 1, 3, 8, 9, 12, 16, and 23. For *n*-pentane the choice of frequencies was considerably more difficult. Each normal mode is expected to be Raman active as well as infra-red active, and the comparison of each spectrum shows this correspondence. Since detailed measurements on the infra-red bands of *n*-pentane have not been made, one must rely upon the polarization measurements given by Fenske.[23] The potential function used in this calculation was

$$2V=2k_{32}(\Delta r_{32})^2+2k_{22}(\Delta r_{22})^2+2k_{\beta 322}l^2(\Delta\beta_{322})^2+k_{\beta 222}l^2(\Delta\beta_{222})^2.$$

For propane, the calculated and experimental frequencies can be made to agree precisely if β is used as the third parameter (see Table V). If one uses the angle $\beta=111°\,30'$ given by electron diffraction, then the errors in the calculated frequencies are of the order of one percent. This is due to the simplicity of the potential function which must be considered only as an approximation. With the use of four adjustable parameters in the potential function of *n*-butane, the frequencies can be calculated

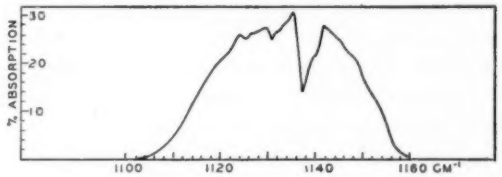

FIG. 6. *n*-Butane gas, 8.8-μ band.

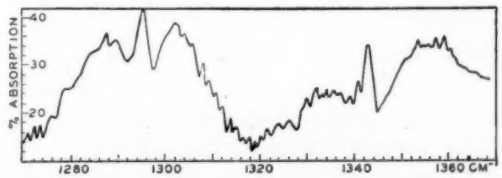

FIG. 7. *n*-Butane gas, 7.7-μ and 7.45-μ bands.

[21] B. L. Crawford, W. H. Avery, and J. W. Linnett, J. Chem. Phys. 6, 682 (1938).
[22] F. Stitt, J. Chem. Phys. **7**, 297 (1939).
[23] M. R. Fenske, W. G. Braun, R. V. Wiegand, D. Quiggle, R. H. McCormick, and D. H. Rank, Anal. Chem. 19, 700 (1947).

TABLE VI. Force constants for skeletal frequency calculations for the normal paraffin hydrocarbons.

Molecule	$k_{32}\times10^{-5}$	$k_{22}\times10^{-5}$	$k_{\beta_{322}}\times10^{-5}$	$k_{\beta_{222}}\times10^{-5}$	β
Ethane $k_{32}=4.36$					180°
Propane	3.88		0.333		115°
n-Butane	3.80	3.525	0.210		120° 41′
n-Pentane	4.09	3.518	0.139	0.212	117° 49′

to better than four percent, which may be considered as satisfactory for a calculation involving the skeletal vibrations only. Using $\beta=111°\ 30'$ the errors become as large as 9 percent, because of an oversimplification of the potential function. The value of β determined for each molecule has little physical significance, since it is actually only an adjustable parameter which corrects for the errors involved by using too simple a potential. The average valence angle probably increases slowly with increasing chain length, but not nearly as rapidly as these values of β might seem to indicate. If one were to make the calculations using additional force constants or parameters of a different nature, then the errors could be taken up with them rather than with β. Furthermore, it must be continually kept in mind that the normal frequencies due to anharmonicities are, in general, not known to within percent deviations of the same order of magnitude as those associated with the calculated frequencies given here.

Table VI gives the values of the force constants and the angle β adjusted by the least squares method. It would be thought that k_{32} would approach a fixed value rather than increasing again in pentane. The other force constants change in the expected fashion. It is not possible to make a different choice of frequencies to bring this constant into line and, if the two frequencies 914 cm^{-1} and 861 cm^{-1} are interchanged with respect to their symmetry representations, the following force constants are obtained: $k_{32}=3.80\times10^{+5}$ dynes/cm, $k_{22}=3.57\times10^{5}$, $k_{\beta322}=0.125\times10^{5}$, $k_{\beta222}=0.241\times10^{5}$, and $\beta=117°\ 25'$. The interchange of the frequencies 914 cm^{-1} and 861 cm^{-1} does not seem possible in view of the depolarization factors given by Fenske.[23] It is felt that the skeletal normal frequencies for the larger paraffin hydrocarbons may be calculated by using the force constants determined here for *n*-pentane, with perhaps small changes applied to them. The infra-red and Raman spectrum of hexane should be extensively studied so that the symmetry classification of its frequencies may be made. This will enable one to continue this type of calculation to larger molecules with more assurance.

ACKNOWLEDGMENTS

I wish to express my sincere appreciation to Dr. David M. Dennison for suggesting this problem and to Dr. Ernest F. Barker for making available to me the equipment at the University of Michigan. I particularly wish to thank the National Institute of Health, Bethesda, Maryland, for the fellowship grant which enabled this research to be carried out.

Zinc Sulfide Phosphor Constitution and Its Effect on Electron Traps

G. F. J. GARLICK, A. F. WELLS,* AND M. H. F. WILKINS**
Department of Physics, University of Birmingham, Birmingham, England
(Received October 29, 1948)

The phosphorescence and thermoluminescence of zinc sulfide phosphors are governed by the mechanism of electron trapping in the phosphor crystal lattice. Experiments have been carried out to find the effect of phosphor constitution and method of preparation on the numbers and the energy distribution of electron traps. In order to investigate the traps, use has been made of the thermoluminescence *vs.* temperature characteristics of the phosphors.

These experiments show that pure zinc sulfide and zinc sulfide activated by silver and manganese possess similar "shallow" electron trap configurations after preparation and that these configurations are not markedly dependent on the particular activator. However, the introduction of copper impurity to zinc sulfide causes a marked change in the number and distribution of electron traps and is responsible for the long afterglow of these phosphors. Investigations of the effect of firing temperature and crystal form on the electron traps show that below the blende-wurtzite transition temperature (1020°C) the proportion of deep traps increases with firing temperature but that above this temperature the trap distribution is independent of the firing temperature or of fluxes and excess of sulfur. Experiments attempting to show that these traps were due to stoichiometric excess of zinc gave inconclusive results, but it is clear that the deep electron traps which produce the long afterglow characteristics of zinc sulfide are due both to the presence of copper impurity and to some change produced in the zinc sulfide lattice at high temperature without copper being present.

Other studies have been made of the effect of the mixed crystal proportions in the ZnS-CdS-Cu phosphor system on the electron traps. At high CdS contents some relatively deep electron traps are produced. Measurements of the fluorescence *vs.* temperature characteristics of the above phosphors show how the phosphor constitution and firing temperature affect the temperature at which the thermal quenching of fluorescence becomes appreciable.

INTRODUCTION

WHEN electrons are raised into the conduction levels of an insulating crystalline solid they frequently become trapped in special positions where localized energy levels, called electron traps, exist just below the conduction levels. Trapped electrons may be raised to the conduction levels by thermal energy and may, in luminescent solids, then produce phosphorescence and thermoluminescence by return to their original ground states in the luminescence centers. Trapped electrons also produce optical absorption and thus often are known as color centers![1] Capture of electrons by traps is shown clearly by studies of photo-conductivity.[2]

In the alkali halides the color centers which constitute the electron traps exist in the localized regions where a halogen ion is missing from the crystal lattice. The chemical nature of trapping centers in other solids is, however, largely unknown, and the present work is an attempt to determine the nature of electron traps in zinc sulfide phosphors. The research was carried out in 1940–41 for the Ministry of Home Security, and though never completed it is of interest as being the first study of zinc sulfide constitution using the "thermal glow curve" technique (Randall and Wilkins[3]) in which the phenomenon of thermoluminescence is used to analyze the distribution of trap energy levels.

THE MODE OF PREPARATION OF PHOSPHORS

The basis of all the phosphors was pure precipitated zinc or cadmium sulfide obtained from Messrs. Levy and West. Heavy metal impurity atoms were added by mixing the sulfide to a paste with a solution of a salt of the heavy metal in redistilled water (Pyrex still); fluxes, such as sodium chloride, were "Analar" chemicals, and these were dissolved in the paste. The mixture was dried on a watch glass in a steam oven and then ground and thoroughly mixed in an agate mortar. The phosphor was then fired in an electric furnace in a silica ignition tube sealed at one end. (The tube was 12 inches long with $\frac{1}{2}$-inch bore, and the mixture occupied approximately 2 inches of the tube length.) The open ends of the tubes were placed in the cold furnace, the temperature raised gradually over a period of one to three hours, and the tubes removed when the required temperature was attained. Experiments were also made with phosphors heated in sealed bulbs made from $\frac{1}{2}$-inch bore silica tubing. The bulbs were outgassed by heating to approximately 1000°C on the pump. Water and sulfur, etc., were removed from the precipitated zinc sulfide by heating to a few hundred degrees centigrade in the bulb in vacuum, and the bulb was then sealed while still connected to the pump.

METHOD OF PRESENTATION OF EXPERIMENTAL RESULTS

Throughout the following sections the results of experiments show how the mode of preparation and chemical constitution of the phosphor affect the energy level distributions of electron traps and therefore the phosphorescence characteristics. In

* Now at I.C.I., Manchester, England.
** Now at King's College, London, England.
[1] R. W. Pohl, Proc. Phys. Soc. **49** (extra part), 3 (1937).
[2] B. Gudden and R. W. Pohl, Zeits. f. Physik **17**, 340 (1923).
[3] J. T. Randall and M. H. F. Wilkins, Proc. Roy. Soc. **A184**, 366 (1945).

TABLE I. Relations between trap depth, thermal glow temperature, and mean phosphorescence decay time at room temperature (291°K) for zinc sulfide type phosphors.

Trap depth in ev	Thermal glow temperature in °K	Mean phosphorescence decay time at 291°K
0.2	100	0.0003 sec.
0.4	200	1 sec.
0.6	300	46 min.
0.8	400	100 days

order to determine the electron trap distributions, use is made of the "thermal glow" experiment as developed by Randall and Wilkins.[3] The phosphor specimen is mounted in a very thin layer on a rhodium plated copper surface forming part of the inner portion of a german-silver Dewar vessel, and is in vacuum during the experiments. The specimen is cooled to liquid air temperature, strongly excited by suitable radiation (in the following experiments filtered radiation of wave-length 0.365μ was used), and then warmed at an approximately uniform rate in the dark. The variation of thermoluminescence intensity with temperature is recorded continuously during this warming by means of an electron multiplier and galvanometer, the temperature being measured by a thermocouple attached to the copper surface, and a second galvanometer. By suitable development of technique both the thermoluminescence emission and the phosphor temperature are recorded manually on a rotating drum by one observer. The horizontal scale in the glow curve diagrams is a linear time scale marked in temperature intervals.

The theoretical interpretation of the thermal glow curve (that is, the recorded variation of thermoluminescence with temperature) has been given by Randall and Wilkins.[3] For a uniform rate of warming, and to the first degree of approximation, the thermoluminescence intensity at the absolute temperature T is proportional to the number of electrons traps of depth E (where E is the activation energy associated with the release of an electron from a trap), and E can be assumed to be proportional to the temperature T over the temperature range used. The proportionality constant between E and T depends on several factors, including the rate of warming, and for the experimental conditions described here (warming rate ~2.5°K sec.) the relation between E and T is such that emission at 300°K is due to electron traps of depth ~0.6 ev. However, in the figures given the temperature scale has been retained, but the approximate trap depths can be deduced from the above relation. Electron traps referred to as "shallow" in the text are those below 0.5 ev—that is, those contributing to thermal glow at temperatures below 250°K and "deep" traps correspond to thermal glow above 250°K. It is useful, with respect to the phosphorescence characteristics of the specimens described, to give a few relations between the thermal glow temperature, the trap depth, and the mean phosphorescence decay time at room temperature due to electron traps of "shallow" and "deep" designations. These relations are contained in Table I for the experimental conditions described above. Throughout this paper the constitution of a phosphor is given by the percent ratio of the number of metallic impurity atoms to the number of metallic matrix atoms. The crystal structure of the phosphor was determined by both x-ray diffraction and polarizing microscope.

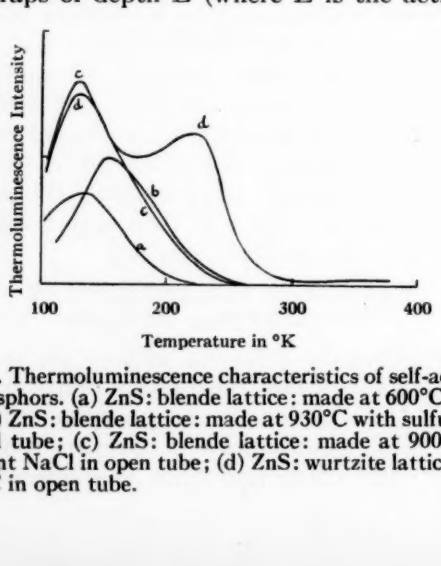

FIG. 1. Thermoluminescence characteristics of self-activated ZnS phosphors. (a) ZnS: blende lattice: made at 600°C in open tube; (b) ZnS: blende lattice: made at 930°C with sulfur vapor in sealed tube; (c) ZnS: blende lattice: made at 900°C with 10 percent NaCl in open tube; (d) ZnS: wurtzite lattice: made at 930°C in open tube.

EXPERIMENTAL RESULTS

(a) Pure ZnS, ZnS-Ag, and ZnS-Mn phosphors

If pure zinc sulfide is heated without any foreign activator metal to a temperature of about 500°C or above, a phosphor luminescing blue is produced.[4,5] The thermal glow curves of Fig. 1 show that the electron traps in this type of phosphor are distributed over a wide range; more deep traps are produced when a higher firing temperature is used between 500° and 900°C, but from 900°C to 1500°C there is no significant change in the thermal glow curve. The curves *b*, *c*, *d* in Fig. 1 were chosen from many dozen curves to show the extreme variation of curve which may occur. Double and single peak curves occur apparently at random, and no significant difference in this respect was found between phosphors having a zinc blende structure and those having a wurtzite structure. Attempts to "kill" the traps and the luminescence, which are both likely to be due to a stoichiometric excess of zinc, by heating the phosphor in about one-atmosphere pressure of sulfur vapor in a sealed quartz tube were unsuccessful.

Zinc sulfide activated by manganese or silver impurity gave the same type of thermal glow curve as

[4] S. Rothschild, Zeits. f. Physik **108**, 24 (1937).
[5] A. Schleede, Zeits. f. angew. Chemie **48**, 276 (1935).

the "pure" specimens. Examples of curves for these phosphors are given in Fig. 2.

(b) Copper Activated ZnS Phosphors

The addition of copper (1 part in 10^4) to zinc sulfide may appreciably alter the electron trap distribution and also change the color of luminescence from blue to yellow-green. The mode of heating and the crystal form (i.e., blende or wurtzite or a mixture of both) can also be important factors in determining the luminescence[6] and the trap distribution. If the phosphor is prepared in an atmosphere of sulfur, the thermal glow curve, for firing temperatures between 400° and 900°C, does not differ appreciably from that of pure zinc sulfide, there being more deep traps the higher the firing temperature (as shown by the curves *a*, *b*, *c*, *d* of Fig. 3); and the sulfide crystallizes in the blende

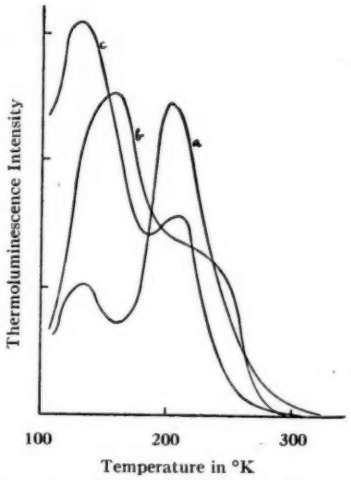

FIG. 2. Thermoluminescence curves of silver and manganese activated zinc sulfide phosphors. (a) ZnS-Ag No. 1; (b) ZnS-Ag No. 2; (c) ZnS-Mn.

form. If, however, the zinc sulfide is heated in an open tube without sulfur, some wurtzite structure is formed, and the trap distribution is quite different if copper is present (curve *e*; Fig. 3). The transition temperature for the blende-wurtzite structure change is given as 1020°C,[7] though it has been suggested that this temperature should be much lower.[8] The transition temperature at 1020°C was confirmed by heating fine grain wurtzite at 1000°C with sulfur or a flux, such as sodium chloride, both of which increase the rate recrystallization, blende being formed. Again, if coarsely crystalline blende or large lumps of natural zinc blende are heated for about an hour at 1040°C, wurtzite is formed though the external shape of the crystals may remain

[6] S. Rothschild, Trans. Faraday Soc. **42**, 635 (1946).
[7] A. T. Allen and J. L. Greenshaw, Zeits. f. anorg. allgem. Chemie **79**, 130 (1913).
[8] F. Seitz, J. Chem. Phys. **6**, 454 (1938).

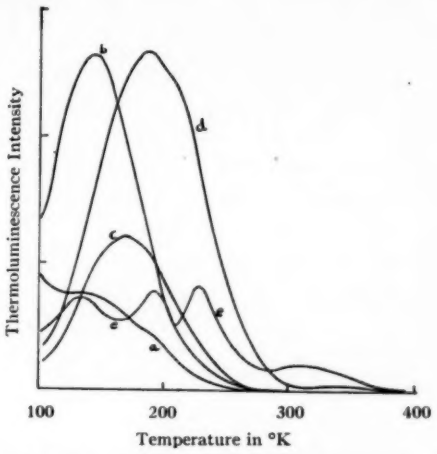

FIG. 3. Effect of crystal form and firing temperature on the thermoluminescence of ZnS-Cu (0.01 percent) phosphors. (a) ZnS-Cu: blende lattice, 600°C; (b) ZnS-Cu: blende made at 765°C in sealed tube; (c) ZnS-Cu: blende: made by firing for 7 hours in sealed tube with sulfur at 850°C; (d) ZnS-Cu: largely blende: made with sulfur in sealed tube at 980°C; (e) ZnS-Cu: partly wurtzite made at 765°C in open tube.

unaltered. Blende only changes to wurtzite below the transition temperature if fine-gained zinc sulfide is heated alone, and it appears that the wurtzite is formed by sublimation, the condensing wurtzite crystals being metastable.

If the zinc sulfide is heated with sulfur or flux to prevent the formation of wurtzite below the transition temperature, more deep electron traps are formed as the temperature is raised from 900° to 1000°C as shown in Figs. 3 and 4. The presence of these deeper traps in blende phosphors is indicated in the thermal glow curve by the development of a "tail" at the high temperature end of the curve (Fig. 4 curves *a* and *b*, Fig. 5 curve *a*, and Fig. 6 curve *a*). This tail, which is associated with an appreciable phosphorescence of many seconds at room temperature, is not present in pure zinc sulfide phosphors or in silver or manganese activated specimens and is produced by the addition of copper. The development of this tail in the thermal glow curve is continuous as the firing temperature is raised, but when approximately 1020°C is reached wurtzite is formed with a characteristic "wurtzite glow curve" (Fig. 4, curves *c*, *e*, and *d*), and the tail, characteristic of blende structure, changes to a large thermal glow peak with a maximum in the region of 320°K. These deep electron traps (~0.65 ev), because of the presence of copper in the wurtzite form of zinc sulfide, produce the afterglow in all commercial long afterglow zinc sulfide phosphors. If the phosphor is prepared at a temperature above 1100°C, the thermal glow curve does not alter and is independent of the presence of flux or of sulfur. It would appear, however, from the above results that the wurtzite structure is not essential for the existence of some deep traps associated with copper in

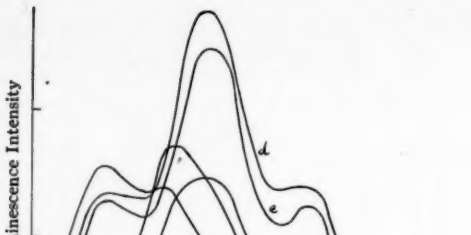

FIG. 4. Development of deep traps in ZnS-Cu phosphors with increase in firing temperature. (a) thermal glow curve of ZnS-Cu: plus 10 percent NaCl: made at 980°C: all blende; (b) thermal glow curve of ZnS-Cu: plus 10 percent NaCl: made at 1000°C: trace wurtzite; (c) thermal glow curve of ZnS-Cu: plus 10 percent NaCl: made at 1028°C: largely wurtzite; (d) thermal glow curve of ZnS-Cu: made at 1180°C; (e) thermal glow curve of ZnS-Cu: made at 1480°C wurtzite.

copper activated zinc sulfide. The blende-wurtzite transition takes place in a temperature range where the number of deep traps produced varies rapidly with the firing temperature and, as a result, a large number of deep traps is only found when the phosphor has been heated sufficiently for the blende-wurtzite transition to take place. The effect of flux below the transition temperature is shown by the thermal glow curves of Fig. 5; wurtzite with a large number of deep electron traps can be formed at firing temperatures as low as 930°C if no flux is used, such phosphors having an afterglow comparable with that of the phosphor fired at 1100° with flux.

(c) The Effect of Sulfur Concentration on Copper Activated ZnS Phosphors

The following incomplete observations have been made on the effect of sulfur vapor pressure during firing on the electron trap distributions in zinc sulfide phosphors. By analogy with oxygen deficient

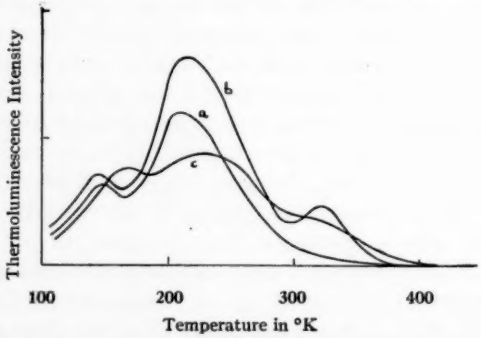

FIG. 5. Effect of flux on thermoluminescence characteristics of ZnS-Cu phosphors. (a) ZnS-Cu (0.01 percent)+10 percent NaCl: blende lattice: made at 980°C; (b) ZnS-Cu (0.01 percent) no flux: wurtzite lattice: made at 980°C; (c) ZnS-Cu (0.01 percent) no flux: largely wurtzite lattice: made at 930°C.

FIG. 6. Suppression of traps by sulfur treatment in blende and wurtzite ZnS-Cu phosphors as shown by thermal glow curves. (a) ZnS-Cu+5 percent $MgCl_2$ fired at 950°C for 20 min. in open tube: blende; (b) ZnS-Cu+5 percent $MgCl_2$+S: fired at 950°C for 4 hr. in sealed tube: blende; (c) ZnS-Cu made at 1030°C (wurtzite) refired at 850°C for 1 hour in sealed tube with sulfur; mainly wurtzite (d) ZnS-Cu made at 1030°C (wurtzite) refired at 850°C with sulfur for 6 hours in sealed tube: blende.

zinc oxide and other excess semiconductors, one would expect that the blue luminescence of pure zinc sulfide and the shallower electron traps in copper activated zinc sulfide might be associated with sulfur deficiency in the sulfide lattice.[9] Experiments designed to test this hypothesis gave no very definite evidence for or against it. In fact, it is not easy to carry out experiments to test the effect of variation in sulfur concentration on the electron trap distribution. It must be recognized that ZnS-Cu phosphors are normally produced in a cloud of sulfur vapor (also sulfur dioxide) resulting from the evaporation of sulfur contained in the original zinc sulfide precipitate. In experiments with phosphors made in sealed quartz tubes the pressure could be increased to one to five atmospheres, but any really effective attempt to remove sulfur vapor also removed the green luminescence characteristic of the copper impurity (and, if anything, also reduced the blue emission). Phosphors prepared by heating in vacuum luminesce a pale blue and cannot be reactivated by adding copper afterwards at 600°C. The same applies to copper activated zinc sulfide phosphors fired in crucibles at temperatures above 1500°C. It appears that copper escapes from the zinc sulfide lattice under these conditions, and some permanent change is produced in the lattice which prevents copper from re-entering. The recent significant observations of Rothschild[6] on the role of halides in zinc sulfide phosphors may lead to an explanation of some of these observations.

A number of experiments were carried out which appeared at first sight to indicate that the deep electron traps in ZnS-Cu phosphors were due to sulfur deficiency. Copper activated phosphors fired at 1100°C did not alter their trap distribution if refired at 1100°C in a closed tube containing a few

[9] J. T. Randall, Trans. Faraday Soc. **35**, 85 (1939).

atmospheres of sulfur vapor but, if refired at 800°–900°C for as long as six hours with sulfur, the deep traps were "killed" (compare curves *c* and *d*, Fig. 6). Heating at 900°C for only one hour did not, however, alter the phosphor and hence, if sulfur deficiency is associated with traps, it would appear that sulfur cannot readily diffuse into the zinc sulfide lattice. After one hour of firing at 850°C the coarsely crystalline phosphor was inappreciably recrystallized, but after six hours the phosphor was entirely converted into plate-like blende crystals. In all experiments which showed sulfur "killing" of electron traps a new recrystallized phosphor was produced at a lower temperature than the original, and it was immaterial whether the constituent atoms of this phosphor were derived from the original phosphor or from unheated zinc sulfide. It appears that sulfur is effective in "killing" deep electron traps only because it is an effective recrystallizing agent or flux. It is clear that an increase of 50°C in the firing temperature (especially in the range 950°C to 1050°C) produces a noticeable increase in the number of deep traps, but an increase in the sulfur vapor pressure, while tending to decrease the number of deep traps, never produces such a clear-cut change as does this small increase in temperature. In no case was it possible (without additional impurity inclusions such as nickel) to produce wurtzite phosphors with the luminescence characteristic of copper but possessing no deep traps. Possibly, if copper activated zinc sulfide phosphors were fired at temperatures slightly in excess of 1020°C with several hundred atmospheres of sulfur vapor, this result could be achieved.

If the deep electron traps in ZnS-Cu phosphors are not associated with excess or deficiency of sulfur, it is possible that they might be due to disorder in the crystal lattice produced at the high firing temperatures and frozen in by rapid cooling. Rapid cooling or slow annealing (six hours to fall in temperature from 1050° to 950°C), however, did not alter the trap distribution in the phosphor.

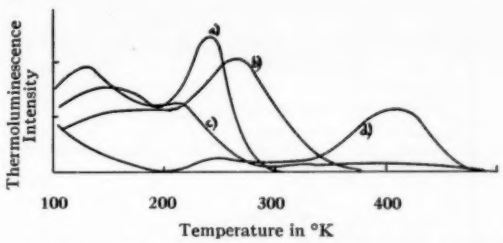

FIG. 8. Thermoluminescence characteristics of ZnS-CdS-Cu phosphors made at 1100°C. (a) ZnS (85 percent)-CdS (15 percent) no copper; (b) ZnS (85 percent)-CdS (15 percent)-Cu (0.01 percent); (c) ZnS (55 percent)-CdS (45 percent)-Cu (0.01 percent; (d) ZnS (45 percent)-CdS (55 percent)-Cu (0.01 percent) curve increased in height approx. 10 times.

Further light is cast on the nature of deep traps in ZnS-Cu phosphors by experiments in which the zinc sulfide was heated to a high temperature without copper and the copper added in a subsequent refiring at 400°–600°C. The effect of this refiring on the glow curve is shown by curves *a* and *b* of Fig. 7. (The small thermal glow between 300° and 400° on curve *a* is due to small traces of copper—probably 0.001–0.0001 percent). The phosphor produced in this way was almost identical in characteristics with that produced by firing the zinc sulfide together with copper impurity at the high temperature. It is clear that high temperature treatment of the zinc sulfide produces some change in the crystal lattice and that the copper impurity may afterwards diffuse into the lattice at a much lower temperature. The presence of copper and the change in the lattice together produce the deep electron traps.

Curve *c* of Fig. 7 shows the "killing" effect of a small amount of nickel impurity on the trap distribution of ZnS-Cu phosphor. Independent measurements of dielectric changes in nickel-killed phosphors, made by Garlick and Gibson (1947)[10] show that the deep traps are destroyed by the nickel and not merely inhibited from supplying electrons to

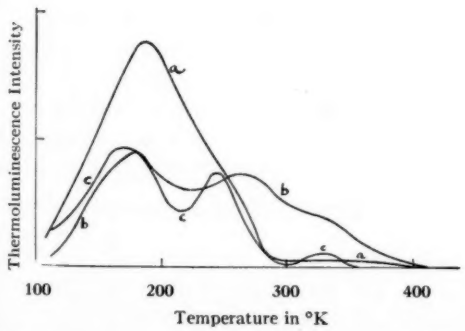

FIG. 7. Effect of copper addition to pure ZnS phosphor at relatively low temperature and destruction of traps by addition of Ni as shown by thermoluminescence curves. (a) pure ZnS phosphor made at 1050°C: wurtzite: blue luminescence; (b) phosphor *a* reheated at 425°C with 0.01 percent Cu: green luminescence; (c) ZnS-Cu phosphor (wurtzite) heated at 1100°C with 0.0005 percent Ni.

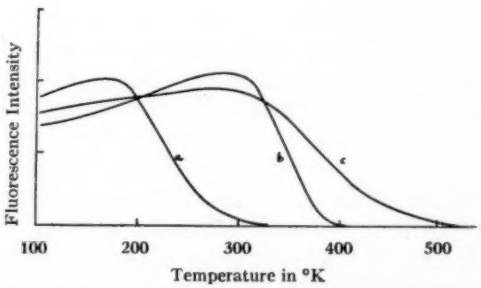

FIG. 9. Fluorescence *vs.* temperature curves for pure ZnS and ZnSAg phosphors excited by 3650A radiation of constant intensity. (a) pure ZnS made at 500°C: blende; (b) pure ZnS made at 1000°C: blende; (c) ZnS-Ag made at 1000°C: blende.

[10] G. F. J. Garlick and A. F. Gibson, Proc. Roy. Soc. **A188**, 485 (1947).

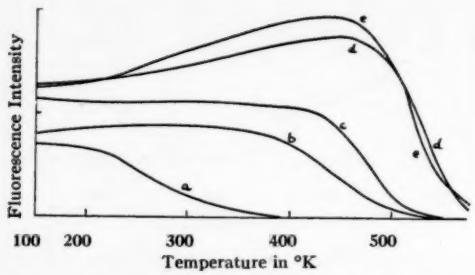

FIG. 10. Fluorescence (green band only) *vs.* temperature curves for ZnS-Cu phosphors excited by constant intensity 3650A radiation. (a) ZnS-Cu made at 500°C; (b) ZnS-Cu made at 700°C; blende; (c) ZnS-Cu made at 900°C: blende; (d) ZnS-Cu made at 1000°C: blende (some wurtzite); (e) ZnS-Cu made at 1160°C: wurtzite.

luminescence centers, as suggested by some workers (cf. Klasens 1946).[11]

Experiments were made to find the effect of oxygen in the air on the phosphors during firing (phosphors being fired in nitrogen, specially exposed to air, and in the normal manner). No clear effect was found, but it must be remembered that all the phosphors probably contained oxide from the hydroxide present in the original zinc sulfide precipitate.

(d) Zinc Sulfide-Cadmium Sulfide Phosphors Activated by Copper

Except for specimens of high ZnS content, the mixed crystal system ZnS-CdS has always the wurtzite structure, but the lattice dimensions depend on the ZnS:CdS ratio. The effect of this ratio on the trap distributions in ZnS-CdS-Cu phosphors all made at the same temperature, and with the same copper concentration, is shown in the four curves of Fig. 8. As shown by curves *a* and *b* of this figure, the introduction of copper into ZnS-CdS phosphors gives rise to deep traps as in ZnS-Cu phosphors. As the cadmium sulfide content increases, for constant copper concentration, marked changes in the trap distributions take place. For phosphors with less than 45 percent CdS the increase in CdS content tends to suppress the deep traps, but for higher CdS concentrations (curve *d*) very deep traps are produced. It is not possible to compare the relative heights of the curves of Fig. 8 as the emission color shifts from green to red with increase in CdS content, and the curves have not been corrected for the rapid decrease in sensitivity of the recording electron multiplier with increase in wave-length of the impinging radiation. Thus the high temperature glow peak of curve *d* may represent a considerable number of deep traps. It is possible that the change in the trap distribution with increasing cadmium content is simply a shift of the distribution towards lower values of trap depth and this, like the corresponding shift of the luminescence spectrum, is to be accounted for by the progressive shift of lattice energy zones relative to impurity levels.

(e) Fluorescence *vs.* Temperature Characteristics and Phosphor Constitution

Measurements of the variation of the fluorescence intensity with temperature under constant high intensity excitation by ultraviolet radiation of 3650A wave-length were made for the phosphors described in the above sections. Experimental curves for representative specimens are given in Figs. 9 and 10. As shown by curves *a* and *b* of Fig. 9 for self-activated "pure" zinc sulfide phosphors, the firing temperature has a marked influence on the upper limit of temperature at which the fluorescence is "quenched." In general, for ZnS with any activator for firing temperatures up to 1000°C the quenching temperature for the fluorescence increases with firing temperature and for higher firing temperatures remains unaltered. Curves *a* and *b* may be supplemented by Randall's[12] observations on pure unheated zinc sulfide which is non-fluorescent under intense excitation at room temperature but shows emission when excited at liquid oxygen temperature (90°K). The addition of silver impurity with subsequent firing at 1000°C (curve *c*, Fig. 9) causes an extension of the fluorescence *vs.* temperature curve to higher temperature. This is a general result for the addition of activating impurities to zinc sulfide.

Measurements of the temperature variation of "green band" fluorescence from copper activated zinc sulfides made at different temperatures are represented by the curves of Fig. 10. As for the specimens of Fig. 9, increase in firing temperature improves the fluorescence efficiency at higher temperatures, but the characteristics change little with firing temperature above 1000°C. For ZnS-Cu phosphors prepared by heating ZnS to a high temperature and adding the copper subsequently at a low temperature the fluorescence temperature curve is the same as that for a ZnS-Cu phosphor fired with impurity at the high temperature. The blue band of emission in ZnS-Cu varies with temperature in the same way as the blue emission of self-activated ZnS.

ACKNOWLEDGMENTS

Our thanks are due Professor M. L. Oliphant, F.R.S., for his encouragement and provision of facilities for this work, Professor J. T. Randall, F.R.S., who initiated this research, for his constant encouragement and helpful discussion, and Mr. A. F. Gibson for the measurements of Fig. 10. Many of the phosphors were prepared by Miss B. M. Browne.

[11] H. A. Klasens, Nature **157**, 306 (1946).

[12] J. T. Randall, Trans. Faraday Soc. **35**, 2 (1939).

Contribution of the Deviation from Perfect Gas Behavior to the Entropy and Heat Capacity. Water and Benzene

J. O. HALFORD
Chemistry Department, University of Michigan, Ann Arbor, Michigan
(Received October 4, 1948)

The properties of water vapor are used to illustrate the point, previously found true for ethyl alcohol, that the modified Berthelot equation of state may not give a satisfactory evaluation of the deviation of thermodynamic properties from those of the hypothetical perfect gas. The entropy deviation for benzene, however, is accurate enough for most purposes, and the heat capacity is not too far out of line.

On limited information, it appears that the Berthelot equation may be satisfactory for the vapors of "normal" liquids up to limited pressures. It is recommended, however, that some attempt be made to check the properties by means of vapor densities, obtained directly or by the Clapeyron equation, before results based upon the Berthelot equation are accepted.

IT is often desired, for practical purposes, to calculate the entropy or heat capacity of a gaseous substance from spectroscopic data and molecular constants. Likewise, it may be desired to calculate these properties for the hypothetical perfect gas from thermal data and vapor pressures. In either case, it is necessary to evaluate the effect of the deviation from perfect gas behavior, an operation which, for maximum accuracy, would require extensive knowledge of the vapor density over a wide range of pressures and temperatures, or the equivalent in the form of an accurate and sufficiently detailed equation of state.

When adequate data are not available it has become broadly customary to use the modified Berthelot equation of state, with constants expressed in terms of the critical properties, to give an approximation to the entropy and heat capacity deviations.

The accuracy of this approximation was recently questioned by the author[1] in a study of the entropy of ethyl alcohol, for which it developed that no reasonable combination of assigned molecular constants could be found which was consistent with the experimental entropy and the Berthelot equation over a sufficiently extended temperature range. Because the vapor pressures and heats of vaporization were apparently reliable and were inconsistent with volumes calculated from the Berthelot equation, it was most reasonable to assume that these volumes and the equation of state from which they were obtained were not acceptable.

In the ethyl alcohol case, the assignment of a potential barrier of at least 15000 cal./mole to the hydroxyl group rotation was required if the Berthelot equation was used, but if the barrier evaluation was based upon the data at a low enough temperature, and larger deviations from perfect gas behavior at high temperature were recognized, a value near 3000 cal./mole was obtained. This illustrates how the inadequacy of the Berthelot equation can lead to serious errors in the description of hindered internal rotations.

The significance of the ethyl alcohol case to the general problem is obscure. It may mean only that inaccuracies will be found for the vapors of associated liquids, but it could be true that serious errors would appear elsewhere as well.

The purpose of the present paper is to compare the correct entropy and heat capacity deviations with those obtained from the Berthelot equation for two substances, water and benzene, chosen as examples, respectively, of the associated and the normal liquid. There are, in fact, very few compounds for which there are enough data to support an accurate calculation of the deviations. In the case of ethane, heat capacity increments calculated by Kistiakowsky and Rice[2] from the vapor densities of Eucken and Parts[3] are substantially the same as those obtained from the Berthelot equation.

WATER

The required information for water vapor appears in a recent article by Keyes,[4] who tabulates the second, third, and fourth virial coefficients and their derivatives as functions of the temperature and gives the explicit expression for the entropy correction. The units at the head of the columns of virial coefficients, however, cannot be correct, the expressions for the coefficients in the entropy equation are not clearly bracketed, and the true entropy coefficients appear to be the negatives of the indicated ones. In using the Keyes expression, therefore, it has been assumed that the virial coefficients are correct for energy in cc atmos., the missing brackets

[1] J. O. Halford, J. Chem. Phys. **17**, 111 (1949).

[2] G. B. Kistiakowsky and W. W. Rice, J. Chem. Phys. **5**, 281 (1939).

[3] A. Eucken and A. Parts, Zeits. f. physik. Chemie **20B**, 189 (1933).

[4] F. G. Keyes, J. Chem. Phys. **15**, 602 (1947).

TABLE I. Entropy of gas imperfection for water vapor at saturation pressures (cal./mole deg.).

T (°K)	p (at.)	S^*-S	S^*-S (Berthelot)
273.2	0.006026	0.006	0.001
283.2	0.01211	0.009	0.001
293.2	0.02306	0.013	0.002
303.2	0.04187	0.018	0.003
313.2	0.07281	0.025	0.005
323.2	0.12179	0.035	0.008
333.2	0.19667	0.045	0.011
343.2	0.30764	0.060	0.016
353.2	0.46752	0.077	0.022
363.2	0.69201	0.098	0.030
373.2	1.0000	0.122	0.040
383.2	1.4137	0.150	0.052
393.2	1.9589	0.183	0.067
403.2	2.6650	0.222	0.085
413.2	3.5648	0.268	0.105
423.2	4.6952	0.313	0.129
433.2	6.100	0.352	0.157
443.2	7.817	0.410	0.187
453.2	9.895	0.478	0.220

have been supplied to the expressions for the coefficients, and the sign of the entire entropy effect has been reversed. The increments finally obtained have been added to the perfect gas entropy and found to agree with the entropy values of Osborne, Stimson, and Ginnings[5] within precisely the same limits as stated in the last paragraph of the paper by Keyes. Units and conversion factors correspond to the following values of the gas constant: 1.9872 cal./mole deg., 82.057 cc atmos./mole deg., 8.3130 int. joule/mole deg. In checking against the entropy values of Osborne, Stimson, and Ginnings, the results obtained from the Keyes' equation were converted to calories defined by the conversion factor 0.238891 cal./int. joule.

Table I shows the entropy of gas imperfection for water vapor at the saturation pressure from 273.2°K to 453.2°K. The second column gives the vapor pressure, the third the entropy correction from the Keyes data and the fourth the corresponding increment from the modified Berthelot equation.

TABLE II. Estimated heat capacity of gas imperfection for water vapor at one atmosphere (cal./mole deg.).

T (°K)	$C-C^*$	$C-C^*$ (Berthelot)
303.2	16.19	0.22
313.2	8.42	0.21
323.2	5.20	0.20
333.2	3.18	0.17
343.2	1.93	0.16
353.2	1.52	0.14
363.2	1.12	0.13
373.2	0.86	0.12
383.2	0.67	0.10
393.2	0.54	0.09
403.2	0.44	0.08

[5] N. S. Osborne, H. F. Stimson, and D. C. Ginnings, J. Res. Nat. Bur. Stand. **23**, 261 (1939).

The vapor pressures up to 423.2° are taken from Keyes, those at higher temperatures come from the International Critical Tables. The last three entropy increments have been obtained by difference from the entropies of Osborne, Stimson, and Ginnings and the Keyes' expression for the perfect gas, and may be low by one or two percent. The critical constants used for the last column are $T_c=643.2$°K, $p_c=217.7$ atmos.

Whether or not the Berthelot values are acceptable depends upon the achievable accuracy of the result. In relation to the limits ± 0.05 cal./mole deg. placed by Giauque and Stout[6] upon their value for the liquid at 298.2°K, the error introduced by the Berthelot equation is negligible (less than 10 percent of the total) only at the lowest temperature where the increment itself is practically negligible. The error becomes equal to the total estimated error in the region of 345°K where the pressure is about 0.35 atmos.

A rough picture of the situation in connection with the heat capacity can also be obtained from the data. It would appear to be very difficult to achieve accuracy in the heat capacity of gas imperfection. For example, if the simplified virial equation of state,

$$pV=RT+Bp \tag{1}$$

is considered, the heat capacity increment is given by $\delta C_p/\delta p=-T\delta^2 B/\delta T^2$. The coefficient B, the difference between the perfect gas volume and the actual volume, is difficult to obtain with accuracy, and, consequently, the second derivative with the temperature will be subject to large errors.

For the present purpose, the entropy increment at one atmosphere has been calculated by the procedure used to set up Table I, and the heat capacity increment has been obtained as a rough graphical estimate of the equivalent quantity $T(\delta S/\delta T)_p$. Table II shows the result.

Obviously the Berthelot equation is not satisfactory. While it prescribes a fixed value of three for the heat capacity/entropy ratio, this ratio is variable and much larger. For example, the heat capacity increment at the boiling point is seven times as large as the entropy increment.

BENZENE

Scott, Waddington, Smith, and Huffman[7] have evaluated the coefficient B in Eq. (1) as

$$B(cc)=-202-53.5\exp[950/T]. \tag{2}$$

This equation has been made consistent with their measured heat capacities and those calculated from

[6] W. F. Giauque and J. W. Stout, J. Am. Chem. Soc. **58**, 1144 (1936).

[7] D. W. Scott, G. Waddington, J. C. Smith, and H. M. Huffman, J. Chem. Phys. **15**, 565 (1947).

molecular constants, subject to the validity of their interpretation of the effect of anharmonicity upon the vibrational entropy. The volumes are also in fair agreement with values obtained from heats of vaporization and vapor pressures by means of the Clapeyron equation.

If Eq. (2) is accepted as correct, then the entropy and heat capacity increments are independent of the pressure and are given by

$$S^*-S=pdB/dT$$

and

$$C-C^*=-pTd^2B/dT^2=(2+950/T)(S^*-S). \quad (3)$$

The entropy and heat capacity increments have been evaluated along the vapor pressure curve, using Young's vapor pressures, as quoted by Fiock, Ginnings, and Holton,[8] as accurate enough for present purposes. The results are presented in Table III. The critical constants used to obtain the Berthelot values are $T_c=561.7°K$ and $p_c=47.7$ atmos.

Here the Berthelot equation gives a remarkably good evaluation of the entropy effect throughout the entire range and is in exact agreement just above the boiling point. The heat capacity, however, is not very good at the lower temperatures but is approaching agreement as the temperature increases.

TABLE III. Entropy and heat capacity of gas imperfection for benzene vapor at saturation pressures (cal./mole deg.).

T (°K)	p (at.)	S^*-S	S^*-S Berthelot	$C-C^*$	$C-C^*$ Berthelot
273.2	0.0349	0.019	0.011	0.102	0.032
283.2	0.0598	0.026	0.016	0.141	0.049
293.2	0.0982	0.036	0.024	0.188	0.074
303.2	0.1556	0.048	0.035	0.245	0.104
313.2	0.2383	0.062	0.048	0.312	0.145
323.2	0.3539	0.079	0.065	0.389	0.196
333.2	0.5113	0.098	0.086	0.476	0.258
343.2	0.7203	0.120	0.111	0.571	0.333
353.2	0.9916	0.146	0.140	0.682	0.420
363.2	1.337	0.171	0.174	0.787	0.521
373.2	1.769	0.199	0.212	0.906	0.635
383.2	2.300	0.230	0.256	1.030	0.764
393.2	2.945	0.263	0.303	1.160	0.907
403.2	3.717	0.300	0.353	1.294	1.059

CONCLUSIONS

From the foregoing examples, including the cases of ethane and ethyl alcohol to which reference has been made, it would appear that the entropy of gas imperfection can be obtained with fair accuracy for the vapors of normal liquids from the modified Berthelot equation of state, but that for water and the lower alcohols, an evaluation by this equation may not be satisfactory.

Heat capacity increments for the associated compounds, when obtained from the Berthelot equation, are seriously in error, and they are not highly dependable even in the case of benzene.

Under the circumstances, it would appear advisable to limit the application of the Berthelot equation to the entropy increment for non-associated substances to pressures well below one atmosphere and to use this equation, or any other selected in a similarly arbitrary manner, for associated substances only when it clearly indicates that the increment is negligible relative to the limits of error from other sources.

Because the number of accurately demonstrable cases is not sufficient to support a broad generalization, it would be most conservative, even for the vapors of normal liquids, to use the Berthelot equation only when some supporting data are available.

USE OF THE CLAPEYRON EQUATION

The virial coefficient of Eq. (1) is given by the exact Clapeyron equation as

$$B=V(l)+\Delta H/(Tdp/dT)-RT/p \quad (4)$$

in which $V(l)$ is the molal volume of the liquid at saturation and is negligible at low pressures. When the vapor pressure and heat of vaporization are known with enough accuracy as functions of the temperature, the deviation volume B can be obtained in relation to the temperature. If it is assumed, as in the case of benzene, that B is a function only of the temperature, the entropy and heat capacity effects can be obtained by Eqs. (3). Since, however, both ΔH and dp/dT are hard to measure accurately, and the error in their ratio will be magnified by the subtraction of the perfect gas volume, it will be difficult to obtain B accurately, and progressively more difficult to obtain the first and second temperature derivatives.

A number of trials with data of ordinary accuracy to be found in the literature have indicated that the highest accuracy will probably be obtained near the boiling point and that at low temperatures and pressures, the results are not dependable. It is therefore suggested that for most purposes it will be satisfactory to evaluate the entropy and heat capacity effects in the region of the boiling point, and to project them into the region of lower temperatures along some arbitrary curve which brings them near zero at temperatures of the order of 100° below the boiling point.

A variation of the method of using the Clapeyron equation is possible which may at some time prove to be useful. Lewis and Randall[9] have shown that, for a gas obeying Eq. (1), if B is a function of the

[8] E. F. Fiock, D. C. Ginnings, and W. B. Holton, J. Res. Nat. Bur. of Stand. **6**, 881 (1931).

[9] G. N. Lewis and M. Randall, *Thermodynamics and the Free Energy of Chemical Substances* (McGraw-Hill Book Company, New York, 1923), p. 197.

temperature alone and is small relative to the volume, the fugacity, defined by the relation $F=RT\ln f$, can be expressed as

$$f=p^2/p(\text{ideal})=pV/V(\text{ideal}). \quad (5)$$

The fugacity can be calculated from vapor densities or from the volumes obtained by means of the Clapeyron equation and, since this property must represent the pressure at which the hypothetical perfect gas would be at equilibrium with the liquid, it follows, if the liquid volume is negligible, that

$$\Delta S^*=RTd\ln f/dT. \quad (6)$$

Equation (6) gives the entropy of vaporization to the ideal gas at the pressure f, and its use should be the practical equivalent of the usual separate evaluation of the entropies of vaporization and of gas imperfection.

THE JOURNAL OF CHEMICAL PHYSICS VOLUME 17, NUMBER 4 APRIL, 1949

Thermal Diffusion in Hydrogen-Hydrocarbon Mixtures

H. G. DRICKAMER, S. L. DOWNEY, AND N. C. PIERCE
Department of Chemistry, University of Illinois, Urbana, Illinois

(Received October 8, 1948)

Thermal diffusion data have been obtained on a series of mixtures of hydrogen plus hydrocarbons. The results indicate that "collision diameter" for these unlike molecules is considerably smaller than the mean collision diameter of the pure compounds. This is consistent with the high critical pressure of such mixtures.

NOMENCLATURE

α—Thermal diffusion ratio
D_{12}—Coefficient of ordinary diffusion
ϵ—Difference between energy of separated molecules and configuration for which they have maximum attraction
E—Potential energy
m—Molecular mass
M_1—(m_1/m_1+m_2)
r—Intermolecular distance
r_0—"Collision diameter"—distance of separation from zero interaction energy
T_1, T_2—Temperatures of upper and lower bulb respectively
T_m—Average temperature
v_1, v_2—Convection velocities of species 1, 2
$W^l r$—Integral involving collision cross sections
x_1, x_2—Mole fractions of species 1, 2

THEORY

THE thermal diffusion ratio α is defined by the equation,

$$x_1x_2(v_1-v_2)=D_{12}(-\text{grad}x_1+x_1x_2\alpha\ \text{grad}\ln T). \quad (1)$$

From the kinetic theory of gases Chapman and Cowling[1] give the following relationship for α:

$$\alpha=5(c-1)\frac{x_1S_1+x_2S_2}{x_1Q_1+x_2Q_2+x_1x_2Q_{12}} \quad (2)$$

which for 50-50 mixtures of gases reduces to

$$\alpha=10(c-1)\frac{S_1+S_2}{Q_1+Q_2+Q_{12}} \quad (2')$$
$$=10(c-1)G,$$

where

$$S_1=\frac{M_1}{M_2^{\frac{1}{2}}}\left(\frac{r_{01}}{r_{012}}\right)^2\frac{W_1^{(2)}(2)^{\sqrt{2}A}}{W_{12}^{(2)}(2)}-M_2\{3(M_2-M_1)+4M_1A\}, \quad (3)$$

$$Q_1=\frac{\sqrt{2}A}{M_2^{\frac{1}{2}}}\left(\frac{r_{01}}{r_{012}}\right)^2\frac{W_1^{(2)}(2)}{W_{12}^{(2)}(2)}\times\{6M_2^2+5M_1^2-4M_1^2B+8M_1M_2A\}, \quad (4)$$

$$Q_{12}=(M_1-M_2)^2(5-4B)+4M_1M_2A(11-4B)+4\left(\frac{r_{01}}{r_{012}}\right)^2\left(\frac{r_{02}}{r_{012}}\right)^2\times\frac{A^2}{(M_1M_2)^{\frac{1}{2}}}\frac{W_1^{(2)}(2)W_2^{(2)}(2)}{(W_{12}^{(2)}(2))^2}, \quad (5)$$

$$A=(W_{12}^{(2)}(2)/5W_{12}^{(1)}(1)), \quad (6)$$

$$B=(5W_{12}^{(1)}(2)-W_{12}^{(1)}(3)/5W_{12}^{(1)}(1)), \quad (7)$$

$$C=(2W_{12}^{(2)}(2)/5W_{12}^{(1)}(1)). \quad (8)$$

S_2, Q_2 can be obtained by reversing subscripts.

The nomenclature has been modified slightly to correspond to that used by Hirschfelder, Bird, and Spotz.[2]

The evaluation of the integrals $W^{(l)}(r)$ involves the use of the collision cross section and therefore depends on the intermolecular force law assumed. Hirschfelder *et al.*,[2] have evaluated these integrals

[1] S. Chapman and T. G. Cowling, *Mathematical Theory of Non-uniform Gases* (Cambridge University Press, Teddington, 1939).

[2] J. O. Hirschfelder, R. B. Bird, and E. Spotz, J. Chem. Phys. 16, 968 (1948).

TABLE I.

100°C—Boiling water
20°C—Tap water
−40°C—Alcohol plus dry ice
−80°C—Chloroform and carbon tetrachloride plus dry ice

for the Lennard Jones model

$$E(r)=4\epsilon[-(r_0/r)^6+(r_0/r)^{12}]. \quad (9)$$

As is discussed in the above paper, it is possible to evaluate ϵ and r_0 for pure compounds from viscosity data. Using Eq. (2′) and experimental values of α it is possible to evaluate ϵ_{12} and $(r_0)_{12}$ for collisions between unlike molecules. The factor G is relatively insensitive to the value of ϵ_{12} and to T, but depends more strongly on the ratios r_{01}/r_{012} and r_{02}/r_{012}. On the other hand $(C-1)$ is very strongly dependent on the value of ϵ_{12} and T, but independent of the ratios r_{01}/r_{012} and r_{02}/r_{012}. This simplifies the evaluation of these quantities from experimental α's.

Before comparison with experiment is possible it is necessary to obtain the temperature corresponding to the experimental α.

For the steady state (1) reduces to

$$\frac{1}{x_1(1-x_1)}\,\mathrm{grad}x_1=\alpha\,\mathrm{grad}\ln T. \quad (10)$$

TABLE II.

T_1	T_2	$\bar{T}_m$	Pressure CmHg	% H_2 Upper	Lower	α
Methane-Hydrogen	°K					
537°	372°	445	102.7	51.34	48.66	0.292
537°	372°	445	96.3	51.34	48.66	0.292
523°	299°	391	97.4	52.01	47.99	0.288
523°	299°	391	94.7	52.00	48.00	0.288
474°	299°	353	100.5	51.14	48.86	0.261
470°	300°	352	98.9	51.16	48.84	0.267
363°	195°	262	104.0	51.90	48.10	0.231
299°	190°	236	89.2	51.22	48.78	0.222
299°	189°	236	87.9	51.18	48.82	0.212
Ethylene-Hydrogen						
532°	372°	443	95.9	51.33	48.66	0.299
523°	301°	392	97.8	51.89	48.11	0.274
523°	301°	392	112.1	51.94	48.06	0.281
364°	194°	262	90.7	51.94	48.06	0.250
363°	195°	262	102.6	51.90	48.10	0.243
302°	192°	239	92.1	51.37	48.63	0.242
301°	191°	239	92.7	51.34	48.66	0.239
Propylene-Hydrogen						
530°	372°	442	105.1	51.47	48.53	0.321
523°	299°	390	93.9	52.18	47.82	0.308
523°	293°	386	86.7	52.11	47.89	0.302
417°	295°	349	97.3	51.18	48.82	0.279
375°	230°	290	92.1	51.75	48.25	0.282
376°	232°	293	89.5	51.72	48.28	0.284
Propane-Hydrogen						
531°	372°	442	81.5	51.48	48.52	0.323
523°	299°	391	105.0	52.18	47.82	0.315
524°	294°	387	97.6	52.30	47.70	0.318
476°	300°	354	93.1	51.22	48.78	0.283
375°	231°	292	93.2	51.78	48.22	0.291

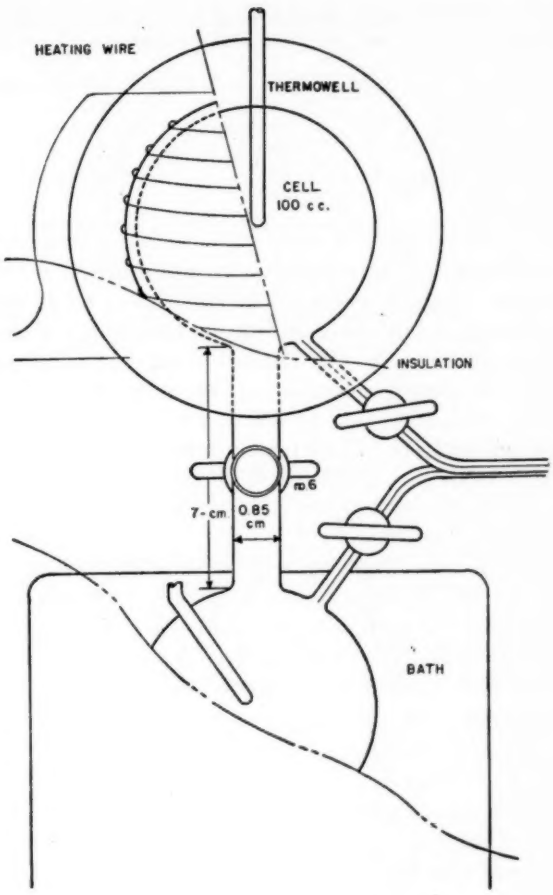

FIG. 1. Thermal diffusion equipment.

To integrate this the dependence of α on T must be known. The actual dependence is somewhat complicated for the Lennard Jones model, but it can be approximated reasonably well in the temperature range considered below by the formula:

$$\alpha=A-(B/T). \quad (11)$$

Brown[3] has shown that using the relationship (11)

$$\bar{T}_m=\frac{T_1T_2}{T_1-T_2}\ln\frac{T_1}{T_2}. \quad (12)$$

EXPERIMENTAL PROCEDURE AND RESULTS

While Eqs. (2) and (2′) were derived specifically for spherically symmetrical molecules, nevertheless it was felt that it would be of interest to obtain values of $(r_0)_{12}$ and ϵ_{12} for hydrogen-hydrocarbon systems.

The essential features of the experimental apparatus are shown in Fig. 1. The temperatures in the upper bulb were obtained by use of the heating wire. For the lower bulb the temperatures were obtained as shown in Table I.

[3] H. Brown, Phys. Rev. **58**, 661 (1940).

TABLE III.

	ϵ	r_0
H_2	33	2.97
CH_4	136	3.88
C_2H_4	200	4.27
C_3H_6	245	4.83
C_3H_8	250	4.94

TABLE IV.

	ϵ_{12}	$r_{0_{12}}$	$(\epsilon_1\epsilon_2)^{\frac{1}{2}}$
H_2-CH_4	88±3	2.90	67
$H_2-C_2H_4$	81±2	2.62	81
$H_2-C_3H_6$	84±3	2.75	90
$H_2-C_3H_8$	80±3	2.70	91

In general it was possible to maintain the temperature in the lower bulb within ±2°C while that in the upper bulb was maintained within ±5°C.

The pressure in the bulbs during the runs was about 1.5 atmospheres. It was maintained constant during each run, but no effort was made to reproduce precisely the same pressure from run to run.

The systems investigated were hydrogen-methane, hydrogen-ethylene, hydrogen-propylene, and hydrogen-propane.

The binary mixtures were made up to contain fifty percent of each gas by pressure. Analyses were performed by measuring the difference in refractive index between the samples in the top and bottom bulbs on a Zeiss laboratory interferometer with a 25-cm cell. All runs were made in duplicate and for different lengths of time to insure that steady state had been reached. The experimental results are shown in Table II.

In Table III are given the values of ϵ and r_0 obtained for the pure components from viscosity data. To evaluate ϵ_{12} and r_{012} from experimental values of α it was first assumed that the ratios r_{01}/r_{012} and r_{02}/r_{012} would be independent of temperature. Then, for any assumed value of these ratios the value of ϵ_{12} could be established by trial, evaluating A, B, C, and $W^{(l)}(r)$ from the work of Hirschfelder *et al.*[2]

For most assumed values of r_{012} the ϵ_{12} obtained were temperature dependent. In Table IV are shown the values of r_{012} and corresponding values of ϵ_{12} for the particular value of ϵ_{12} which are independent of the temperature. It can be seen that the effective collision diameter for hydrogen-hydrocarbon collisions is slightly less than the collision diameter for hydrogen-hydrogen collisions, also, ϵ_{12} is considerably less than the geometric mean of the ϵ values.

The precise significance of these results for molecules which are so far from spherically symmetrical is open to considerable question. At least one physical fact can be pointed out which is consistent with these values. Hydrogen-hydrocarbon mixtures are known to have a critical pressure considerably higher than the critical pressure of the pure gases which would correspond to interaction only at very small separations.

The Application of Ultrasonic Waves to the Study of Electrolytic Solutions

II. The Detection of the Debye Effect*

ERNEST YEAGER, JOHN BUGOSH, FRANK HOVORKA, AND JOHN MCCARTHY
Departments of Chemistry and Physics, Western Reserve University, Cleveland, Ohio
(Received October 13, 1948)

The existence of the alternating potentials which Debye predicted should accompany the passage of ultrasonic waves through an electrolytic solution has been established experimentally by means of a stationary acoustical field. The effect has been shown (i) to depend on velocity variations within the ultrasonic waves, (ii) to be a function of the electrolyte, and (iii) to be independent of concentration for practical purposes in the range 0.005 to 0.0005 molar for uni-univalent electrolytes. These characteristics are in agreement with theoretical considerations.

IN 1933 Peter Debye[1] proposed a method for the determination of the masses of solvated electrolytic ions which involved the introduction of ultrasonic waves into an electrolytic solution and the subsequent measurement of periodic differences in potential within the solution arising from the dynamic reactions of the ions to the acoustical waves. Debye obtained for the alternating potential the approximate equation[2]

$$\Phi=\frac{a_0 g m_H \sum p_j z_j M_j/\rho_j}{\epsilon \sum p_j z_j^2/\rho_j} \cdot \frac{4\pi\lambda/\omega D}{[1+(4\pi\lambda/\omega D)^2]^{\frac{1}{2}}} \exp i(\omega t-\sigma x-\Delta),$$

where

$$\Delta=\arctan(\omega D/4\pi\lambda),$$

a_0 and ω are the velocity amplitude and angular frequency of the ultrasonic waves, g is the velocity of propagation in the solution, σ is equal to ω/g, λ is the specific conductance of the solution (neglecting ionic interaction), D is the dielectric constant of water, m_H is the mass of the hydrogen atom ($1.67\cdot10^{-24}$ g), ϵ is the fundamental electric charge ($4.80\cdot10^{-10}$ e.s.u.), and $p_1, p_2, \cdots p_j, \cdots p_n$ are the relative numbers per unit volume of the different types of ions of valences $z_1, z_2, \cdots z_j, \cdots z_n$, gram-ionic-weights $M_1, M_2, \cdots M_j, \cdots M_n$, and frictional coefficients $\rho_1, \rho_2, \cdots \rho_j, \cdots \rho_n$. For an electrolytic solution such as 0.001 normal potassium chloride and ultrasonic waves of unit velocity amplitude and angular frequencies of the order 10^6 radians per sec., the amplitude of the alternating potential should be of the order of 10^{-6} volt according to the Debye equation if the difference between the effective gram-ionic-weight of the anions and cations is of the order 10. For solutions of 0.001 normal or greater and for ultrasonic waves with angular frequencies of 10^7 radians per sec. or less, the observed effect according to the Debye equation should be essentially independent of conductance or concentration, provided the effective masses of the solvated ions remain constant.

Although Debye, as well as other prominent investigators, expressed considerable optimism concerning the existence of the Debye effect as well as its utilization for the determination of the masses of solvated ions, no one had detected the effect in the case of electrolytic solutions[3] prior to the present investigation. The lack of experimental results can be traced to the difficult circumstances under which the investigation must be carried out. Whether the ultrasonic waves are produced by means of piezoelectric effects or magnetostriction, the possibility of direct electromagnetic coupling between the ultrasonic generator and the detection apparatus is very great.

CONSTRUCTION OF APPARATUS

The source of the ultrasonic waves which have been used in the detection of the Debye effect is a circular x-cut quartz crystal with a natural frequency of 265.5 kc. The quartz crystal is driven with a radiofrequency generator consisting of a Hartley electron-coupled oscillator and three stages of class C amplification, the last of which is a push-pull stage utilizing two Eimac 250 TH tubes. Link coupling is used between the plate coil of the last stage of the radio-frequency generator and a coil matched to the quartz crystal. The radiofrequency generator, as well as the coil matched to the quartz crystal, is housed in a copper case. The high po-

* A portion of the thesis submitted by E. Yeager and J. Bugosh in partial fulfillment of the requirements for the degree of Doctor of Philosophy in Chemistry at Western Reserve University, June 1948.

[1] P. Debye, J. Chem. Phys. 1, 13 (1933).

[2] A more exact form of this equation has been developed in the first paper of this series—Bugosh, Yeager, and Hovorka, J. Chem. Phys. 15, 592 (1947).

[3] Although unable to detect the effect for electrolytes, Rutgers and his co-workers have found a similar effect for a colloidal suspension. A. Rutgers, Physica 5, 46 (1938); Nature 157, 74 (1946); J. Vidts, Koninkl. Vlaamsche Acad. voor Wetenschappen 7, 5 (1945).

tential lead from the matching coil to the crystal is also shielded.

The circular quartz crystal, which has a diameter of 6.21 cm, is coated with a film of silver on both flat surfaces and is mounted within a thermostatic bath (Fig. 1), maintained at 25.0±0.1°C. The mounting

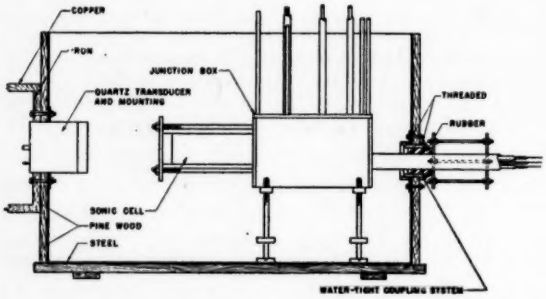

FIG. 1. Propagation apparatus: Vertical cross section.

(Fig. 2), which is constructed of brass and Plexiglass, permits the propagation of ultrasonic waves directly into the water. Electrical contact is made to the edge of the film of silver on the front face of the quartz crystal by means of three short, brass spring contacts, which are mounted on the grounded case. Electrical contact is made at the rear silvered face by means of a small brass brush which is held in place by a spring. Dow-Corning silicone stopcock grease is used as a packing about the circular edge of the crystal to prevent electrical breakdown.

Opposite the quartz transducer in the thermostatic bath is the cylindrical "sonic" cell (Fig. 3), which contains the electrolytic solution under investigation and the electrode assembly. The cell container is a Plexiglass tube with an internal diameter of 5.4 cm and a length of approximately 25 cm. Surrounding the plastic tube is a copper jacket. The end of the sonic cell through which the ultrasonic waves enter from the water in the outer tank is covered with a brass plate, 0.72 cm thick,[4] and a stretched latex membrane which isolates the brass plate from the electrolytic solution within the sonic cell. At the end of the sonic cell farthest from the quartz crystal is a brass piston or reflector, 0.99 cm thick, completely encased by a film of polystyrene. Mechanical connection is made to the piston by means of a polystyrene shaft, which enables the piston to be moved by controls located outside the thermostatic bath. By means of the reflector, standing waves are produced in the sonic cell. During most of the experimental work the sonic cell was located approximately 10 cm from the quartz transducer.

Theoretically, two electrodes are necessary for the detection of the Debye effect; in practice, one electrode appears to be sufficient. The electrolytic solution within the sonic cell at radiofrequencies is connected to ground by a rather low impedance which is primarily capacitive in nature. In effect, this low impedance to ground is equivalent to an electrode which is at the average potential of the solution. Hence it has been necessary to use only one electrode to detect the Debye effect and to measure its potential relative to ground. For a check, however, a platinum electrode has been placed behind the piston and provisions made for grounding this electrode. This electrode exposes to the solution a 6-mm length of No. 20 (B. and S.) platinum wire. Potentials have been measured between ground and one of two movable electrodes. The movable electrodes consist of No. 26 (B. and S.) platinum wire sealed in polystyrene holders with the dimensions of the exposed areas of the platinum wires small compared with the wave-length. Each electrode holder

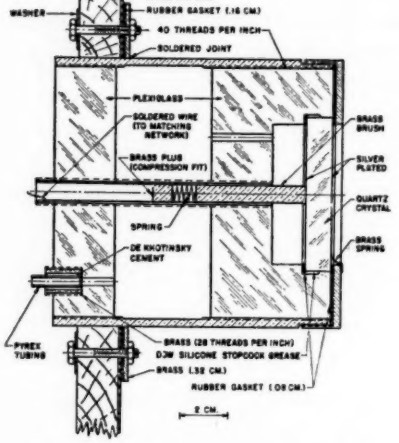

FIG. 2. Underwater transducer.

consists of a polystyrene tube of 0.925 cm in outer diameter with a brass tube inside to give structural strength. Through the center of each brass tube runs a shielded cable to the platinum electrode. Each electrode holder is connected to a mechanical drive by which it can be moved back and forth along the axis of the sonic cell. Changes in the position of each electrode as well as the reflector can be determined with an accuracy of approximately 0.002 cm. During most of the experimental work one of the movable electrodes was used as a "dummy" electrode by covering the surface of the platinum with a film of polystyrene which prevented direct contact between the platinum and the solution.

Acoustically produced phenomena can be distinguished from electromagnetically produced phenomena by moving the electrodes through the stationary sound field. The amplitude of the acoustically produced effects is a periodic function of the

[4] Theoretically a plate which is one-half wave-length (in brass) or 0.66 cm thick should transmit the ultrasonic waves with maximum efficiency. Experimentally, a slightly thicker plate 0.72 cm was found to be more efficient.

position of the electrode with respect to the velocity loops in the stationary field.

A shielded cable with a capacity of approximately 20 micromicrofarads per ft. extends from each electrode through a junction box and then a copper pipe to the detection apparatus, which is located approximately nine feet from the sonic cell. After passing through a switching network, the signal from the electrode assembly in the sonic cell enters a three-stage intermediate-frequency amplifier where it is amplified by a factor of approximately 10^5. The output from the last stage of the amplifier is fed into a Du Mont oscillograph, model 241. Quantitative measurements are made with an accuracy of ± 10 percent ± 1 microvolt by the substitution method with a Hickok standard microvolt signal generator, model 19X.

The switching network preceding the amplifier permits either one of the two movable electrodes in the sonic cell or the standard signal generator to be connected to the amplifier. Provisions have also been made for passing current through either platinum electrode with the detection apparatus connected simultaneously to the same electrode. In order to prevent direct coupling through the direct current source, a resistance-capacitance trap has been installed. The switching network is shielded by a separate copper case.

The three-stage amplifier is of conventional design. To minimize the possibility of direct coupling between the individual stages of the amplifier, as well as between the amplifier and the ultrasonic generator, radiofrequency wave traps have been placed in the plate leads of each stage, which shunt any radiofrequency components in these leads to ground. In addition, each stage has a separate, shielded filament transformer to reduce coupling through the heater circuit. A regulated power supply is used for the plate and screen voltages of the

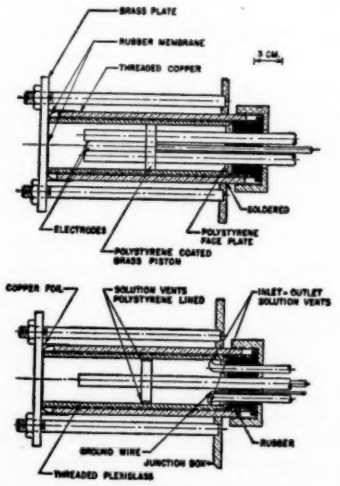

FIG. 3. Sonic cell. Horizontal and vertical cross sections.

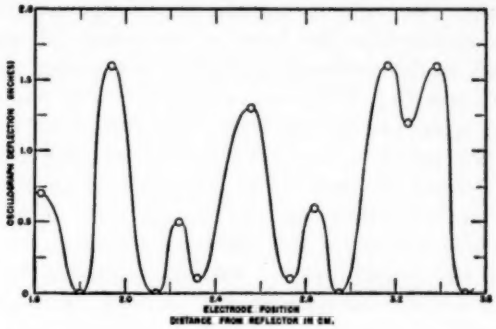

FIG. 4. Nature of acoustical field within sonic cell.

amplifier. An input of one microvolt to the detection apparatus from the Hickok standard microvolt signal generator produces a sinusoidal trace on the oscillograph with an amplitude of more than one inch when the detection apparatus is adjusted for maximum sensitivity. Background noise within the amplifier is equivalent to less than a 0.1-microvolt input. The copper case housing the switching network, the three-stage intermediate-frequency amplifier, and the power supply for the amplifier are contained in a double-layer copper box with the inner copper layer insulated from the outer by pine wood, $\frac{5}{8}$ in. thick.

EXPERIMENTAL RESULTS

With the sonic cell empty and the ultrasonic generator in operation at 264 kc with as much as 300 watts input to the last stage, the detection apparatus indicated an input signal of less than 0.5 microvolt with either the working or "dummy" movable electrode connected to the detection apparatus. When an electrolytic solution such as 0.001 normal potassium chloride was placed in the sonic cell, however, a much greater effect was produced with the working movable electrode connected to the detection apparatus. The amplitude of the effect was found to be a periodic function of the position of either the working electrode or the reflector. In Fig. 4 is shown the variation in the amplitude of the trace on the oscillograph for a 0.001-normal lithium chloride solution as the working electrode was moved in the sonic cell with the reflector in a fixed position. The gain on the oscillograph was adjusted so that a deflection of one inch on the cathode-ray tube corresponded to an input signal to the detection apparatus with an amplitude of six microvolts. The positions of the maxima are separated by approximately 0.29 cm or one-half wave-length in water. The maximum effect for the "dummy" electrode was less than one-tenth of that for the working electrode. This is in agreement with the concept of the film of plastic over the platinum surface of the "dummy" electrode as the dielectric of a small condenser which couples the electrode loosely to the

solution. The velocity amplitude of the ultrasonic waves incident to the front of the sonic cell was 2 cm/sec. as determined by radiation pressure measurements with a deflection pendulum.[5] The reflected waves were prevented from interfering with the radiation pressure measurements by placing a brass plate behind the deflection pendulum at an oblique angle to the direction of propagation. The low acoustical output of the ultrasonic generator minimized the possibility of thermal changes in the quartz crystal as well as the solution within the sonic cell.

Unfortunately, it has not been possible to establish either experimentally[6] or theoretically the velocity amplitude of the ultrasonic waves in the cell producing the observed effect, primarily because of the complex nature of the acoustical field within the sonic cell. The irregularity of the field as is evident from Fig. 4 is attributable to (i) the fact that the diameter of the electrode holder was appreciable compared with the diameter of the cell and (ii) the fact that the plane of the quartz transducer and the plane of the brass reflector were not exactly perpendicular to the axis of the cylindrical sonic cell. In addition, a standing field was set up not only between the front of the sonic cell and the reflector, but also between the quartz transducer and the reflector. Evidence of the interaction between the quartz transducer and the brass reflector within the cell was the periodic dip in the plate current of the last stage of the ultrasonic generator as the piston or reflector was moved in the sonic cell.

The fact that the alternating potentials are acoustically produced is not conclusive evidence that the Debye effect has been detected. Although the possibility is rather remote, the electrical effect might be the result of some other acoustically produced phenomenon. Unfortunately, it has not been possible to determine whether the observed effect is of the magnitude which might be expected on the basis of the Debye equation, because the velocity amplitude of the ultrasonic waves could not be determined and considerable doubt exists concerning the values now available for the masses of solvated ions. Other evidence is available, however, which indicates that this is the Debye effect. While absolute measurements in terms of velocity amplitude could not be made with the present apparatus, comparative values have been obtained for the effect in the case of different solutions. The results of these measurements are given in Table I. In order to minimize the possibility of any changes in the nature of the acoustical field within the sonic cell, the temperature of the solution within the cell was maintained at 25.0 ± 0.1°C and only dilute solutions have been considered. The ultrasonic generator was operated continuously for the period during which the comparative measurements were made. During this time the frequency[7] was 263.27 ± 0.02 kc. The velocity amplitude of the ultrasonic waves incident to the front of the sonic cell was 2.7 ± 0.3 cm/sec. as determined by radiation pressure measurements.

All of the values listed in Table I for the Debye effect have been determined relative to a reference solution, 0.005-normal potassium chloride, as 10. In each case the magnitude of the effect was established for the reference solution under investigation and the effect measured. The cell was then refilled with the reference solution and the magnitude of the effect remeasured. If the first and the last reading for the reference solution showed reasonable agreement, this implied that the acoustical conditions within the sonic cell had remained constant during the series of measurements. For the values listed in Table I the initial and final values for the reference solution agreed to within at least 15 percent. The sonic cell was rinsed out with distilled water prior to the introduction of each solution. To lower the possibility of gas formation on the electrode surfaces and on the front inside surface of the sonic cell, all the solutions were boiled under reduced pressure and then transferred to the sonic cell by displacement with argon. The conductance of each solution was determined after the solution was removed from the sonic cell and the concentration calculated.

From Table I it can be seen that a tenfold change in conductance or concentration for either lithium chloride or potassium chloride solutions produced an increase of less than 20 percent in the magnitude of the effect which is within experimental error. This is to be expected experimentally, since the effect is essentially independent of conductivity and, hence, concentration under these experimental conditions

TABLE I. A comparison of the Debye effect for different electrolytic solutions.

Electrolyte	Specific conductance $\text{ohm}^{-1}\,\text{cm}^{-1}$ $\times10^4$	Concentration (calculated) normality $\times10^3$	Relative values for alternating potentials
KCl (ref.)	7.57	5.26	(10)
KCl	0.706	0.474	12
KOH	6.39	2.4	15
LiCl	7.6	6.6	9
LiCl	0.65	0.56	11
NaCl	7.32	6.07	10
$CaCl_2$	7.56	6.08	8

[5] L. King, Proc. Roy. Soc. London **147**, 212 (1934); F. Fox, J. Acous. Soc. Am. **12**, 147 (1946).

[6] The Debye effect itself will be useful for the determination of the velocity amplitude of ultrasonic waves in liquids. Figure 4 demonstrates the utilization of the effect for exploring complex fields within cylindrical acoustical elements.

[7] The fundamental frequency was checked by means of beating the nineteenth harmonic against the 5-mc carrier of WWV, the National Bureau of Standards station in Washington, D. C. Frequency stability was of prime importance since even small frequency changes would alter the nature of the acoustical field within the sonic cell.

according to the Debye equation as indicated above. The effect appears to be a function of the particular electrolyte as would be expected for the Debye effect.

The mathematical treatment of the Debye effect predicts that the alternating potential should be in phase with the velocity variations in the ultrasonic field except for the factor

$$\Delta = \text{arc tan}(\omega D/4\pi\lambda).$$

For a 0.001-normal solution of a uni-univalent electrolyte and a frequency of 265 kc/sec., Δ is less than four degrees and thus the alternating potentials are almost in phase with the velocity variations. Experimentally, the observed effect has been shown to be a maximum at the velocity loops in the stationary field within the sonic cell. In order to demonstrate this dependence, use has been made of the effect of ultrasonic waves on a hydrogen electrode.[8] If a hydrogen electrode is exposed to ultrasonic radiations, an alternating component is produced in the electrode potential primarily as a result of pressure and temperature variations in the gas phase. The hydrogen electrode effect, however, is in phase with pressure variations in the ultrasonic field.

Hydrogen gas was formed on the surface of the platinum of the working electrode by passing a current through the solution with the working electrode as the cathode and the grounded platinum electrode behind the reflector or piston as the anode. The positions of the pressure loops in the stationary field were then established by adjusting the position of the working electrode (with the hydrogen gas film on it) for a maximum effect in terms of the trace on the oscillograph of the detection apparatus. In Fig. 5 is a graph of the amplitude of the traces on the oscillograph before passage of the current and after the passage of the current for a 0.001-normal lithium chloride solution in the sonic cell. In both cases the position of the piston was constant. The acoustical output from the quartz crystal was approximately 2 cm/sec. in terms of the incident waves to the sonic cell. A deflection of one inch on the Du Mont oscillograph was equivalent to an input to the detection apparatus of 5 microvolts. The data for the curve in Fig. 5 representing the effect before the passage of current were obtained in a period of five minutes. Current was then passed through the working electrode at 87 microamp. for 40 minutes,

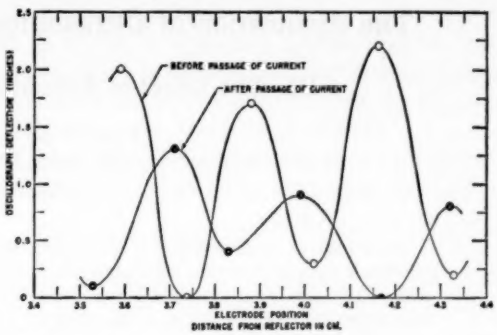

FIG. 5. Effect of passing current through working electrode.

after which the readings for the second curve were made in a period of three to four minutes with the current off. Utmost haste was necessary in making measurements after the passage of the current, for after approximately five minutes the positions of the maxima and minima started to drift back towards the original positions in an irregular fashion.

From Fig. 5 it can be seen that the positions of the maxima and the minima have been shifted approximately one-quarter wave-length after the passage of the current through the working electrode. Since the hydrogen electrode effect depends on the pressure variations in the ultrasonic field, the shift implies that the effect before the passage of the current depended on the velocity amplitude. When hydrogen gas was formed on the working electrode, the resistance between the solution and the platinum electrode became very high. The gas film was equivalent to the polystyrene film on the "dummy" electrode as far as the Debye effect was concerned. Hence the contribution of the Debye effect to the observed effect dropped practically to zero after the formation of the hydrogen gas film. The hydrogen electrode was also expended in the form of an internal voltage drop across the gas film, but the hydrogen electrode effect is much greater than the Debye effect—according to the calculations in the following paper of this series. Thus the effect after the passage of the current was almost entirely the hydrogen electrode effect.

CONCLUSIONS

On the basis of this evidence, the existence of the Debye effect for electrolytic solutions has been established experimentally beyond all reasonable doubt.

The authors wish to express their appreciation to the General Electric Company who supported this research in part through a Coffin fellowship.

[8] The hydrogen electrode effect will be considered mathematically in the next paper in this series.

The Application of Ultrasonics to the Study of Electrolytic Solutions

III. The Effect of Acoustical Waves on the Hydrogen Electrode

ERNEST YEAGER AND FRANK HOVORKA
Department of Chemistry, Western Reserve University, Cleveland, Ohio
(Received October 13, 1948)

An equation is developed for the alternating component in the electrode potential of a hydrogen electrode exposed to acoustical radiations. According to these calculations, the effect is of the magnitude 10^{-2} volt for acoustical waves with a pressure amplitude of 0.1 atmos. The hydrogen electrode should prove very useful as a means for absolute measurements of pressure amplitude as well as the detection of underwater sound.

I

THE passage of ultrasonic waves through a fluid is attended by variations in pressure and temperature as a result of the tremendous periodic accelerations imparted to the medium. Since the potential of a gas electrode is a function of pressure and temperature, an alternating component would be expected in the electrode potential of a hydrogen electrode exposed to ultrasonic waves. If the magnitude of this alternating component is sufficiently large to permit quantitative measurements and can be expressed as a definite function of acoustical intensity and characteristic parameters of the electrode, this effect can be utilized for the determination of absolute acoustical intensities in water and aqueous solutions. The purpose of the present paper is to show that such is the case.

II

Consider an electrolytic cell consisting of two hydrogen electrodes without liquid junction potential:

(Pt) H_2	H^+	H^+	H_2 (Pt)
P_g°, T_g°	$P_1^\circ, T_1^\circ, a_1^\circ$	P_1, T_1, a_1	P_g, T_g
(reference electrode)		(detection electrode)	

The half-cell on the left-hand side is isolated from the ultrasonic field with the conditions P_g° (pressure) and T_g° (temperature) in the gas phase[1] and P_1°, T_1°, and a_1° (activity of hydrogen ions) in the liquid phase. The half-cell on the right-hand side is exposed to the ultrasonic waves with the instantaneous pressure P_1, temperature T_1, and hydrogen-ion activity a_1 in the liquid phase and the pressure P_g and temperature T_g in the gas phase of the hydrogen electrode. Furthermore, let P_g°, T_g°, P_1°, T_1°, and a_1° of the reference electrode be such as to represent the time averages of the corresponding variables at the detection electrode. The over-all reaction for the cell may be expressed by the equation:

$$\tfrac{1}{2}H_2(P_g^\circ, T_g^\circ)+H^+(P_1, T_1, a_1)\rightleftharpoons H^+(P_1^\circ, T_1^\circ, a_1^\circ)+\tfrac{1}{2}H_2(P_g, T_g).$$

For the purpose of evaluating the free energy change for the cell reaction, the over-all cell reaction may be reduced to the two processes:

(a) $$\tfrac{1}{2}H_2(P_g^\circ, T_g^\circ)\rightleftharpoons\tfrac{1}{2}H_2(P_g, T_g)$$

and

(b) $$H^+(P_1, T_1, a_1)\rightleftharpoons H^+(P_1^\circ, T_1^\circ, a_1^\circ).$$

For the first reaction the free energy change ΔG may be expressed as a function of the two independent variables, temperature and pressure. Hence,

$$dG=(\partial G/\partial P)_T dP+(\partial G/\partial T)_P dT. \quad (1)$$

For a perfect gas

$$(\partial G/\partial P)_T = V = RT/P, \quad (2)$$

where V is the molar volume and R is the gas constant per mole. From the second law of thermodynamics,

$$(\partial G/\partial T)_P = -S_g, \quad (3)$$

where S_g is the molar entropy of the gas. For these calculations the entropy of hydrogen gas may be considered as a constant, since the periodic temperature variations produced by the ultrasonic waves in the gas phase are only a small fraction of a degree. Combining Eqs. (2) and (3) with Eq. (1), and integrating between the limits P_g and P_g° with respect to pressure and T_g and T_g° with respect to temperature, we have for reaction (a)

$$\Delta G=\tfrac{1}{2}RT_g^\circ \ln(P_g/P_g^\circ)-\tfrac{1}{2}S_g(T_g-T_g^\circ). \quad (4)$$

A similar equation could be developed for reaction (b). Its contribution to the total free energy change attending the propagation of the ultrasonic waves would be very small[2] because the temperature varia-

[1] The pressure on the hydrogen gas at the reference electrode will be assumed equal to the pressure in the liquid phase and the partial pressure of the water vapor neglected. For the purposes of these calculations this assumption is perfectly justified.

[2] The contribution of reaction (b) to the total free energy change is approximately 0.1 percent.

tions in the liquid phase and the molar volumes of the hydrogen ions are much smaller than the corresponding quantities in the gas phase. The total free energy change for the cell is then given approximately by Eq. (4). If the approximation $\ln(1+x)=x$ for $x \ll 1$ is applied to Eq. (4),

$$\Delta G=[RT_g^\circ/2](\Delta P_g/P_g^\circ)-\tfrac{1}{2}S_g(T_g-T_g^\circ), \quad (5)$$

where S_g is assumed to be constant.

For adiabatic expansion and compression it can be shown from thermodynamics[3] that

$$(\partial T/\partial P)_S=[T/C_p](\partial V/\partial T)_P, \quad (6)$$

where C_p is the molar heat capacity at constant pressure. Integrating Eq. (6) between the limits T_g and T_g°, P_g and P_g°, respectively, for the gas phase and assuming the simple gas law applicable, we have

$$\ln[T_g/T_g^\circ]=[R/C_p]\ln[P_g/P_g^\circ] \cong[R/C_p](\Delta P_g/P_g^\circ)\cong[\Delta T_g/T_g^\circ] \quad (7)$$

with C_p assumed to be constant.

If Eq. (7) is combined with Eq. (5),

$$\Delta G=(RT_g^\circ/2)[1-(S_g/C_p)](\Delta P_g/P_g^\circ). \quad (8)$$

In order to apply Eq. (8) experimentally, the excess acoustical pressure in the gas phase must be related to the intensity or the pressure amplitude of the incident waves in the liquid phase. For simplicity, only the situation in which a plane wave is propagated in a direction normal to the surface of the electrode will be considered. Furthermore, the assumptions will be made that the acoustical waves are completely reflected from the surface of the platinum[4] of the hydrogen electrode and that the effective thickness of the film of hydrogen on the electrode is negligible compared to the wave-length. If p is the pressure amplitude of the incident waves, then the excess acoustical pressure in the gas phase is approximately

$$\Delta P_g=p[\exp i(\omega t-\sigma_1 x)+\exp i(\omega t+\sigma_1 x)], \quad (9)$$

since the boundary conditions include continuity of pressure between the liquid phase and the gas phase.

If Eqs. (8) and (9) are combined,

$$E=\Delta G/-F=[RT_g^\circ/2FP_g^\circ][(S_g/C_p)-1]p \times[\exp i(\omega t-\sigma_1 x)+\exp i(\omega t+\sigma_1 x)], \quad (10)$$

where E is the alternating component in the electrode potential produced by the interaction of the acoustical waves with the detection electrode and F is the faraday, i.e., 96,494 coulombs.

Consider the application of Eq. (10) to experimental conditions with the following parameters:

$T_g^\circ=292.2°\text{A}$,
$P_g^\circ=1$ atmos.,
$R=1.987$ cal./mole °C,
$S_g=31.23$ cal./mole °A,
$C_p=6.99$ cal./mole °C,
$F=9.65\cdot 10^4$ coulombs.

Thus,

$$E=4.28\cdot 10^{-8}p[\exp i(\omega t-\sigma_1 x)+\exp i(\omega t+\sigma_1 x)]. \quad (11)$$

For a pressure amplitude of 0.1 atmos. for the incident waves, the alternating component E from this cell would have an amplitude of approximately 0.01 volt, a value which could be easily measured by the usual electronic methods.

Provided the mathematical development is correct, it should be possible to use this effect for the measurement of absolute acoustical intensities. In addition, the alternating components in the electrode potential of a hydrogen electrode may prove practical as a means for the detection of underwater sound in general. With the usual electronic apparatus, measurements could be extended to at least 10^{-7} volt, which would correspond to an acoustical intensity of less than 10^{-12} watt/cm^2. If designed properly, the response of the hydrogen electrode to acoustical waves would be independent of frequency for practical purposes for frequencies as high as 10^6 cycles per sec. Experimental work may demonstrate that this means of detecting underwater sound ranks with the methods now in use.

The Debye effect, discussed in the previous paper,[5] may also prove useful as a means for absolute intensity measurements. Its use would be considerably more restricted than the hydrogen electrode effect, however, since the Debye effect is of a much smaller magnitude. While the hydrogen electrode depends on the excess acoustical pressure, the Debye effect depends for practical purposes on velocity variations. Since both of these effects can be measured in the form of very small electrodes or probes which are virtually points, they should prove useful in exploring complex acoustical fields.

[3] G. Lewis and M. Randall, *Thermodynamics* (McGraw-Hill Book Company, Inc., New York, 1923), p. 137.

[4] This assumption is justified only if the thickness of the platinum is not close to a multiple of half the wave-length or negligible compared to the wave-length.

[5] Yeager, Bugosh, Hovorka, and McCarthy, J. Chem. Phys. 17, 412 (1949).

Hydrogen Exchange Reactions of the Butanes in Sulfuric Acid

O. BEECK, J. W. OTVOS, D. P. STEVENSON, AND C. D. WAGNER
Shell Development Company, Emeryville, California
(Received October 25, 1948)

IN this note there are described observations on the reactions of the four monodeuterobutanes in the presence of a typical alkylation catalyst (conc. sulfuric acid) at 25°C.[1] The gaseous butanes, 30 cc-atmos. at 30 cm Hg initial pressure, were circulated through a 5-cm column of sulfuric acid (10 ml) by means of a magnetic piston pump.

Neither the primary nor the secondary hydrogens of *n*-butane undergo measurable reaction in the presence of 96.2 percent sulfuric acid in three hours at 25°C since there was no measurable change in the mass spectra of *n*-butane-1-d_1 or *n*-butane-2-d_1. Isobutane exchanges primary hydrogens with sulfuric acid. This was proved by the observation that isobutane-1-d_1 exchanged D for H with sulfuric acid. Between sulfuric acid concentrations of 91.5 and 98.3 percent this reaction has a pseudo first-order rate constant, k, such that $-\log k \cong 2H_0 + A$, where H_0 is the acidity function[2] and A is a constant. Under the experimental conditions, the half-times for the reaction of isobutane-1-d_1 with sulfuric acid,

$$(CH_3)_2(CH_2D)CH + H_2SO_4 \rightarrow (CH_3)_3CH + HDSO_4 \quad (1)$$

increased from 48 minutes in 98.3 percent H_2SO_4 to 1700 minutes in 91.5 percent H_2SO_4.

That the tertiary hydrogen of isobutane does not exchange readily with sulfuric acid was shown by the observation that the mass spectrum of isobutane-2-*d* was unchanged after five hours contact with 96.2 percent H_2SO_4 at 25°C, while only 1.2 percent isobutane-d_0 was formed in three and one-half hours by reaction in 98.3 percent H_2SO_4. In the latter experiment appearance of sulfur dioxide in the vapor phase and slight discoloration of the acid indicated oxidation of the isobutane. The small exchange observed may have been initiated by an oxidation product. In spite of the absence of exchange between tertiary hydrogens and acid, it was found that isobutane molecules undergo direct intermolecular exchange of their tertiary hydrogens at 25°C in the presence of sulfuric acid. The reaction,

$$(CH_3)_3CD + (CH_3)_2(C^{13}H_3)CH \rightleftharpoons (CH_3)_3CH + (CH_3)_2(C^{13}H_3)CD, \quad (2)$$

takes place as a pseudo first-order reaction at the same specific rate as reaction (1) in both 93.5 percent and 96.2 percent H_2SO_4, the two acid concentrations in which reaction (2) was studied.

Both reactions (1) and (2) showed evidence of short induction periods which could be largely eliminated by the addition of 0.1 percent isobutylene to the original butane, known to contain less than 0.01 percent olefin. The added isobutylene caused a forty to fifty percent increase in the specific rates.

The exchange reactions of the two butanes in the presence of 96.2 percent sulfuric acid are summarized in Table I.

The fact that the specific rates of reactions (1) and (2) remain equal while changing by a factor of five between sulfuric acid concentrations of 93.5 and 96.2 percent can best be interpreted by the assumption that reactions (1) and (2) have a common rate-determining step. The equality of these rates further implies that, in each molecule undergoing tertiary-tertiary exchange, all primary hydrogens undergo exchange with the acid. Furthermore, the existence of an induction period which may be shortened by the addition of isobutylene suggests that the rate-determining step of reactions (1) and (2) may be related to that of the alkylation reaction. Stewart and Calkins[3] have found an induction period for the consumption of isobutane by normal butylenes and sulfuric acid and noted that this induction period may be shortened by the addition of isobutylene to the reaction mixture.

The definite correlation of the rates of the two types of hydrogen exchange, shown by isobutane with the strength of the sulfuric acid (as measured by the acidity function, H_0), strongly suggests the rate-determining factor to be either the concentration or the rate of formation of a salt-like complex between the very weak base, isobutane, and the strong acid, sulfuric. The absence of hydrogen exchange between paraffin and catalyst in the pres-

TABLE I. Intermolecular hydrogen exchange reactions of butanes in 96.2 percent sulfuric acid at 25°C.

Compound \ Reaction	Primary with primary	Primary with secondary	Primary with tertiary	Secondary with secondary	Tertiary with tertiary	Primary with acid	Secondary with acid	Tertiary with acid
n-Butane	no	no	—	no	—	no	no	—
i-Butane	no	—	no	—	yes	yes	—	no

[1] See Wagner, Beeck, Otvos, and Stevenson, J. Chem. Phys. **16**, 255 and 745 (1948); see also accompanying paper in this issue.

[2] L. P. Hammett, Chem. Rev. **16**, 67 (1935).

[3] T. D. Stewart and W. H. Calkins, J. Am. Chem. Soc. **70**, 1006 (1948).

ence of the presumably stronger acid "aluminum chloride"[1] no doubt results from the lack of mobility of the acid in this latter case.

The observation of tertiary-tertiary hydrogen exchange in isobutane in the presence of both sulfuric acid and the aluminum chloride catalyst, together with the correlation of the rate of this exchange reaction with acid strength in the case of sulfuric acid, makes possible a new quantitative measure of the strengths of very strong acids.

THE JOURNAL OF CHEMICAL PHYSICS VOLUME 17, NUMBER 4 APRIL, 1949

Hydrogen Exchange Reactions of Paraffins in the Presence of Aluminum Chloride—Alumina Catalyst

C. D. WAGNER, O. BEECK, J. W. OTVOS, AND D. P. STEVENSON
Shell Development Company, Emeryville, California
(Received October 25, 1948)

As a part of a comprehensive investigation of the reactions of hydrocarbons in the presence of acid-type catalysts by means of isotopic tracer methods,[1] we have recently studied the reactions of a group of monodeuteroparaffins in the presence of (1) a typical isomerization catalyst and (2) a typical alkylation catalyst. Inasmuch as certain features of the reactions are quite unexpected on the basis of hitherto published theories of the nature of acid catalyzed reactions, it seems desirable to present a summary of the results thus far obtained. This communication deals with the reactions of the seven monodeutero C_2, C_3, and C_4 paraffins in the presence of the isomerization catalyst. The accompanying communication deals with the reactions of the four monodeuterobutanes in the presence of the alkylation catalyst.

The isomerization catalyst consisted of alumina (4 mesh), vapor-impregnated with "anhydrous" aluminum chloride (0.25 g Al_2Cl_6 per g of catalyst and 0.7 mg-atom of hydrogen per mg-atom of chlorine). The catalyst (25 g) was contained in a vertical tube (50 cc) attached by standard taper joints to a vacuum system into which was incorporated a small volume, magnetic piston-type, circulating pump. In a typical experiment the reaction system was charged with 60 cc-atmos. of gas, the pump started, and one cc-atmos. samples were periodically removed for mass spectrometric analysis. The ratio of the amount of catalyst hydrogen to hydrocarbon deuterium was greater than 100.

During the time within which the experiments with the deuteroparaffins were carried out, the half-time for the equilibrium conversion of normal butane to isobutane increased from 180 minutes to 1900 minutes, owing to loss of isomerization activity of the catalyst. No disproportionation products were ever observed. No effort was made to reactivate the catalyst for isomerization (as by the addition of hydrogen chloride or water). Contrary to expectation, there was no detectable exchange of hydrogen between any of the paraffins (ethane-d_1, propane-1-d_1, propane-2-d_1, *n*-butane-1-d_1, *n*-butane-2-d_1, isobutane-1-d_1, and isobutane-2-d)[2] and the catalyst, as measured by the total deuterium content of the paraffins in the gas phase. However, as enumerated in the following paragraphs, a variety of intermolecular hydrogen exchange reactions was observed in the paraffins.

Extremely rapid intermolecular exchanges of secondary hydrogens in propane and of tertiary hydrogens in isobutane were found in the following reactions:

$$2CH_3CHDCH_3 \overset{\text{catalyst}}{\rightleftharpoons} CH_3CH_2CH_3+CH_3CD_2CH_3 \quad (1)$$

$$(CH_3)_3CD+(CH_3)_2(C^{13}H_3)CH \overset{\text{catalyst}}{\rightleftharpoons} (CH_3)_3CH+(CH_3)_2(C^{13}H_3)CD. \quad (2)$$

The half-time for equilibration at 25°C was 2.5 ±0.5 minutes for reaction (1) and less than two minutes for reaction (2). The temperature coefficient for the over-all reaction (1) was zero between 0° and 25°C, and the initial rate of this reaction was decreased by a factor of 5 by dilution with 90 percent argon.

A slow intermolecular exchange between primary and secondary hydrogens of propane was established by the formation of propane-1,2-d_2 and propane-d_0 from propane-1-d_1, as well as by the formation of propane-d_3 and propane-d_4 both from propane-1-d_1 and from propane-2-d_1.

Rapid intermolecular exchange of secondary hydrogens in *n*-butane was established by the reactions of *n*-butane-2-d_1. Slower intermolecular exchange of primary and secondary hydrogens in

[1] J. Chem. Phys. **16**, 255 and 745 (1948).

[2] For clarity the substances properly designated 2-methylpropane-1-*d* and 2-methylpropane-2-*d* are designated herein as isobutane-1-*d* and isobutane-2-*d*, respectively.

TABLE I. Intermolecular hydrogen exchange reactions of ethane, propane, *n*-butane, and *i*-butane in the presence of aluminum chloride on alumina at 25°.

Reaction / Paraffin	Primary with primary	Primary with secondary	Primary with tertiary	Secondary with secondary	Tertiary with tertiary	Paraffin with catalyst
Ethane	no	—	—	—	—	no
Propane	?	very slow	—	fast	—	no
n-Butane	?	slow	—	fast	—	no
i-Butane	no	—	slow	—	very fast	no

normal butane (much more rapid than in propane) was demonstrated in the reactions of *n*-butane-1-d_1 and of *n*-butane-2-d_1. Both of these compounds produced the same final mixture of butanes after about five hours. The composition of this final mixture corresponded, within the experimental error, to a random distribution of hydrogen and deuterium among the butane molecules. The mole fraction of $C_4H_{10-n}D_n$ is given by $(10!/(10-n)!n!) \times (9/10)^{10-n}(1/10)^n$.

The intermolecular exchange reactions of *n*-butane-1-d_1 also had a zero temperature coefficient between 0° and 25°C, but the initial reaction rate was not changed by dilution with 90 percent argon. The rate of this reaction did not decrease during the period that the catalyst was used.

Isobutane was shown to undergo slow intermolecular exchange between primary and tertiary hydrogens through the formation from isobutane-2-*d* of isobutane-d_0 (33.3 percent), isobutane-d_2 (6.9 percent), isobutane-d_3 (4.9 percent), isobutane-d_4 (2.8 percent), isobutane-d_5 (1.9 percent), isobutane-d_6 (1.2 percent), isobutane-d_7 (0.5_8 percent), and isobutane-d_8 (0.2_7 percent) in 24 hours at 25°C. Isobutane-1-d_1 also showed intermolecular hydrogen exchange, but the product after 24 hours was quite different from that resulting from the reaction of isobutane-2-*d*. From isobutane-1-d_1 in 24 hours there was only formed 7 percent each of isobutane-d_0 and isobutane-d_2 and less than 0.2 percent isobutane-d_3. It will be noted that the concentrations of isobutane-d_6, isobutane-d_7, and isobutane-d_8 resulting from the reaction of isobutane-2-*d* are 100-, 1000-, and 10,000-fold greater, respectively, than their random distribution values.

The above described hydrogen exchange reactions of the various paraffins are summarized in Table I.

The fact that several of the isotopic species concentrations in the reaction of isobutane-2-*d* increase so far beyond their equilibrium values indicates that the life of the reactive complex which the molecule forms with the catalyst is sufficiently long that several exchanges of tertiary hydrogen from the gas phase with primary hydrogen of the adsorbed isobutane can take place before decomposition of the complex occurs.

The observation that only isobutane-d_0 and isobutane-d_2 were formed in significant amounts from isobutane-1-d_1 proves the extreme relative slowness of intermolecular exchange between primary hydrogens of isobutane.

Although the activity of the catalyst for isomerization of normal butane to isobutane decreased by a factor of ten during the course of this work, there was no corresponding change in the rate of the intermolecular exchange reactions as exemplified by the exchanges of *n*-butane-1-d_1. Thus it seems reasonable to conclude that different degrees of activation of the adsorbed paraffin are required for isomerization and for intermolecular exchange of hydrogens. Furthermore, the range of the rates of the various types of intermolecular hydrogen exchanges that a single paraffin can undergo clearly demonstrates different degrees of activation of the adsorbed paraffin for such exchanges.

These experiments provide no evidence that a primary transfer of hydrogen to the catalyst is a necessary prerequisite for the isomerization reaction since no hydrogen exchange with the catalyst was detectable under isomerization conditions. As will be shown in the accompanying communication, it seems that a necessary condition for hydrogen exchange with the catalyst is that another catalyst molecule can react with the reactive complex formed by the paraffin and the catalyst, a circumstance which can readily occur only in a liquid phase system. It will also be shown that hydrogen exchange with the catalyst can take place without isomerization.

In conclusion, there are in preparation papers which will describe in detail not only the results summarized in this and the accompanying note, but also the preparation, purity, and mass spectra of the various isotopic compounds employed in these investigations. For the purposes of these communications it will suffice to state that the upper limit to the olefin content of any one of the deuteroparaffins is 0.01 percent.

Neutron Absorption Cross Sections of Radioactive La^{140} and Two Stable Cerium Isotopes*

S. KATCOFF,** J. A. LEARY, K. A. WALSH, R. A. ELMER, S. S. GOLDSMITH, L. D. HALL, E. G. NEWBURY, J. J. POVELITES, AND J. S. WADDELL
Los Alamos Scientific Laboratory, University of California, Los Alamos, New Mexico

(Received September 13, 1948)

Two multi-curie samples of 40-hr. La^{140} were irradiated with slow neutrons at the Los Alamos homogeneous pile for 24 hours. The small amount of 3.7-hr. La^{141} formed was allowed to decay to 28-day Ce^{141} which was then radio-chemically extracted and counted. From the activity measured, the neutron flux, and the known half-lives, a value of 3.1 ± 1.0 barns was calculated for the cross section of 40-hr. La^{140}. The thermal neutron absorption cross sections of stable Ce^{140} and Ce^{142} were also measured and found to be 0.27 ± 0.06 and 0.105 ± 0.020 barn, respectively, per atom of the naturally occurring element.

INTRODUCTION

THE activation method, which has been used extensively for the determination of cross sections of stable nuclei,[1] has also been applied in several cases to the measurement of neutron absorption cross sections of radioactive isotopes.[2] One method of attack is to irradiate in a high neutron flux a stable isotope, S, which by a single neutron capture gives rise to active isotope J, whose cross section is to be measured. Further capture of neutrons by J yields radioactive isotope B which frequently has an active daughter, C:

$$\text{stable } S \xrightarrow{(n,\gamma)} \text{active } J \xrightarrow{(n,\gamma)} \text{active } B$$
$$\qquad\qquad\qquad\quad \downarrow \beta^- \qquad\qquad\quad \downarrow \beta^-$$
$$\qquad\qquad\qquad\quad K \qquad\quad \xrightarrow{(n,\gamma)} \text{active } C.$$

The saturation number of atoms of J is given by

$$N_J = N_S(nv)\sigma_S\left(\frac{1}{\lambda_J}\right), \tag{1}$$

where N_S is the number of S atoms, σ_S is the thermal neutron activation cross section of S, λ_J is the disintegration constant of J, and (nv) is the neutron flux. If the half-life of J is short compared to the time of bombardment and also to the half-life of B, then the activity of B at the end of bombardment time, t, is given by

$$A_B = (1/\lambda_J)N_S(nv)^2\sigma_S\sigma_J(1-\exp(-\lambda_B t)). \tag{2}$$

By measuring A_B, (nv), N_S, and t, the cross section of J, σ_J, can be calculated from this equation. The cross section σ_S is known or can easily be measured. In cases where the time of irradiation is not long compared to the half-life of J, the above equations must be replaced by more general ones.[2] It should be noted that the activity of B is proportional to the square of the neutron flux. Since it is usually more advantageous to analyze radiochemically for C rather than for its parent B, account must be taken of the amount of C which is formed by the alternate process involving neutron capture by K, the daughter of J[2]. However, in the favorable cases where the half-life of C is short compared to that of its parent B, this alternate process does not interfere because C can be separated radiochemically from B at periodic intervals. Only the first extraction can contain C which originated from neutron capture by K. All succeeding extracts can contain only that C activity which comes from β-decay of its parent B.

By applying the above method, upper limits have been set on the cross sections of a few fission products,[2,3] and the thermal neutron capture cross section of 85-min. Ba^{139} was determined to be 3.8 ± 1.0 barns.[4]

A slightly different method for measuring cross sections of unstable nuclei involves the isolation of as much radioactive J as possible from its source of supply and then irradiating it in a high neutron flux. The product of neutron capture, B (or its daughter C), can be measured as above. In this case the activity of B at the end of bombardment time t is given by[2]

$$A_B = (N_J{}^0 T_J\sigma_J(nv)/T_J - T_B) \times(\exp(-\lambda_J t)-\exp(-\lambda_B t)), \tag{3}$$

where $N_J{}^0$ is the number of atoms of J present at the beginning of the irradiation, and T_J and T_B are the half-lives of J and B, respectively. The activity of C arising from neutron capture by stable K (the daughter of J) is given by the following equation:

$$A_C = (N_J{}^0\sigma_K(nv)/T_J - T_C)[T_J(1-\exp(-\lambda_J t)) - T_C(1-\exp(-\lambda_C t))], \tag{4}$$

* Based on AEC Report LA-630 (May 26, 1947).
** Now at Brookhaven National Laboratory, Upton, Long Island, New York.
[1] L. Seren, H. N. Friedlander, and S. H. Turkel, Phys. Rev. 72, 888 (1947).
[2] S. Katcoff, Plutonium Project Record, IX B, 7.59.1 (1946).
[3] N. Sugarman and A. Turkevich, Manhattan Project Report CC-2485 (Dec. 15, 1944); Plutonium Project Record, IXB, 7.59.2 (1946).
[4] S. Katcoff, Manhattan Project Report CC-2908 (April 7, 1945); Plutonium Project Record IXB, 7.59.4 (1946).

where σ_K is the neutron absorption cross section of K. Equation (3) can be used to calculate the cross section of J. However, when the activity of C is measured instead of the activity of B and when the half-life of C is long compared to that of its parent B, then the activity of C, which is formed by neutron activation of K, must be subtracted from the total activity of C. This amount is calculated by use of Eq. (4).

This method has been applied in work with some of the transuranic isotopes, in a rough determination[5] of the cross section of long-lived I^{129}, and in measuring the cross section of 40-hr. La^{140} as reported here. The nuclear processes involved in the latter were:

$$\begin{array}{ccc} \text{40-hr. } La^{140} & \xrightarrow{(n,\gamma)} & \text{3.7-hr. } La^{141} \\ \downarrow \beta^- & & \downarrow \beta^- \\ \text{stable } Ce^{140} & \xrightarrow{(n,\gamma)} & \text{28-day } Ce^{141}. \end{array}$$

A quantity of 40-hr. La^{140}, corresponding to a number of curies, was irradiated at the Los Alamos homogeneous pile for a period of 24 hours. Several days later radiochemical analysis was made for the 28-day Ce^{141} resulting from the irradiation.

EXPERIMENTAL PROCEDURE AND RESULTS

Before starting the major portion of the experiment, a determination was made of the neutron absorption cross sections of the two major stable cerium isotopes, Ce^{140} (88.5 percent abundance) and Ce^{142} (11.1 percent abundance). The former had not been measured previously, and the latter had been measured only roughly.[6] For this determination 2.0 g of Ce, as $Ce(NO_3)_3 \cdot 6H_2O$, was irradiated for one hour at a point in the graphite 8″ from the edge of the "water boiler" sphere. A piece of uranium was used as a monitor for the neutron flux. Three weeks of cooling was allowed for the 33-hr. Ce^{143} to decay to a negligible value. Then the cerium was dissolved, and aliquots were withdrawn for radiochemical analyses. Two samples were analyzed for 28-day Ce^{141} and two others for 13.8-day Pr^{143}, the daughter of 33-hr. Ce^{143}. The decay of the samples was followed for several weeks by means of a mica-window bell-shaped Geiger counter. Aluminum absorption curves were also taken of the activities in order to check their purity and also for making corrections to zero absorber. Correction was also made to 100 percent counter geometry (by means of a standard), to 100 percent chemical yield, and for decay. The neutron flux was measured by analyzing the uranium monitor for the 12.8-day Ba^{140} fission product. From the latter's fission yield and the thermal fission cross section of uranium the flux was calculated. Then by applying the parent daughter relation and Eq. (1), the neutron absorption cross sections which are given in Table I were calculated. These values are for thermal neutrons if the fission cross section of uranium and the cross sections measured here change by the same ratio when a purely thermal neutron flux is substituted for the approximately thermal flux actually used. This assumption is probably valid within the limits of error given. The value listed here for Ce^{142} checks the tentative value of 0.1 barn reported earlier[6] for the natural atom cross section.

TABLE I. Neutron capture cross sections of stable Ce.

	Isotopic abundance	Natural atom cross section	Isotopic cross section
Ce^{140}	88.5 percent	0.27 ±0.06 barn	0.31±0.07 barn
Ce^{142}	11.1 percent	0.105±0.020	0.95±0.18

Two runs were made to determine the cross section of 40-hr. La^{140}. In the first one, a solution of 12.8-day Ba^{140} was used which had been milked of its 40-hr. La daughter several times before. After the last milking four days were allowed for more 40-hr. La to grow in. Then 10 mg of stable La carrier was added and precipitated with NaOH as $La(OH)_3$. This was filtered, redissolved, and precipitated twice more as $La(OH)_3$ in order to purify it from 12.8-day Ba. Then a final precipitation was made as lanthanum "fluo-oxalate."[7] These operations were performed by means of remote control apparatus which was made available for this work by Dr. R. W. Spence. Most of the radioactive La^{140} was contained in a stainless steel container of 0.020-in. wall thickness. It was transported to the pile in a thick lead shield and then transferred quickly by means of two 6-foot rods and a string to a position in the graphite 9″ from the "water boiler" sphere. Two small uranium foils were used as neutron flux monitors. The sample was irradiated for 24 hours at maximum pile power. However, a portion of this La^{140} sample was not bombarded but reserved for comparison with the irradiated sample.

After a two-week cooling period, both samples were radiochemically analyzed, in duplicate, for 28-day Ce^{141}, 40-hr. La^{140}, and 12.8-day Ba^{140}. The La^{140} analyses served as assays for the size of the samples. In the Ce analyses it was necessary to reprecipitate $Ce(IO_3)_4$ eight times to decontaminate completely from the vastly greater activity of 40-hr. La. Aluminum absorption curves of the radiations from the Ce samples indicated the presence of both 28-day Ce^{141} and 275-day Ce^{144}. It became obvious that these isotopes were present as small but im-

[5] S. Katcoff, Phys. Rev. **71**, 826 (1947).
[6] S. Katcoff, Manhattan Project Report CC-2739 (February 23, 1945).
[7] G. Friedlander, R. Spence, and R. G. Steinhardt, Jr., Manhattan Project Report LA-557 (May 6, 1946).

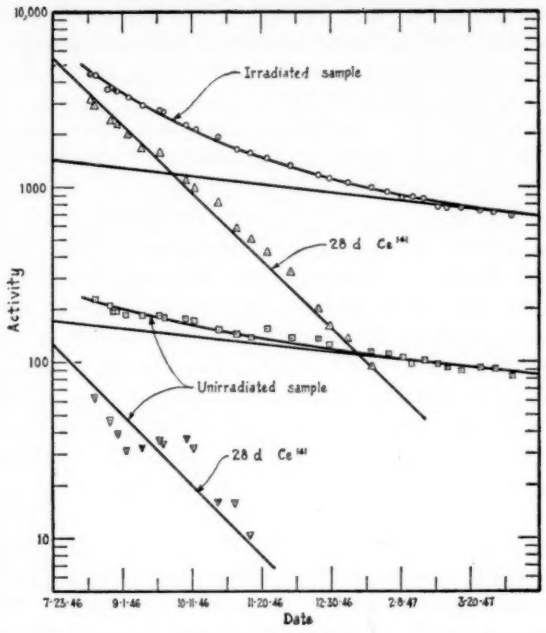

FIG. 1. Decay of Ce activity extracted from irradiated and unirradiated 40-hr. La^{140}.

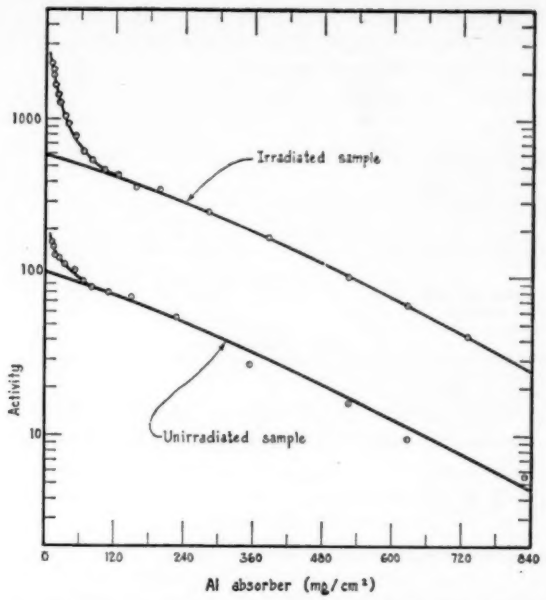

FIG. 2. Aluminum absorption curves of Ce activity from irradiated and unirradiated 40-hr. La^{140}.

portant impurities in the original active La^{140} samples. A small increase in the 28-day Ce^{141}, however, was found in the irradiated sample. This was used to calculate a rough upper limit of about 2 barns on the neutron absorption cross section of 40-hr. La^{140}. The barium analyses indicated that an appreciable quantity of 12.8-day Ba^{140} was also present. This isotope can also absorb neutrons to give 18-min. Ba^{141} which decays to 3.7-hr La^{141} and then to 28-day Ce^{141}. Therefore the Ba^{140} had not been removed sufficiently in this run.

In the final run an attempt was made to overcome the above difficulties. A Ba^{140} solution similar to the first one was scavenged three additional times by precipitating $Fe(OH)_3$ four days before finally extracting the La^{140} sample. These precipitations were designed to remove any radioactive Ce that may have been present. For the final La^{140} extraction 10 mg of stable lanthanum carrier was used again, but this time the two $La(OH)_3$ reprecipitations were done in the presence of about 500 mg of stable Ba carrier. This was designed to reduce further the amount of 12.8-day Ba^{140} carried along. Subsequent operations were essentially identical with those of the previous run. The radio-chemical analyses for La^{140} showed that 22.6 curies of this isotope were present at the beginning of the neutron irradiation.

The radio-chemical analyses for active Ce in both the irradiated and unirradiated samples were performed in duplicate on two aliquots (0.400 of total) from each sample. A considerable improvement over the previous run was observed. Although active Ce was not completely eliminated from the La^{140} samples before irradiation, a large increase in the amount of 28-day Ce^{141} was observed in the irradiated sample. This is seen from the decay curves and aluminum absorption curves shown in Figs. 1 and 2. The soft part of the radiation is from 28-day Ce^{141} and 275-day Ce^{144}; the hard beta-ray is from 17.5-min. Pr^{144}, daughter product of 275-day Ce. In Table II the data are presented. The time of irradiation was 24.0 hours, starting 7.9 hours after the La^{140} was separated from the Ba^{140}.

The data in both the second and third columns represent an average of two aliquot samples; column 4 represents an average of four aliquots, and the last column an average of three aliquots. The data of column 3 are based on the very poor decay curve shown at the bottom of Fig. 1, but fortunately these data affect the final result to only a small extent. The activity of 28-day Ce^{141} which was formed by the neutron irradiation of the La sample was (968−221) or 747 disintegrations per second. From this must be subtracted 115 d/s, which is the calculated activity of 28-day Ce^{141} formed by neutron activation of the stable Ce^{140} arising from the beta-decay of 40-hr. La^{140} before and during the irradiation. It is assumed that essentially all of the stable cerium was removed from the Ba^{140} solution when the latter was scavenged with $Fe(OH)_3$ precipitations, and that the Ce^{140} which grew into the solution in the subsequent four days was carried down completely with the final separation of 40-hr. La^{140}. Of the 115 d/s, 101 d/s was formed from the Ce^{140} which grew in before the bombardment, and 14 d/s from the Ce^{140} which grew in during the bombardment. The latter quantity was calculated by means of Eq. (4). Thus the net activity of 28-day Ce^{141}

TABLE II. Data for La^{140} cross-section determination.

	28-day Ce from irradiated La sample	28-day Ce from unirradiated La sample	40-hr. La from irradiated La sample	40-hr. La from unirradiated La sample
Observed activity corrected to 100% chemical yield and extrapolated to end of bombardment	5250 c/m	113 c/m	1.05×10^{7} c/m	0.989×10^{7} c/m
Correction to zero absorber	1.42	1.42	1.04	1.04
Correction to 100 percent counter geometry	3.12	3.12	3.04	3.04
Correction for aliquot (and to equal amounts of 40-hr. La for column 3)	2.50	26.5	10×10^{5}	1×10^{5}
Corrected activity	968 d/s	221 d/s	5.53×10^{11} d/s	0.521×10^{11} d/s
Corrected number of atoms at *beginning* of bombardment			1.74×10^{17}	0.164×10^{17}

which arose from neutron capture by 40-hr. La^{140} was (747−115) or 632 d/s. Then the cross section of 40-hr. La^{140} was calculated from Eq. (3) after substituting the subscript *C* for the subscript *B*. This is permissible because the half-life of B (3.7 hours) is very short compared to the half-life of C (28 days). The neutron flux (5.87×10^{10} n/cm² sec.) was derived from the radio-chemical analyses of the uranium monitors for the 12.8-day Ba^{140}, the fission yield of the latter (6.1 percent), the weights of the monitors, and the known thermal fission cross section of normal uranium. The value for the neutron absorption cross section of La^{140} is then 3.1 barns, probably reliable to within one barn.

DISCUSSION

The radiochemical analysis for 12.8-day Ba^{140} in the La^{140} sample of the final experiment indicated that much less of it carried through than in the preliminary experiment. By comparing the amounts from the two experiments, it can be shown that the maximum amount of 28-day Ce^{141} which could have resulted from neutron capture by Ba^{140} was only a few percent of the amount actually observed. Thus the 28-day Ce^{141} formed in both the final and preliminary runs must have resulted mostly from neutron capture by 40-hr. La^{140}.

If the lanthanum carrier used in the experiments had contained 25 percent stable cerium as an impurity, the same amount of 28-day Ce^{141} would have been formed as that observed. Therefore a separate neutron bombardment was made on a sample of the carrier, and then this was analyzed for 28-day Ce^{141}. Only a very small amount was found, proving that the lanthanum carrier was of sufficient purity. Another possible source of 28-day Ce^{141}, which could have interfered with the measurements, is a small uranium or plutonium impurity. By neutron irradiation 275-day Ce^{144} would be formed as well as 28-day Ce^{141}. In the final sample the 275-day Ce activity would have increased by 30 percent. Instead, a decrease of about 22 percent was found from a comparison of the cerium decay curves for the irradiated and unirradiated samples. This apparent decrease may be involved in measuring the soft radiations of the 275-day Ce^{144}. The relative amounts could have been estimated somewhat more accurately by carefully measuring the activity through 180 mg/cm² of aluminum so that essentially only the hard radiations of 17.5-min. Pr^{144} would be measured. The absorption curves of Fig. 2 cannot be applied accurately for making this comparison because the two samples were at slightly different distances from the Geiger counter. Furthermore, the distance had to be considerably greater for the absorption curves than for the decay curves in order to make room for the absorbers. That resulted in a low counting rate for the Pr^{144} from the unirradiated sample. If the necessary chemical yield and (inaccurate) geometry corrections are applied, an apparent decrease of about 14 percent is found for the Pr^{144} after irradiation. It seems improbable, therefore, that the La^{140} sample was contaminated by an important amount of a fissionable isotope.

The probable error in the cross section of La^{140} is estimated as large as 33 percent mainly because of the difficulty in measuring neutron flux and absolute disintegration rates accurately and because of the uncertainty introduced by the 275-day Ce impurity. In addition, it is still possible that some part of the induced 28-day Ce activity came from a small fissionable impurity. Circumstances did not permit the repetition of the experiment so as to further minimize these difficulties.

This paper is based on work performed at the Los Alamos Scientific Laboratory of the University of California under Government Contract W-7405-eng-36, and the information contained therein will appear in the National Nuclear Energy Series as part of the contribution of the Los Alamos Laboratory.

Letters to the Editor

THIS section will accept reports of new work, provided these are terse and contain few figures, and especially few half-tone cuts. The Editorial Board will not hold itself responsible for opinions expressed by the correspondents. Contributions to this section should not exceed 600 words in length and must reach the office of the Managing Editor not later than the first of the month preceding that of the issue in which the letter is to appear. No proof will be sent to the authors. The usual publication charge ($4.00 per page) will not be made and no reprints will be furnished free.

An Attempt to Find Cross Products in the Benzidine Rearrangement

G. W. WHELAND AND J. R. SCHWARTZ*
Department of Chemistry, University of Chicago, Chicago, Illinois
February 25, 1949

SINCE cross-products have never been observed in the benzidine rearrangement, the reaction is considered to be purely intramolecular. One may, however, doubt whether the methods employed heretofore in the search for cross-products have been sensitive enough to detect the presence of small amounts of these substances. We have accordingly studied the problem with the use of C^{14} as a radioactive tracer.

The most reliable method for determining whether cross-products are formed in the benzidine rearrangement is doubtless that of Ingold and Kidd,[1] in which a mixture of two *symmetrical* hydrazobenzenes is rearranged. Although we have not yet solved all the problems connected with the practical application of this method, we have obtained some preliminary results for the rearrangement of an *unsymmetrical* hydrazobenzene. 2-Methyl-2′-ethoxyhydrazobenzene, with C^{14} in the methyl group, was rearranged in absolute ether by the addition of the calculated amount of alcoholic hydrogen chloride. To the resulting precipitate was then added an approximately equivalent quantity of non-radioactive *o*-tolidine dihydrochloride, a possible cross-product. The mixture was transformed into a mixture of Schiff's bases by refluxing with benzaldehyde and potassium acetate in absolute ethanol. The resulting dibenzal-*o*-tolidine, being practically insoluble in ethanol, remained undissolved. This material, after two crystallizations from benzene, had a residual radioactivity only 0.2–0.5 percent as great as would have been expected if the original rearrangement had produced *only* the two cross products, *o*-tolidine and 3,3′-diethoxybenzidine. This residual activity was still decreasing when the smallness of the remaining sample required the purification to be discontinued; hence, a completely inactive material might ultimately have been obtained. In any event, the cross-product clearly amounts to much less than one percent of the total product of the rearrangement.

Materials. Benzoic acid[2] was reduced to benzyl alcohol with lithium aluminum hydride,[3] and then to toluene with hydrogen and palladium on charcoal. The toluene was nitrated in acetic anhydride, and the isomeric nitrotoluenes were separated by distillation. The *o*-nitrotoluene was then transformed into *o*-nitrosotoluene, which was condensed with *o*-phenetidine in ligroin containing a little glacial acetic acid. The resulting 2-methyl-2′-ethoxyazobenzene melted at 70–71°C. Anal. Calcd. for $C_{15}H_{16}N_2O$: N, 11.68. Found: N, 11.31. Reduction with hydrogen sulfide in alcoholic ammonia gave the hydrazo compound, melting at 95–97°C. Anal. Calcd. for $C_{15}H_{18}N_2O$: N, 11.58. Found: N, 11.4. Dibenzal-*o*-tolidine melted at 157–158°C. Anal. Calcd. for $C_{28}H_{24}N_2$: N, 7.22. Found: N, 7.13.

Radiochemical technique. The standard procedures, as described by Kamen[4] and by Libby,[5] were employed. The counter used was of the end-window type.

The authors gratefully acknowledge much help with the radiochemical measurements from Professor W. F. Libby and Mr. E. C. Anderson.

* Present address, Department of Chemistry, University of California at Los Angeles, Los Angeles, California.
[1] C. K. Ingold and H. V. Kidd, J. Chem. Soc., 984 (1933).
[2] U. S. Atomic Energy Commission, Isotope Branch Research Division, Isotope Branch Circular C-2 (January 10, 1947).
[3] R. F. Nystrom and W. G. Brown, J. Am. Chem. Soc. **69**, 2548 (1947).
[4] M. D. Kamen, *Radioactive Tracers in Biology* (Academic Press, Inc., New York, 1947), Chapter VIII.
[5] W. F. Libby, Ind. and Eng. Chem., Anal. Ed. **19**, 2 (1947).

Isotope Effect in the Decarboxylation of Labelled Malonic Acids

JACOB BIGELEISEN
Brookhaven National Laboratory, Upton, Long Island, New York
January 28, 1949

RECENTLY Yankwich and Calvin[1,2] have synthesized and decarboxylated malonic and brom-malonic acids with tracer C^{14} in the carboxyl group. They find that the specific activity of the carbon dioxide formed in the decarboxylation is significantly different from that calculate on the assumption that the rate constant for the evolution of $C^{14}O_2$ is one-half that of $C^{12}O_2$ in the normal acids. Their results are reported as the relative probabilities of rupture of $C^{12}-C^{12}$ bonds as compared with $C^{12}-C^{14}$ bonds. They find for malonic acid at 150°C $C^{12}-C^{12}/C^{12}-C^{14}=1.12\pm0.03$ and for brom-malonic acid at 115°C $C^{12}-C^{12}/C^{12}-C^{14}=1.41\pm0.08$.

It has been estimated[3] that an upper limit for the ratio of rates for a compound containing C^{12} compared with one containing C^{14} is 1.5 at 298°K, apart from a factor arising from symmetry numbers. The deviation of the ratio from unity decreases rapidly with increasing temperature and this estimated upper limit becomes 1.35 at 400°K. This estimate is made for reactions which proceed through monatomic carbon gas (chemically improbable at these temperatures) as the activated complex. In view of the fact that the results reported by Yankwich and Calvin approach this upper limit so closely even after decarboxylation of *all* of the substrate, it seems worth while to consider the reaction in a little detail from a theoretical viewpoint.

Kinetically the reaction is very simple and has been shown to be first order for malonic acid both in glacial acetic acid[4] and in the pure liquid.[5,6] A summary of the kinetic data on the molten malonic acid is given in Fig. 1. The point marked *S* is for supercooled liquid. After correcting the entropy of activation (calculated assuming unity for the transmission

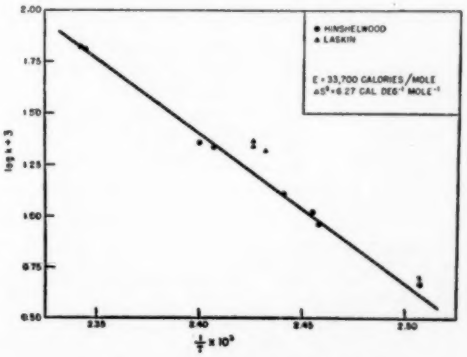

FIG. 1. Decomposition of malonic acid.

TABLE I.

	Brom-malonic acid		Malonic acid		
	ω	$\Delta\omega$	ω	$\Delta\omega$	ω (Infra-red, see reference 8)
ω_1	458	7.1	756	2.4	765
ω_2	196	3.3	230	4.4	
ω_3	505	6.6	905	3.6	894

TABLE II. Calculated isotope effect in the decarboxylation of malonic acids.

	Brom-malonic acid		Malonic acid	
$T°K$	$k_1/2k_2$	$k_1/2k_3$	$k_1/2k_2$	$k_1/2k_3$
300	1.044	1.0063	1.042	1.0041
350	1.043	1.0048		
385	1.042	1.0040		
400	1.042	1.0037	1.041	1.0029
425	1.041	1.0033	1.041	1.0026
500			1.040	1.0019

coefficient) for the destruction of symmetry in the activated complex ($R1n2$) we find the activated complex 4.9 e.u. higher than the liquid. There is no evidence of any type of chain reactions.

The specific activity of the CO_2 formed at any time can be calculated in terms of the initial specific activity and the rate constants defined by the following equations:

$$CH_2(COOH)_2 \xrightarrow{k_1} CO_2+CH_3COOH, \quad (1)$$

$$CH_2\begin{matrix}C^{14}OOH\\COOH\end{matrix} \xrightarrow{k_2} C^{14}O_2+CH_3COOH, \quad (2)$$

$$CH_2\begin{matrix}C^{14}OOH\\COOH\end{matrix} \xrightarrow{k_3} C^{12}O_2+CH_3C^{14}OOH. \quad (3)$$

The initial numbers of moles of ordinary and labeled malonic acids are defined as Mo^{12} and Mo^{14}, respectively. Then

$$\frac{C^{12}O_2}{C^{14}O_2}=\frac{Mo^{12}(1-e^{-k_1 t})(k_2+k_3)}{Mo^{14}(1-e-(k_2+k_3)t)k_2}.$$

For t small,

$$\frac{C^{12}O_2}{C^{14}O_2}=\frac{Mo^{12}k_1}{Mo^{14}k_2};$$

at $t=\infty$,

$$\frac{C^{12}O_2}{C^{14}O_2}=\frac{Mo^{12}}{Mo^{14}}\frac{k_2+k_3}{k_2}.$$

We shall estimate the ratios $k_1/2k_2$ and $k_1/2k_3$ by the method[7] previously applied to the calculation of the isotope effect in the rupture of C−C bonds in propane $-1-C^{13}$. This model should give an upper limit to the ratios and in addition predicts that the entropy of activation will be positive.

The force constants for the skeletal vibrations are chosen[8] as $k_{C-C}=4.1\times10^5$ dynes/cm and $k\delta=0.35\times10^5$ dynes/cm. The calculated and found frequencies[8] are given in Table I. The ratio $(k_2+k_3)/k_2$ depends upon the masses of the carbon atoms alone[7] and equals 2.0378 for both acids. The calculated ratios for $k_1/2k_2$ and $k_1/2k_3$ are given in Table II.

The disagreement between theory and experiment is independent of the model of the activated complex chosen since the reciprocal of the specific activity of CO_2 at complete decarboxylation is proportional to $(k_2+k_3)/k_2$, which is a function of the masses in the normal molecules alone.

[1] P. E. Yankwich and M. Calvin, University of California Radiation Laboratory Document 145; J. Chem. Phys. 17, 109 (1949).
[2] P. E. Yankwich, Brookhaven Conference on Kinetics, December 1, 1948.
[3] J. Bigeleisen, Science, in press.
[4] J. Linder, Sitzungsber. K. Akad. Wiss. Wien 116, 945 (1907).
[5] C. N. Hinshelwood, J. Chem. Soc. 117, 156 (1920).
[6] J. Laskin, Trans. Siberian Acad. Agr. Forestry 6, No. 1 (1926).
[7] J. Bigeleisen, J. Chem. Phys. 17, 345 (1949).
[8] M. Wehrli, Helv. Phys. Acta 14, 516 (1941).

Ultraviolet Absorption by Hydrogen-Bridged Molecules*

GLADYS A. ANSLOW, HSI-TEH HSIEH, AND RUTH C. SHEA
Department of Physics, Smith College, Northampton, Massachusetts
January 27, 1949

THE short wave-length continua appearing in the 220–190 mμ region in the spectra of fatty and amino acids have been ascribed by the senior author[1] to the dissociation of hydrogen bridged bonds in the respective associated molecules, the absorbed photon energy being dissipated according to the equation

$$E_{photon}=E_e(OH)^*+D_v'(OH)+D_v'(H\cdots O),$$

where $E_e(OH)^*$ is the electronic energy of the excited state, i.e., of the (O,O) transition, 4.02 ev (32410 cm^{-1} for the 3064A OH band in water vapor, and $D_v'(OH)$ and $D_v'(H\cdots O)$ are the excited state vibrational energies of the bond and the bridge, which are equivalent as a result of the resonating structure.

The dissociation energy of a polyatomic molecule is determined by the vibration frequencies and anharmonicity constants which appear in infra-red stretching vibrations.[2] Consequently, the energies required to dissociate molecules with similar electronic configurations in the vibrating bonds must vary approximately as $D_v'(1)/D_v'(2)=\{\mu_2/\mu_1\}$, where μ_1 and μ_2 are the reduced masses of the respective molecules. Consequently the dissociation energies of the bonds and the bridges in OH···O polymers may be calculated from the dissociation energy of water vapor in the excited state, approximately 2.4 ev[3] and the respective reduced masses of the corresponding molecules. Such calculations indicate dissociation energies which agree within one percent with the energies indicated by the long wave-length edges of the ultraviolet continua reported by the senior author and others[4] for glycine, alanine, butyric acid, cysteine, phenylalanine, and tryptophane, and within three percent with the energies indicated by the continua in the spectra of aspartic acid, succinic acid, glutamic acid and tyrosine.

A search for OH··O dissociation bands in the spectra of the heavy alcohols and the starches and for NH··O dissociation bonds in the spectra of the amides and related molecules has resulted in the identification of such bands and also of three weaker absorption bands; the (O,O) electronic excitation with center near 32400 cm^{-1}, the D'' vibrational dissociation of the OH or the NH unassociated bonds, and the OH··O or the NH··O dissociation of hydrogen bridged bonds in the unexcited state. These are easily identified in the spectra of the alcohols, shown for amyl alcohol in Fig. 1. Relative values of the maximum extinction coefficients of the two vibration bands indicate the degree of association. The long wave-length edges indicate OH bond energies in the lighter alcohols of 4.47–4.49 ev, approximately the 4.46-ev value calculated for the OH bond energy in water by Gaydon[3] or the 4.36-ev value calculated by Dwyer and Oldenberg.[5] The energy of the hydrogen bridge in the unexcited state, $D_v''(OH\cdot\cdot O)-D_v''(OH)$, is approximately 0.31 ev per molecule, (7.1 kcal./mol).

Similarly values of the electronic energy for the (O,O) band, and of vibrational energies of the NH bond in unassociated and associated molecules, as well as the energy required to dissociate both the NH bond and the H··O bridge in the excited state have been calculated from bands appearing in the absorption spectra of urea, acetamide, propionamide, butyramide, allantoin, and hydantoin solutions. Some of these specimens had been heat treated to produce different types of association.[6] A typical spectrum for propionamide is shown in part 2 of the figure. The average value of $D_v''(NH)$ given by these spectra is 3.71 ev, very close to the thermodynamically calculated value 3.74 ev given by Glockler.[7] The onset of absorption near 32000–33000 cm^{-1} may be ascribed

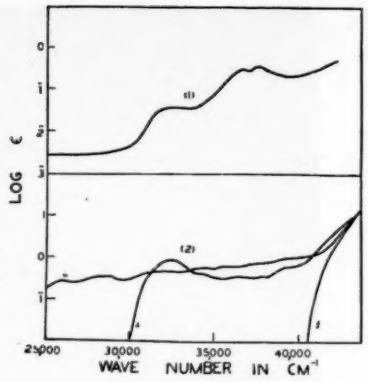

FIG. 1. Electronic excitation and vibration dissociation bands in ultraviolet spectra of (1) 4.6 M isoamylic alcohol in methanol; (2) 0.1 M propionamide in water, "*u*" untreated, "*s*" slowly cooled, "*f*" fast cooled to 0°C after heat treatment on steam bath.

to $D_v''(\mathrm{NH}\cdots\mathrm{O})$ and indicates that the strength of the hydrogen bridge in these molecules is approximately 0.25–0.30 ev (5.7–6.9 kcal./mol). The wave numbers ascribed to the (0,0) electronic transition run between 29400 and 29000 cm^{-1}, close to the 29750 cm^{-1} value observed for the origin of this absorption band in the emission spectrum of nitrogen hydride. The strong absorption continua appearing between 230–260 $m\mu$ in these spectra must result from the dissociation of hydrogen-bridged bonds in the respective dimers or trimers.

* Research supported by the ONR, U. S. Navy Contract N8onr-579, T.O. 1.

[1] Gladys A. Anslow, Phys. Rev. **61**, 547 (1942).
[2] G. A. Anslow and Hilda Hsi-Teh Hsieh, to be published.
[3] A. G. Gaydon, *Dissociation Energies and Spectra of Diatomic Molecules* (John Wiley & Sons, Inc., New York, 1948), pp. 190–191.
[4] G. A. Anslow *et al.*, J. Biol. Chem. **97**, 37 (1932); **103**, 81 (1933); G. A. Anslow and S. Nassar, J. Opt. Soc. Am. **31**, 118 (1941).
[5] R. J. Dwyer and O. Oldenberg, J. Chem. Phys. **12**, 35 (1944).
[6] G. A. Anslow and Ruth Shea, Bull. Am. Phys. Soc. **24**, No. 1, R4 (1949).
[7] George Glockler, J. Chem. Phys. **16**, 602 (1948).

Thermal Conductivity of Gases and Aggregate Matter

H. S. STRICKLER
Research Laboratories, Westinghouse Electric Corporation, East Pittsburgh, Pennsylvania
February 10, 1949

THE production of more data on the conductivity of gases has recently been considered to be of major importance.[1] It appears to the writer that since the direct determination of thermal conductivities of gases at high temperatures is practically impossible (due to the magnitude of radiation corrections, etc.), the need may be met in two other ways. One is from computation as the theory of gases is extended, the other is from thermal conductivity measurements of powdered or aggregate matter. This note gives some preliminary results as obtained in the study of heat flow in aggregates now under way in these laboratories, together with some data from the literature, and a few calculated values for zero pressure gases, using the Eucken assumption.

Our data[2] for a fused magnesia powder of 51.5 percent porosity may be expressed by

$$k(\text{c.g.s.}) = 6.^2\times10^{-4}(1+0.843\times10^{-3}t°\text{C}).$$

The data of Borelius and Wilner[3] for a magnesia powder of apparent density 0.456 (87.2 percent porosity with $d_0=3.57$) may be expressed by $k=2.205\times10^{-4}(1+0.8057\times10^{-3}t)$.

The three points of Pierce and Austin[4] for a finely divided (precipitated) calcined magnesia, porosity not known, may be expressed reasonably well by $k=1.7\times10^{-4}(1+2.3\times10^{-3}t)$. The writer's computed values for air may be expressed approximately for comparison by

$$k=0.585\times10^{-4}(1+2.15\times10^{-3}t).$$

The data of Knapp[5] for a single crystal of synthetic periclase may be expressed approximately as

$$k=111\times10^{-4}(1+2.117\times10^{-3}t) \quad \text{to} \quad 499°\text{C}.$$

Borelius and Wilner[3] also have data on pure kieselguhr ($d=0.267$; for $d_0=2.65$, porosity is 90 percent). For comparison

$$k=1.175\times10^{-4}(1+1.^{5-7}\times10^{-3}t)(0\text{–}600°\text{C}).$$

All of the above were at atmospheric pressure. With accumulation of more data on aggregates, it therefore seems that the proper functions may be deduced to permit extrapolation to 100 percent porosity, thus giving the thermal conductivity of the gas (see Fig. 1). Too high porosities of aggregate evidently should not be employed for experimentation (danger of radiation and convection effects).

Obviously determinations on the same aggregate with different gases present would seem to offer a means of obtaining relative conductivities. However, the proper treatment of data is by no means clear as yet. Budrin and Golubev[6] report increases, on replacing nitrogen with hydrogen, of 1.7 and 2.9 times for vermiculite and diatomite powders at 700°C and 0°C, respectively, less for diatomite bricks. Unfortunately, this paper could not be obtained for study. From our calculated values for gases, kH_2/kN_2 at 700° is 0.945 times that (6.987) at 0°C. Hence the effect is not as large as would be anticipated. It may well be that the light gases, helium and hydrogen, behave abnormally in conduction, a behavior which may be indicated by their accommodation coefficients at much lower temperatures. One may also cite the results of Kannuluik and Martin[7] with a very low density magnesia powder ($d=0.20$, porosity with $d_0=3.57$, 94.5 percent). At 757 mm Hg, k in air was 17.5×10^{-5}, in hydrogen 46.6×10^{-5} and 762 mm Hg (both probably near 0°C). The ratio here was 2.66, while the ratio kH_2/k air at 0°C is 7 (data of Johnston *et al.*[8]). The accommodation coefficients (a') on bright platinum given by Johnston *et al.*[9] are for hydrogen, 0.40; for air 0.75 (at 279–80°K).

The writer obtained k in He/k in air at 700°C = 1.24[8] but this probably was due to incomplete replacement of air by helium, due to the design of the first unit.

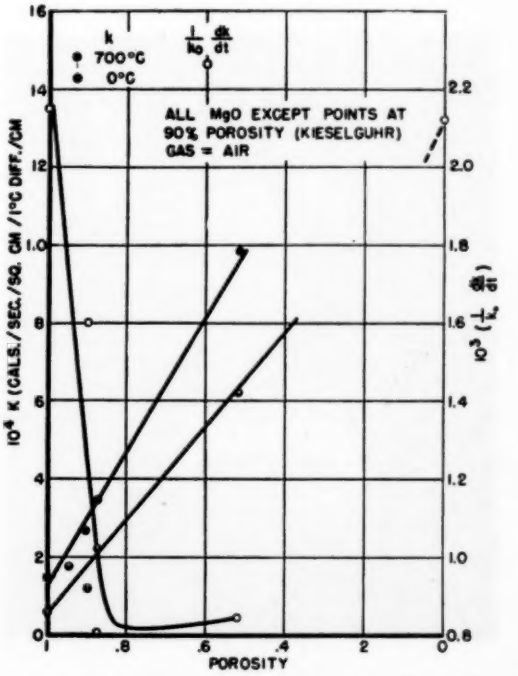

FIG. 1. Thermal conductivity *versus* porosity for various materials.

TABLE I. Gas $k \times 10^4$ calculated.

Hydrogen	3.990 (0°C)	9.444 (700°C)
Nitrogen	0.5582 (0°C)	1.431 (700°C)

and the preceding equation for air.

For the calculated gas thermal conductivities the writer used the viscosity data of Trautz and Zink[10] and C_{p_0} and C_v^∞ as given by Justi[11] and by Heck.[12] On the basis of Hirschfelder's paper[13] and a personal communication from him such values of thermal conductivity should be regarded as tentative values originally computed of necessity for the discussion of results on powders.

[1] G. A. Hawkins, Trans. Assoc. Mech. Eng. **70**, 621 (1948).
[2] C. W. Childers and H. S. Strickler, unpublished.
[3] G. Borelius and T. Wilner, Tekn. Tidsk. (Mekan.) **58**, 93 (1928).
[4] J. B. Austin, A.S.T.M., Symp. Thermal Insul. Materials (1939).
[5] W. J. Knapp, J. Am. Ceram. Soc. **26**, 48 (1943).
[6] D. V. Budrin and I. I. Golubev, Chem. Abstr. **40**, Col. 3861[8] (1946).
[7] W. G. Kannulink and L. H. Martin, Proc. Roy. Soc. **141A**, 144 (1933).
[8a] W. J. Taylor and H. L. Johnston, J. Chem. Phys. **14**, 219 (1946).
[8b] H. L. Johnston and E. R. Grilly, J. Chem. Phys. **14**, 233 (1946).
[9] Grilly, Taylor, and Johnston, J. Chem. Phys. **14**, 435 (1946).
[10] M. Trautz and R. Zink, Ann. Physik, (5), **7**, 427 (1930).
[11] E. Justi (Verlag Julius Springer, Berlin, 1938).
[12] R. C. H. Heck, Mech. Eng. **63**, 126 (1941).
[13] Joseph O. Hirschfelder, J. Chem. Phys. **16**, 968 (1948).

Cell Structure of Propane Flames Burning in Tubes*

G. H. MARKSTEIN
Cornell Aeronautical Laboratory, Buffalo, New York
January 21, 1949

IN the course of an investigation of flame propagation in tubes, flames of unusual structure have been observed in propane-air and propane-air-nitrogen mixtures. The experiments were performed in vertical glass tubes of $2\frac{3}{4}$-inch and 4-inch inner diameter. The premixed gases entered with constant flow velocity near the closed bottom of the tube. Tube length and range of flow velocities were chosen so as to insure laminar flow in the upper part of the tube.

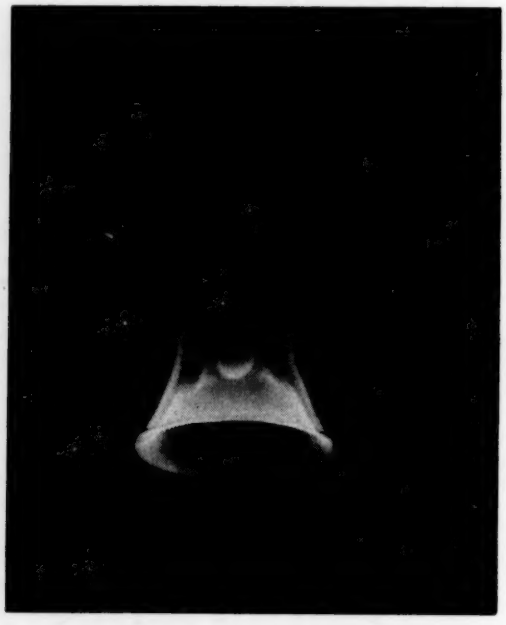

FIG. 1. First appearance of cell structure in the primary combustion zone of a rich propane flame.

FIG. 2. Fully developed cell structure of propane flame in 4-inch tube.

Starting with a diffusion flame burning in a rich mixture at the upper end of the tube, the propane concentration was gradually decreased, leaving air and nitrogen flow unchanged. When certain rather well-defined compositions were reached, one or more approximately hemispherical cusps, convex toward the unburned gas, formed near the tube axis in the primary combustion zone ("inner cone") (Fig. 1). Upon decreasing the propane concentration further, the primary combustion zone entered the tube, assuming a structure composed of many cusps of fairly uniform size. These cusps, which again were convex downward towards the unburned gas and separated by dark narrow ridges, filled the whole cross section of the tube in a single horizontal layer (Fig. 2); they were in continuous irregular motion. By proper adjustment of flow velocity and mixture composition these "cellular" flames could be kept almost stationary, moving downward only very slowly owing to gradual heating up of the tube wall. A similar structure was also observed in the case of slightly faster propagating flames. When the flames entered the lower half of the tubes, oscillations of the gas column were generally excited which often lead to rapid flash-back of the flames. Sometimes a different structure, composed of somewhat larger cells arranged more regularly and rotating, often quite rapidly, around the tube axis, was observed. It was found that this phenomenon occurred only when the flame was made to move upward into a region of the tube which had been previously heated by the flame.

The first appearance of cells in the primary combustion zone was found to occur at the rich limit of inflammability of propane-air-nitrogen flames.[1] A lean limit of cell structure was found at a C_3H_8-air ratio of about 0.06 by volume for mixtures containing more than 28 percent added nitrogen. When this limit was approached from the rich side the ridges separating the cells flattened out and beyond the limit the flames formed a single smooth disk filling the whole tube cross section. The average diameter of the cells was found to be of the order of $\frac{1}{2}$ inch and was independent of tube diameter and mixture composition.

This cell structure of almost stationary flames in tubes has apparently not been observed by previous investigators. Polyhedral flames[2] may constitute a special case of this structure. Interpretation of the phenomenon as a flow instability

is suggested by the resemblance to cellular convection,[3] which has been treated successfully as a stability problem.[4] A connection between cellular convection and combustion phenomena has been anticipated by Chandrasekhar.[5] Instability of an infinitely thin plane flame front, taken as a surface of discontinuity of normal velocity and density in incompressible and inviscid flow has been established.[6] This treatment cannot explain, however, the finite size of the cells and the existence of limits of composition beyond which the cell structure disappears. A theory in which the finite thickness of the combustion zone is taken into account is being developed.[7] Dimensional analysis shows that in such a treatment the diameter of the cells should be proportional to the thickness of the combustion zone under otherwise unchanged conditions. Since a reduction of pressure causes an increase of combustion zone thickness without affecting other variables to a large extent, exploratory observations of cellular flames burning under reduced pressure have been performed in the Cornell Aeronautical Laboratory Altitude Chamber. The size of the cells was found to vary roughly inversely proportional to pressure, in accordance with the above-mentioned theoretical conclusion.

* This work was supported by the U. S. Navy under Project SQUID.

[1] H. F. Coward and G. W. Jones, U. S. Bur. of Mines Bull. **279**, 65 (1938).
[2] F. A. Smith and S. F. Pickering, J. Research Nat. Bur. Stand. **3**, 65 (1929).
[3] H. Bénard, Revue générale des Sciences **12**, 1261, 1309 (1900).
[4] Lord Rayleigh, Phil. Mag. **32**, 529 (1916), and others.
[5] S. Chandrasekhar, Meetings on Fundamentals of Combustion, Applied Physics Laboratory, Johns Hopkins University, March 1947.
[6] L. Landau, Acta Physicochimica URSS **19**, 77 (1944).
[7] H. Einbinder, forthcoming paper.

Errata: Rate of Nucleation in Condensed Systems

[J. Chem. Phys. **17**, 71 (1949)]

J. C. FISHER
General Electric Company Research Laboratory, Schenectady, New York

THE first line of the second column, page 71, should end

$$i^* = (2A/3B)^3,$$

and Eq. (15) should read

$$R = n \Big/ \int_{i_0}^{\infty} \exp(\Delta F_i/kT) i^{-1} di.$$

On the Electric Dipole Moment and Vibrational States of $H_3B^{10}CO$*

M. W. P. STRANDBERG, C. S. PEARSALL, AND M. T. WEISS
Research Laboratory of Electronics, Massachusetts Institute of Technology, Cambridge, Massachusetts

February 18, 1949

THE $J=1\rightarrow2$ rotation absorption due to bordine carbonyl has been observed by Gordy, Ring, and Burg,[1] from which they deduce a value of 3 for the B^{10} spin.

We have observed the $J=0\rightarrow1$ rotational transition in $H_3B^{10}CO$ for the ground vibrational state, and for two excited vibrational states (v_1,v_2), with negative α's but as yet unassigned. The quadrupole hyperfine structure was not observed, since at room temperature (~23°C), the compound decomposed so rapidly (~ a few seconds) under pumping, that lines less than 1 Mc/sec. could not be observed. The Stark effect was measured for two of the unresolved lines. The relevant data may be listed as follows:

$H_3B^{10}C^{12}O^{16}$			
$\nu_{J=0\rightarrow1}$	= 17,961.20	±0.05	Mc/sec.
B_0	= 8980.36	±0.025	Mc/sec.
B_{v1}	= 9002.66	±0.03	Mc/sec.
B_{v2}	= 8985.80	±0.03	Mc/sec.
D_J	= 0.177	±0.03	Mc/sec.
$(\mu_{J=0\rightarrow1})_0$	= 1.795	±0.01	debye
$(\mu_{J=0\rightarrow1})_{v1}$	= 1.770	±0.01	debye
γ_0/γ_{v1}	≃ 3.		
γ_0/γ_{v2}	≃ 10.		

These measurements were made with a spectroscope which we have been using for some time, and which exhibits high sensitivity. The system combines a modified f-m method[2] with a Stark detection scheme.[3] The oscillator source is frequency-modulated at a frequency greater than the line breadth (instead of less than the line breadth as is usual), and of an amplitude such that the modulation index $m=\Delta f/f\simeq1$. This gives a carrier with essentially two strong sidebands at $\pm f$ from the carrier. A strong square-wave Stark field at about 6-kc/sec. repetition rate is imposed on the gas sample. The microwave field transmitted through the absorption sample is detected in a silicon crystal and amplified by a receiver tuned to the frequency-modulation rate, f, ±6 kc/sec. The detected receiver output is further amplified in a narrow-band 6-kc/sec. amplifier. The theory of operation will be published later but, briefly, the high frequency f-m allows superheterodyne amplification with detection removed from the low frequency region of high crystal noise. In all detection processes, phase is preserved, so that band width narrowing at 6 kc/sec. increases the signal-to-noise power ratio by an amount inversely proportional to the band width. The band widths used by us are about 3 c.p.s., 10 c.p.s., and 800 c.p.s., and are stable since a phase-sensitive detector at 6 kc/sec. is used. The near d.c. signals (with 3- and 10-c.p.s. band widths) are remodulated to 6 kc/sec. and are displayed on a long-persistence (P7 screen) cathode-ray oscilloscope. The sensitivity has not been accurately checked except on the 800-c.p.s. band width, where $\alpha_{\min.}\simeq5\times10^{-8}$. The 10-c.p.s. band width has been checked against that for 800 c.p.s., and the expected tenfold increase seems achieved. This means that with the 10-c.p.s. system, and $\alpha_{\min.}$ of about 5×10^{-9} with oscilloscope presentation may be achieved.

We would like to acknowledge the use of a sample of diborane kindly supplied by G. B. Kistiakowsky and H. S. Gutowsky of Harvard University and the University of Illinois.

* This work has been supported in part by the Signal Corps, the Air Materiel Command, and ONR.

[1] W. Gordy, H. Ring, and A. Burg, Phys. Rev. **74**, 1191 (1948).
[2] W. D. Hershberger, J. App. Phys. **19**, 411 (1948).
[3] R. H. Hughes and E. B. Wilson, Phys. Rev. **71**, 562 (1947).

The Unsteady Shock Wave

BRUNO W. AUGENSTEIN
School of Aeronautics, Purdue University, Lafayette, Indiana

January 28, 1949

THE following comments concern the Letter to the Editor of F. Cap, entitled "A new equation for the non-stationary shock wave" (J. Chem. Phys. **17**, 106, (1949)). The letter contains numerous misprints which make the equations and results unintelligible. In particular, the symbol u has throughout been used for both the particle speed before the wave, and for the ratio of specific heats, C_P/C_V.

Since the results obtained are of interest, a very brief alternative derivation is given here. If, as in the letter of Cap, we denote by w the wave speed relative to the gas in front of it, by u the particle speed, by P the pressure, by a the speed of sound, by $\gamma=C_P/C_V$ the ratio of specific heats, and if we use a subscript $(\,)_0$ to denote states before the wave, and the subscript $(\,)_s$ to denote the states after the wave, then it is known that the following relations hold for the unsteady shock:[1]

$$\left(\frac{w}{a_0}\right)^2=\frac{1}{2\gamma_0}\frac{(\lambda-1)[(\gamma_s+1)\lambda+(\gamma_s-1)]}{\lambda-[(\gamma_s-1)/(\gamma_0-1)]},$$

$$\left(\frac{a_s}{a_0}\right)^2=\frac{\gamma_s}{\gamma_0}\lambda\frac{(\gamma_s-1)\lambda+(\gamma_s-1)+2[(\gamma_s-1)/(\gamma_0-1)]}{(\gamma_s+1)\lambda+(\gamma_s-1)}, \qquad (1)$$

$$\left(\frac{u_s-u_0}{a_0}\right)^2=\frac{2}{\gamma_0}\frac{(\lambda-1)(\lambda-[(\gamma_s-1)/(\gamma_0-1)])}{(\gamma_s+1)\lambda+(\gamma_s-1)},$$

where we have put: $\lambda=(P_s/P_0)$. For the limiting case of intense shock waves, $\lambda\rightarrow\infty$, we derive from Eq. (1) putting $u_0=0$, the following relations:

$$(u_s/a_s)^2=(2/\gamma_s(\gamma_s-1)),$$
$$(w/a_s)^2=[(\gamma_s+1)^2/2\gamma_s(\gamma_s-1)], \quad (2)$$
$$(w/u_s)^2=(\gamma_s+1/2)^2=(w/a_s\cdot a_s/u_s)^2.$$

For the case where $\gamma_0=\gamma_s=1.4$, we have, therefore:

$$u_s/a_s=1.89, \quad w/a_s=2.27, \quad w/u_s=1.20, \quad (3)$$

and these are the results of the last line of the letter of Cap, as it should read. It is not to be implied that it is necessarily correct that $\gamma_s=\gamma_0$ is compatible with $\lambda\rightarrow\infty$. To answer such questions, the detailed structure of the shock wave and its wake must be investigated. Such questions and related ones are satisfactorily treated only by the higher order approximations of kinetic theory; an account of the techniques involved is given in reference 2. Relations (1) are derived under the assumption of a perfect gas equation of state, and zero relaxation time for all degrees of freedom of the gas swept over by the shock wave.

[1] H. Pfriem, Forsch. Ing. Wesen. Bd., 12 (1941).
[2] S. Chapman and T. G. Cowling, *Mathematical Theory of Non-Uniform Gases* (Cambridge University Press, London, 1939).

The Infra-Red Absorption Spectrum of *n*-Butane in the Solid State*

D. W. E. Axford and D. H. Rank
Physics Department, Pennsylvania State College, State College, Pennsylvania
February 21, 1949

A SERIES of investigations,[1-4] carried out recently in this laboratory, on the Raman spectra of the normal hydrocarbons has established the co-existence of rotational isomers in the liquid phase and has demonstrated that only one of the isomers persists, in general, on solidification. Since there is no reason to doubt that the infra-red spectra would show a similar behavior, we have attempted to obtain the spectrum of solid *n*-butane in the hope of obtaining a corresponding simplification.

Previous investigations of infra-red spectra of organic compounds at low temperatures are few in number. Avery and Ellis[5] studied the spectra of several simple hydrocarbons, including ethane, at liquid air temperature. Halford *et al.*[6,7] have studied the spectrum of benzene and cyclohexane at low temperature, and Thompson and his co-workers[8] have recently studied a considerable number of compounds in the liquid and solid states with a view to obtaining information about the effect of state of aggregation on the spectra.

The cell employed was based on a design at present being used by Dr. R. C. Lord at the Massachusetts Institute of Technology. It consists in essence of an ordinary infra-red absorption cell for liquids, with silver chloride windows, suspended inside an evacuated container, also with silver chloride windows. By cooling with liquid air it was possible to freeze the liquids completely and obtain a satisfactory spectrum of the frozen substance. The method probably does not allow a very accurate determination of percentage transmission because the liquid may leave gaps on freezing, but it is quite adequate to observe the general character of the spectra. In order to fill the cell with *n*-butane which boils at -0.3°C, it was necessary to cool the cell in dry ice before filling it and placing it in the outer jacket. However, with a little practice, this proved to be a fairly simple operation. The spectrometer employed was a standard Perkin-Elmer instrument, Model 12c, used in conjunction with a Brown recorder.

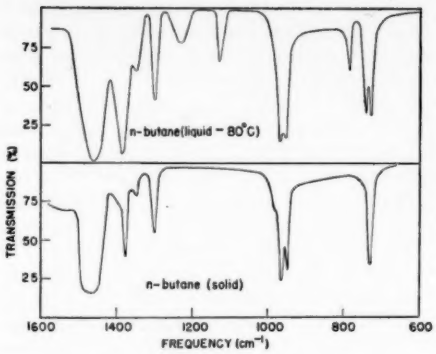

FIG. 1. Infra-red absorption spectrum of liquid *n*-butane at -80°C and solid *n*-butane at liquid air temperatures. Cell thickness 0.1 mm.

The infra-red spectrum of gaseous *n*-butane is available,[9] but not so that of the liquid, so we carried out experiments at -78°C also in order to get a trace for liquid *n*-butane. The traces for the liquid and solid are shown in Fig. 1. The spectra were investigated in the regions 7.5–14 μ since it is in this region that the most interesting changes are likely to occur on solidification.

The bands observable in the liquid and solid are listed below.

Gas[9] cm^{-1}	Liquid cm^{-1}	Solid cm^{-1}
1466(*s*)	1462(*s*)	1461(*s*)
1390(*s*)	1392(*s*)	1382(*s*)
1340(*w*)	1350(*w*)	1350(*w*)
1297(*s*)	1297(*m*)	1299(*m*)
1244(*w*)	1233(*w*)	—
1134(*m*)	1133(*m*)	—
—	—	984(*w*)
970(*s*)	971(*s*)	965(*s*)
959(*s*)	961(*s*)	951(*s*)
795(*w*)	788(*m*)	—
751(*m*)	747(*s*)	—
734(*m*)	731(*s*)	732(*s*)

Our results agree well with conclusions already made[1] about the symmetry of the more stable isomer. The existence of, at the most, 8 lines in the infra-red where 10 are permitted in this region on the basis of the C_{2h} symmetry, is good evidence for the *trans*-isomer being the one formed on solidfication. A few minor modifications in the assignment already made are required:

(1) The frequency 732 cm^{-1} belongs to the low energy *trans*-form, not 751 cm^{-1}, as previously had been arbitrarily suggested.
(2) It would appear likely that, since the bands at 1340 and 795 cm^{-1} disappear on cooling, they correspond to the less stable isomeric molecule rather than that they are summation or difference bands. However, this might occur due to the disappearance of one or both of the combining frequencies, and until data in the region below 650 cm^{-1} is available, this point cannot be unambiguously decided. In view, however, of their intensity in the liquid, we are inclined to assign them to the weak isomer.
(3) There is no doubt that both the bands at 970 and 959 cm^{-1} belong to the *trans*-isomer. The only curious feature of the solid spectrum is the appearance of a marked shoulder at 988 cm^{-1} which is not detected in the gas or liquid. This may be because in the liquid and gaseous states it is obscured in the broad contour of the 970-951 cm^{-1} band. It is apparently genuine, as it was obtained on three separate occasions.

The results with *n*-butane show that the infra-red spectra of the solid supports the conclusions made previously. Experiments which we have made with the straight-chain hydrocarbons up to C_7 also show simplification in the spectra on freezing. It is intended to publish a full account of this work directly.

* This research was carried out on contract N6onr-269, Task Order V of ONR.
[1] Szasz, Sheppard, and Rank, J. Chem. Phys. **16**, 704 (1948).
[2] Rank, Sheppard, and Szasz, J. Chem. Phys. **17**, 83 (1949).
[3] N. Sheppard and G. Szasz, J. Chem. Phys. **17**, 86 (1949).
[4] G. Szasz and N. Sheppard, J. Chem. Phys. **17**, 93 (1949).
[5] W. M. Avery and C. F. Ellis, J. Chem. Phys. **10**, 10 (1942).
[6] R. S. Halford and G. B. Carpenter, J. Chem. Phys. **15**, 99 (1947).
[7] R. S. Halford and O. A. Schaeffer, J. Chem. Phys. **14**, 141 (1946).
[8] R. E. Richards and H. W. Thompson, Proc. Roy. Soc. (London) **195**, 1 (1948).